Determining drought sensitivity of the Amazon forest: does plant hydraulics matter?

Determining drought sensitivity of the Amazon forest:

does plant hydraulics matter?

A dissertation presented

by

Thomas L. Powell

to

The Department of Organismic and Evolutionary Biology

in partial fulfillment of the requirements

for the degree of

Doctor of Philosophy

in the subject of

Biology

Harvard University

Cambridge, Massachusetts

July 2015

Professor Paul R. Moorcroft Thomas L. Powell

Determining drought sensitivity of the Amazon forest:

does plant hydraulics matter?

Abstract

Climate change is projected to cause significant shifts in precipitation patterns across the Amazon basin. This dissertation is designed to address key uncertainties surrounding our ability to predict the fate of the Amazon rainforest in a drier climate. The second chapter is an assessment of the ability of four leading dynamic vegetation models—CLM3.5, ED2, IBIS and JULES—to replicate observation from two long-term ecosystem-scale drought experiments in the eastern Brazilian Amazon. This analysis revealed that these four models can reliably predict plant and ecosystem carbon fluxes under the present climate, but still require substantial development for predicting the consequences of severe drought. These four models were not parameterized to mechanistically represent soil water-stress or the competitive differences in plant hydraulics that exist between tree species. Therefore, chapter three is a field-based study designed to quantify the range of variation in two plant hydraulic traits—xylem-P_{50} and turgor loss point (TLP)—that exists in mature tropical trees. The field measurements were made on four genera common to both experimental study sites. Each genus was categorized *a prior* into one of four plant functional types: early- versus late-successional that were each subdivided into drought-tolerant versus intolerant. Xylem-P_{50} and TLP occurred at water potentials that were 0.7 to 1.1 MPa and 0.75 MPa higher, respectively, in the drought-intolerant genera compared to the tolerant genera. In comparison, the early- versus late-

successional genera showed no significant differences in xylem-P_{50} and TLP, thereby revealing two orthogonal axes of competition: one along a successional gradient and the other along a soil moisture gradient. The results from chapter three were then used to parameterize and test a new mechanistic water-stress formulation in the Ecosystem Demography (ED2) model, which became the basis of chapter four. With the new water-stress formulation, ED2 successfully replicates the observed reductions in total aboveground biomass in the drought experiments. It also more realistically captures the compositional and structural shifts that occur as a result of severe droughts. This dissertation makes an important contribution that advances the science of tropical forest drought ecology and enhances our ability to make reliable predictions about the fate of tropical forests in a future drier climate.

Table of Contents

Abstract	iii
Table of Contents	v
Acknowledgements	vi
Chapter 1: Introduction	1
Chapter 2: Confronting model predictions of carbon fluxes with measurements of Amazon forests subjected to experimental drought	28
Chapter 3: Do differences in xylem cavitation resistance and leaf hydraulic traits explain differences in drought tolerance among mature tropical rainforest trees?	78
Chapter 4: Improving tropical forest drought responses in dynamic vegetation models: are drought-tolerance plant functional types or a mechanistic representation of plant water movement required?	110
Chapter 5: Conclusions	167
Appendix A: Protocol for drought manipulations	173
Appendix B: Chapter 2 Supporting Information	184
Appendix C: Chapter 3 Supporting Information	205

Acknowledgements

I am deeply indebted to the numerous people and organizations that have made this dissertation possible.

First and foremost, I thank my advisor and mentor Paul Moorcroft. Paul has been a powerful influence on the way I approach scientific inquiries and understand ecology. Paul has also provided me with the necessary support and freedom a student needs to develop as an independent professional.

I thank my committee members, Missy Holbrook, Stuart Davies and Andrew Richardson, for their time, professional advice and valuable input about my research.

I thank members of the Moorcroft lab and the greater ED community for all of the assistance they provided me on learning how to use the ED model. I am also grateful to them for their academic and professional advice and friendship. Chapter 4 of this dissertation would not have been possible without the instruction and model development of Marcos Longo, Naomi Levine, Ryan Knox, Alex Antonarakis, and Ke Zhang. Carla Barger and Erin Sullivan provided valuable logistical support in organizing the field campaigns.

I thank Xiangtao Xu and David Medvigy of Princeton University for generously providing me with the hydrodynamics code used for Chapter 4. I thank the Drought Team from the AAI project for their modeling contributions in Chapter 2. I thank Lola da Costa of Universidade Federal do Pará, Brazil, Patrick Meir of the University of Edinburgh, and Scott Saleska of the University of Arizona for helping me to gain access to the Brazilian field sites, sharing ancillary data and for providing logistical support for

my field work. I am grateful to the Holbrook lab for generously providing me with their time, expertise, lab space and instruments to facilitate my field work. Jim Wheeler and Tony Rockwell in particular provided me with several hours of training. Alex Oliveira, a student and field technician of Lola da Costa, was my indispensible field assistant, logistical coordinator, language trainer and friend during the Caxiuanã and final Tapajós field campaigns. Kathy Ran, a Harvard undergraduate, helped with field measurements during the first Tapajós field campaign. I would also like to acknowledge Collin Johnson for his council and insight in learning the craft of teaching ecology.

I am grateful for the generous financial support provided by the Department of Organismic and Evolutionary Biology, the Gordon and Betty Moore Foundation, the National Science Foundation Doctoral Dissertation Improvement Grant (NSF award # DEB-1110540), the National Science Foundation Partnership for International Research and Education in Amazon Climate Interactions grant (NSF award #OISE-0730305). In Brazil, the Museu Paraense Emilio Goeldi in Belem and the LBA office in Santarém provided logistical support and assistance during the field campaigns.

Finally I thank my family, which includes the entire Arlington Heights community. Thank you for your support, encouragement and fellowship throughout this entire process. More than anyone, I am most grateful to my wife Julie—this is an accomplishment that belongs to both of us.

Chapter 1

Introduction

Anthropogenic climate change is likely to be one of the most consequential events to affect the terrestrial biosphere of our planet over the coming century (IPCC, 2014). Quantifying the relative sensitivity of various ecosystems to climate change is critical to finding a balance between fostering human development, sustaining ecosystem services and transferring vast stores of terrestrial organic carbon to the atmosphere and oceans. Accordingly, tropical forests are one of the most important ecosystems to understand because of their influence on the global climate system and the global carbon budget (Bonan *et al*., 2008; Malhi *et al*., 2008). Amazonia is the largest continuous tropical forest in the world; covering approximately 5.4 million km^2 (Malhi *et al*., 2008) and accounting for 25% of the world's biodiversity (Dirzo *et al*., 2003) and 15% of terrestrial productivity (Field *et al*., 1998). This research addresses the fundamental question: what is the fate of the Amazon forest in a future drier climate?

Currently, the Amazon region appears to be more strongly limited by light availability compared to precipitation and temperature (Nemani *et al*., 2003). Indeed, direct phenological and gas exchange measurements have verified that the present assemblage of species has been selected to optimize for light by "greening up" and increasing net carbon assimilation during the dry season when incident radiation is the highest (Saleska *et al*., 2003; Huete *et al*., 2006; Hutyra *et al*., 2007). A comparative study of plant functional types (PFT) conducted in a subtropical region of South America corroborates this light-limiting hypothesis (Nemani *et al*., 2003), where early successional trees adjusted their hydraulic architecture to increase water transport efficiency in response to increased irradiance while late successional trees did not (Campanello *et al*., 2008).

Many global climate models (GCMs) are predicting a regime shift for the Amazon region as anthropogenic global change evolves over the 21st century, where higher temperature and lower precipitation are projected to become more limiting (Cox *et al*., 2000; Huntingford *et al*., 2008; Malhi *et al*., 2009). Consequently, early predictions by both a GCM that was unidirectionally coupled to a dynamic vegetation model (DVM) (Huntingford *et al*., 2008) and a fully coupled GCM (Cox *et al.*, 2000) suggest widespread die-back of the Amazon forest by the end of the 21st century. Alternatively, an analysis of 21st century precipitation predictions by 19 GCMs found that the climate for eastern Amazonia tended toward that indicative of a seasonal deciduous forest (Malhi *et al.,* 2009). The positive feedback from the release of CO_2 resulting from either of these two cases could significantly accelerate global climate changes (Cox *et al*., 2000). A more recent analysis of 22 different climate models coupled to a single DVM suggested that changes in vegetation resulting from changes in precipitation would be minor in comparison to the negative effects of higher temperatures and the positive effects of CO_2 fertilization (Huntingford *et al*., 2013). However, are any of these predictions realistic?

The paleo-record offers some insight into how Amazonia has historically responded to precipitation changes. According to various proxies obtained through dendrochronology (Schöngart *et al*., 2004; Jones *et al*., 2009), stable isotopes (Stute *et al*., 1995; Thompson *et al*., 1995, 1998), palynology and limnology (Baker *et al*., 2001; Bush *et al*., 2002, 2004), the Amazon forest experienced a range of climatic conditions through the Cenozoic. Contrary to the "refugia hypothesis" (Haffer, 1969; Haffer and Prance, 2001), $\delta^{13}C_{OM}$ (organic matter carbon) and lignin phenol sampled from a deep

sea core collected from the Amazon river fan (Leg 155 of the Ocean Drilling Program) showed that the average species composition between C_4 grasses, C_3 angiosperms and C_3 gymnosperms has changed little over the past 70 ky BP (Kastner and Goñi, 2003). Continental sources of pollen also suggest that the extent of forest expansion and contraction has only been limited to the margins of the Amazon basin (Colinvaux *et al*., 2001; Mayle *et al*., 2004). A GCM simulation through the last glacial maximum also supported the lack of vegetation change between C_3 and C_4 functional groups (Mayle *et al*., 2004). Interestingly, the model predicted a shift in southern Amazonia from the widely distributed evergreen forests typical of today's more humid climate to an extensive deciduous forest, while the evergreen forest remained in the north (Mayle *et al*., 2004). Therefore, direct evidence and model simulations suggest that there was an inherent degree of resilience among the assemblage of tree species that allowed for alternative forested configurations rather than transitions between savanna and forested states as the climate changed.

Three caveats should be noted when drawing comparisons between today's situation and the past. First, although individual plasticity or competitively mediated changes in canopy composition may enable persistent forested states, a considerable amount of C may still be released to the atmosphere as the balance between productivity and respiration shifts in response to changes in precipitation and temperature (Schuur *et al*., 2001). Second, global change is occurring more than an order of magnitude faster now than during the Pleistocene to Holocene transition (Bush *et al*., 2004). Third, unlike the past 22ky BP (Monnin *et al*., 2001), profound changes in atmospheric chemistry will be an important feature of anthropogenically driven climate change (IPCC, 2014). For

example, recent increases in water–use efficiency have been widely observed in forests around the world, which is likely the result of increasing atmospheric CO_2 (Keenan et al., 2013).

A broad range of drought resistance has been found across tree species in today's tropical forests through ample biogeographical and physiological studies. For example, Engelbrecht *et al*., (2007) showed that drought sensitivity explained the distribution of 48 species across a precipitation gradient in Panama. A wide range of functional traits such as wood density (e.g. Baker *et al*., 2004), specific leaf area (Fyllas *et al*., 2009), leaf shape (Malhado *et al*., 2009), branch architecture (Meinzer *et al*., 2008), root architecture (Markesteijn & Poorter, 2009; Metcalfe *et al*., 2008), lethal leaf water potential, turgor loss point, lethal leaf relative water content (Baltzer *et al*., 2008), stem xylem conductivity (Fonti *et al*., 2010), leaf conductivity (Brodribb and Holbrook, 2003), stem capacitance (Pineda-García *et al*., 2013), and whole-plant leaf-area specific conductivity (Meinzer *et al*., 2008) have been associated with spatial variation in available soil moisture. Given these results, making generalizations about trade-offs between fitness under either a light or water limited regime is complex.

Ecological studies in the Tapajós (TNF) (Nepstad *et al*., 2002, 2007; Brando *et al*., 2008), and Caxiuanã (CAX) National Forests (Fisher *et al*., 2007; da Costa *et al*., 2010) were established in the eastern Brazilian Amazon to directly measure the effects of severe long-term experimental drought on a 1 ha forested ecosystem. Interestingly in both studies, tree mortality increased 2.5 to 4.5 times among the largest trees, but smaller trees (<20cm DBH) were marginally affected (Nepstad *et al*., 2007; da Costa *et al*., 2010). LAI also was reduced in the drought plots of both studies (Fisher *et al*., 2007;

Brando *et al*., 2008). However, Nepstad *et al*. (2002) reported that leaf-shedding as an early response to drought was not the cause of lower LAI; rather, leaf production declined later in the second year indicating a possible shift in C-allocation properties. It is possible that additional carbohydrate energy was required to repair leaf embolism (Brodribb and Holbrook, 2003), or more C was allocated below ground to scavenge for water. Yet, the plasticity of functional traits was not examined in these two drought experiments, and has been poorly studied in general (but see Fonti *et al*., 2010). But perhaps even more fundamental is that mechanism causing the larger trees to succumb to the drought was not identified.

Given these uncertainties, a properly parameterized mechanistic model can be useful for *i*) identifying the fundamental processes and associated trade-offs that lead to survival or mortality within a dynamic tropical ecosystem, and *ii*) predicting how compositional shifts will play out as climate changes, which is impractical to address experimentally in a field setting over several decades. The Ecosystem Demography (ED) model can meet this objective because it tracks competitive dynamics between plant functional types (PFT) and can be run into the future dynamically coupled to atmospheric models (Moorcroft *et al*., 2001; Medvigy *et al*., 2009). However, ED is not well configured to realistically predict responses to changes in precipitation regimes. The current parameterization incorporates successional differences between species by representing early, mid and late successional PFTs. But, many of the functional traits known to both control plant water-use and adjust to water stress are either not included in the current model parameterization, are a fixed property of individuals, or are the same across PFTs. Hence, it is therefore not surprising the ED simulation in Huntingford *et*

al., (2008) caused the forest to collapse under a higher temperature and lower precipitation regime.

Currently, most land surface models parameterize the hydraulic system of trees using resistor (e.g. Farquhar *et al*., 1980) or resistor-capacitor (e.g. Čermák *et al*., 2007; Kumagai *et al*., 2009) schemes; see for example: CLM (Oleson *et al.,* 2008), IBIS (Foley *et al*., 1996), JULES (Cox, 2001; Clark *et al*., 2011), SiB3 (Sellers *et al.,* 1996; Baker *et al.,* 2008). These models, however, neglect the architecture of water-transport systems within vascular plants. Ultimately, hydraulic architecture is simultaneously responsible for the efficient, yet safe, transport of water in vascular plants, which reflects trade-offs necessary for enhancing fitness in a given environment (Fonti *et al*., 2010). In the tropics, little is known about how inherent structural differences between species will influence long-term community dynamics between competing species. Also, individuals are known to modify their conductive tissue in response to environmental changes (Campanello *et al*., 2008; Fonti *et al*., 2010); yet, the magnitude of this plasticity and how it differs within and between functional groups is poorly quantified.

Even in light of our growing knowledge about morphological and physiological adaptations to water-stress, little is known about the exact process by which trees succumb to intense water-stress. McDowell *et al*. (2008) proposed a framework that divides drought survival strategies between tolerance and avoidance and then sub-divided tolerance between isohydric and anisohydric. Isohydric plants use their stomata to maintain leaf water potential above a critical threshold, thereby restricting CO_2 exchange when water is limited. Anisohydric plants keep their stomata open under water-stress, thus allowing CO_2 exchange to continue to the point that cavitation may occur.

McDowell *et al*. (2008) used a piñon-juniper woodlands (*Pinus edulis-Juniperus monosperma*) that was affected by the 2001-2003 severe drought in the American Southwest as an example for this framework because the two dominant species were either isohydric (pinon pine) or anisohydric (juniper). Interestingly, the isohydric piñon pines suffered wide spread mortality while the anisohydric junpers generally survived the drought. Carbon starvation was identified as the likely process that caused piñon pine mortality (Breshears *et al*., 2009). The framework proposed by McDowell *et al*., (2008) is particularly relevant for studying severe drought in the Amazon forest because Fisher *et al*. (2006) showed that of the seven species measured for physiological properties in the CAX drought experiment, all were isohydric. This result suggests there may be a limited range of strategies for coping with water-stress in tropical regions that have not been water limited over an evolutionary time scale.

Research Framework

This dissertation is organized around an integrated modeling and empirical framework (Medlyn *et al*., 2015). Once a scientific inquiry is motivated, the research flows in the following manner: (1) evaluate the state of our theoretical understanding within a model, (2) develop new hypotheses, (3) test the hypotheses through experimentation, (4) use experimental results to parameterize new model formulations, then return to 1 and identify new model uncertainties (Fig. 1.1).

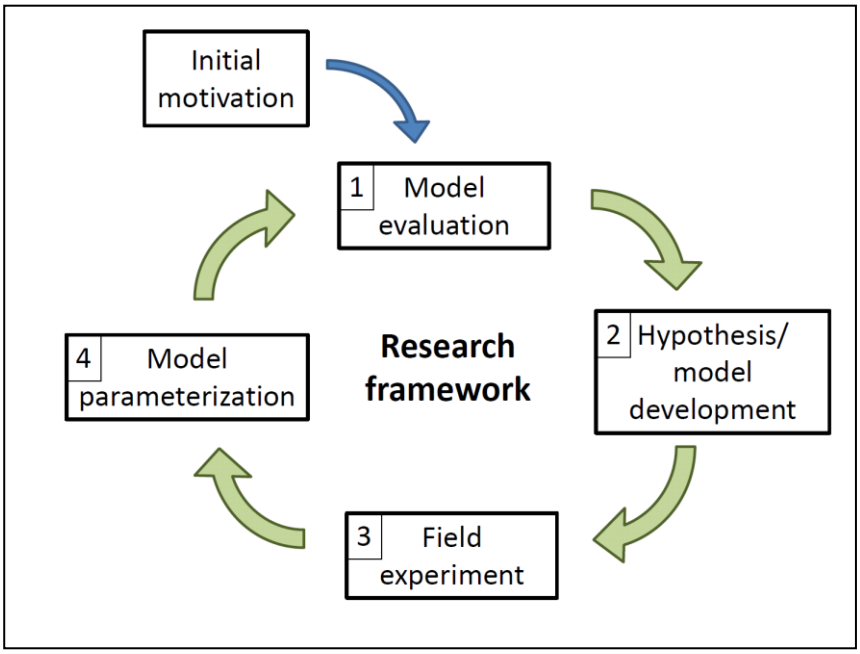

Figure. 1.1 Framework guiding the research of this dissertation. The research was initially motivated by scientific uncertainties identified from a literature review. These uncertainties were evaluated theoretically using the Ecosystem Demography model. 2. Hypotheses were developed to resolve the highest impact uncertainties. 3. Field experiments were conducted to test the hypothesis. The ED model was updated to reflect the results of the field experiment. The model was evaluated again. New hypotheses will be developed for future research.

Initial model evaluation

Part 1. The Ecosystem Demography model, version 2 (ED2, Medvigy *et al*., 2009) is a state of the art terrestrial biosphere model that simultaneously tracks hydrology, land-surface biophysics, soil carbon and biogeochemistry (Moorcroft *et al*., 2001). An important innovation of ED2 relevant to this study is that it links fine-scale (sub-grid) and landscape level processes by representing competition between discrete demographic groups. Competition is tracked through sub-grid scale mortality and subsequent

reproduction and growth of similarly aged cohorts and PFTs. This unique feature can be adapted to also evaluate the competitive advantages of differing drought tolerance strategies within and between PFTs. ED2 incorporates a complete representation of land-surface biophysics that explicitly solves for the carbon, water and energy fluxes of the land surface including a multilayer soil model.

ED2 is presently configured to represent competition between three successional (early, mid, and late) tropical tree PFTs, each with different parameterizations for photosynthesis, growth and mortality. ED2 contains the following structural and functional traits that have been related to plant water-use: rooting depth, specific leaf area (*SLA*), leaf size, canopy roughness, wood density, tree height, C-allocation between leaves and fine roots (q), and ratio of sapwood area to leaf area (q_{sw}, *sw*: sapwood). ED2 also includes a tunable parameter that encompasses the conductivity of the soil-to-leaf system (K_W, m^2 kg-C^{-1} yr^{-1}). However, these traits and K_W are static at the cohort level.

A preliminary analysis was conducted to evaluate how the original formulation of ED2 predicts the drought response of the throughfall exclusion site at TNF. Several drought levels were simulated over a 9 year period (2000-2008). The model was run using NCEP reanalysis meteorological data. The simulations were initialized from a 500-year spin-up forest generated from recycled NCEP data for 1969 – 2008 for the TNF coordinates. The parameterization of ED2 (Medvigy *et al*., 2009) includes the original parameterization for tropical forests used in ED (Moorcroft *et al*., 2001). The drought levels tested were 0%, 25%, 40% and 50% to 70% by 5% increments; each imposed for the entire 9 yr simulation period. Hereafter, drought nomenclature is denoted as dr0 = drought 0%, dr25 = drought 25%, etc.

After a 500 year spin-up, the equilibrium aboveground biomass (AGB) is 3.2 and 13.8 kg C m^{-2} for PFT_{early} and PFT_{late}, respectively (Fig. 1.2a). The PFT_{mid} did not establish itself during the spin-up. The change in AGB under each drought scenario relative to dr0 is insignificant up to dr60 (Fig. 1.2b). Reducing precipitation by 5% more to dr65 causes a 75% reduction in AGB in the 5th year (Fig. 1.2c). Under dr70, the ecosystem completely collapses in the 3rd year of drought (Figure 1.2d). The mortality under dr65 occurs across all size classes (Fig. 1.3). This large-scale decline in AGB in all size classes sharply contrasts with the results of the TNF and CAX drought experiments, which observed a decline of 22% of total AGB in only the larger size classes (Nepstad *et al*., 2007; da Costa *et al*., 2010)

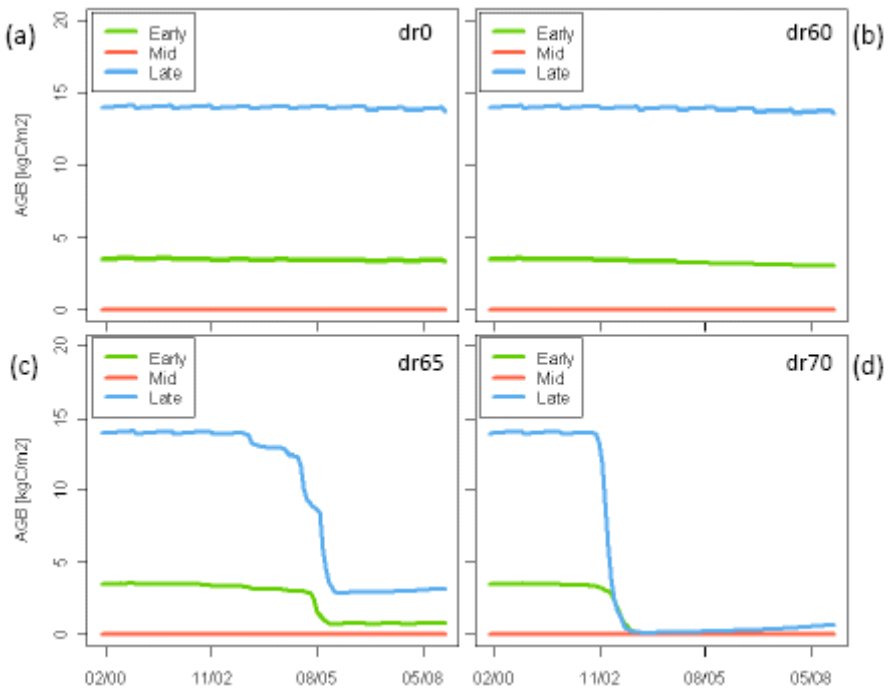

Figure 1.2. Simulations of Tapajós National Forest aboveground biomass (AGB, kg C m^{-2}) between 2000 to 2008 for drought (dr) levels (a) 0%, (b) 60%, (c) 65% and (d) 70%. Early, mid and late are the succession plant functional types.

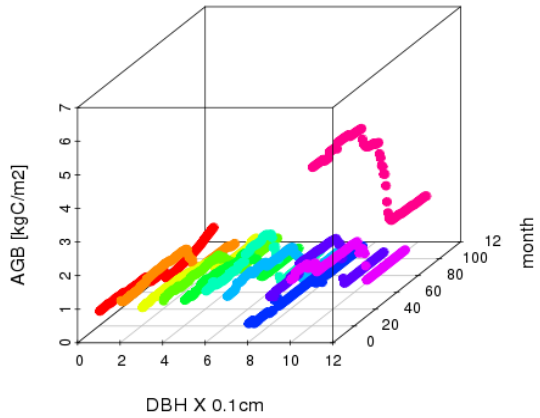

Figure 1.3. Monthly time series of Tapajós National Forest aboveground biomass (AGB) according to stem diameter class (DBH). Month 0 = January 2000.

A sensitivity test was performed on the functional traits K_W, q, and SLA to evaluate how much they alter ecosystem drought tolerance as measured by AGB. Both positive and negative adjustments of q and SLA by 40% to 50% had only a minor effect on the response of AGB to drought. The greatest gain for drought tolerance came from adjusting downward the K_W conductivity parameter from a baseline of 150 to 50 m^2 kg-C^{-1} yr^{-1} (Fig. 1.4a,b). Again the threshold was dr65; yet AGB was only reduced by half when K_W was set to 50 m^2 kg-C^{-1} yr^{-1}. In comparison, adjusting K_w downward to 100 m^2 kg-C^{-1} yr^{-1} had a marginal effect on AGB (Fig. 1.4c), while adjusting it upward to 200 m^2 kg-C^{-1} yr^{-1} resulted in even greater losses in AGB (Fig. 1.4d). The relationship between K_W and soil moisture is curvilinear where conductivity becomes increasingly sensitive with declining soil moisture. This prediction by ED2 is consistent with the general observation that species growing in xeric regions have relatively lower xylem hydraulic conductivity (Lambers *et al*., 2008). The sensitivity analysis showed that regardless of which of the three trait parameter were adjusted the ecosystem was largely insensitive to reduced precipitation until a critical threshold was breeched. This prediction is consistent

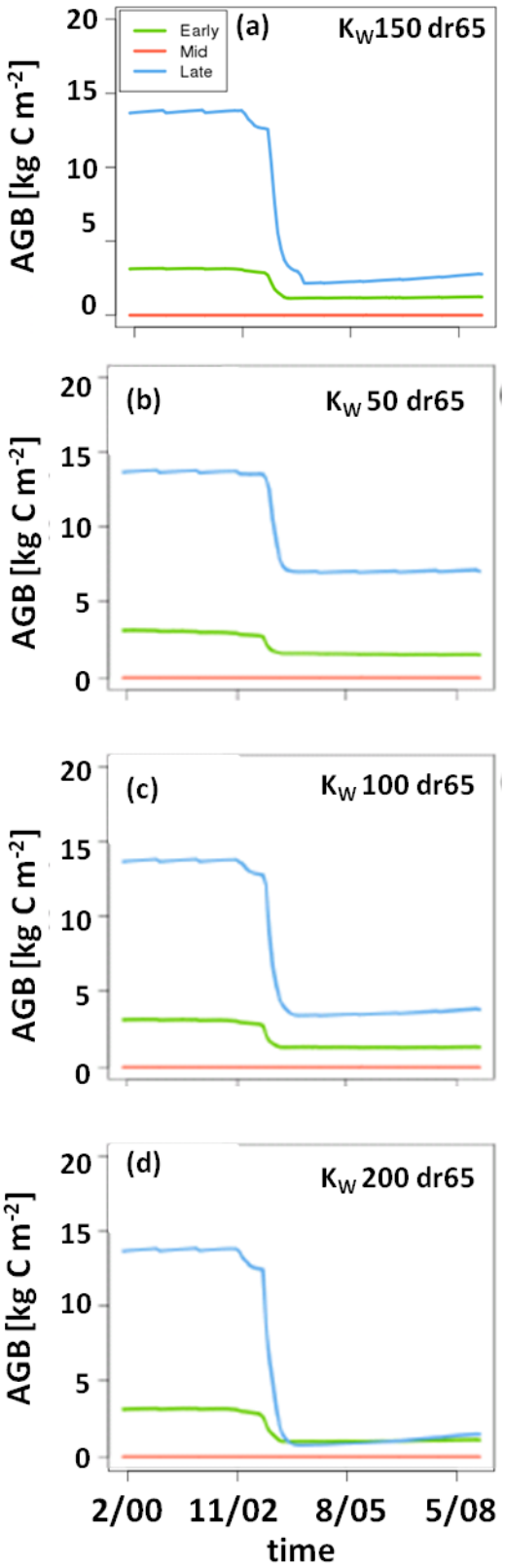

Figure 1.4 Sensitivity test of aboveground biomass (AGB, kg C m^{-2}) of the Tapajós National Forest during a 9 yr (2000-2008) simulation with a 65% reduction in precipitation (dr65). For each simulation, only the plant hydraulic conductivity parameter, K_W, was adjusted. (a) baseline parameterization, K_W = 150 m^2 kg-C^{-1} yr^{-1}, (b) conductivity is severely reduced, K_W = 50, (c) conductivity is moderately reduced, K_W = 100, (d) conductivity is increased, K_W = 200.

with the Tapajós drought experiment where the reduction in AGB occurred only after soil moisture available to the plants declined below a critical threshold (Nepstad *et al*., 2007). K_W showed the most promise for future inquiry since it conserved the greatest amount of AGB after the threshold was breeched.

Part 2. ED2 is one of several terrestrial biosphere models being used to evaluate the effects of drought on the Amazon forest (e.g. Baker *et al*., 2008; Sakaguchi *et al*., 2011; Huntingford *et al*., 2013). There is a range of predictions among these studies about both the magnitude of the response (e.g. Sakaguchi *et al*., 2011; Huntingford *et al*., 2013) and the key biological and ecological processes governing the response to drier soils (Baker *et al*., 2008; Castanho *et al*., 2013) . While similar in many ways, there are fundamental differences between all of the models in how they represent key biological and ecological processes relevant to drought. Moreover, these previous modeling studies generally used different spin up procedures and prescribed different physical environments—e.g. soil texture, soil moisture drainage, partitioning of radiation, etc.—thus making it challenging to generalize the biological and ecological responses to a future drier climate in the Amazon. Therefore, Chapter 2 is a rigorous intercomparison between ED2 and four other terrestrial biosphere models (Community Land Model version 3.5 (CLM3.5), Integrated BIosphere Simulator version 2.6.4 (IBIS), Joint UK Land Environment Simulator version 2.1 (JULES) and Simple Biosphere model version 3 (SiB3)) and a hydrodynamic terrestrial ecosystem model (the Soil–Plant–Atmosphere (SPA) model). For the first time, the spin-up procedure, physical environments and prescribed drought simulations were standardized between the models. In Chapter 2, differences and

similarities in the model formulations are elucidated in order to parse out where the greatest uncertainties exist in our understanding of the biological and ecological responses to drought.

Hypothesis evelopment

The research described in Chapters 3 and 4 is designed to build on the specific model evaluation of ED2 and the model intercomparison in Chapter 2. The role conductive tissue plays in water transport within the soil-plant-atmosphere continuum is not explicitly represented in ED2. Rather, ED2 uses a phenomenological relationship between soil water supply and canopy water demand to represent the effect of soil water stress on gas exchange (Moorcorft *et al*., 2001). In this relationship, stomatal conductance is down-regulated as a function of soil moisture. Although still not directly causal, a more realistic representation would have stomatal conductance be a function of leaf water potential, not soil moisture. Therefore, Chapter 4 explores formally representing hydrodynamic flow of water through the tree within the ED2 model.

A porous-media, pipe model that explicitly represents capacitance and hydraulic conductivity can be used to simulate hydrodynamic flow through the xylem. The fundamental assumption of a pipe model is that water movement through the xylem is analogous to soil water movement and is governed by Darcy's law. One major advantage of this approach is that the parameters represent the underlying physiological mechanisms that control water movement through plants and can be directly measured. Therefore, this formulation can realistically be extrapolated to novel environments

because the parameters remain within observed biological boundaries; whereas the K_W parameter from ED2 cannot be directly measured.

Field experiments

The field campaign served as the basis for Chapter 3. Its underlying aim was to obtain the measurements required to parameterize the new hydrodynamic formulation for ED2 described above and evaluated in Chapter 4. Estimates of turgor loss point (TLP) and xylem-P50 are the two plant traits needed for the new parameterization. Turgor loss point is the integrated leaf water pressure when the cells lose turgor and is correlated with stomatal closure (Brodribb *et al*., 2003). Xylem-P_{50} is the xylem water pressure when the xylem loses 50% of its conductivity. Xylem-P_{50} is one metric of xylem cavitation that allows for a direct comparison between species (Meinzer *et al*., 2009).

Prior to this study it was not known how strongly the observed variation in tropical tree hydraulic traits (Baltzer *et al*., 2008; Anderegg *et al*., 2014) correlated with functional diversity associated with both succession and drought tolerance. Therefore, the field campaign was designed to test if a successional axis of competition among tropical trees is the same as or orthogonal to a drought-tolerance axis of competition. By extension, the quantitative results from this study were used to test the validity of the current PFT representation of tropical trees in the ED2 model (as well as terrestrial biosphere models in general—e.g. those in Chapter 2), which includes only three PFTs that operate along a successional axis of competition, versus the need to include additional PFTs that operate along a drought tolerance axis.

Model parameterization

Chapter 4 tests three alternative soil water-stress formulations within the structure of the ED2 model: (1) the original ED2 formulation that accounts for both soil moisture supply and atmospheric demand for plant water, (2) a more simplistic single-resistor formulation that is only a function of soil moisture supply and is typical of many terrestrial biosphere models, and (3) a more detailed and mechanistic hydrodynamic formulation that accounts for both supply and demand as a function of leaf water potential. Formulas 2 and 3 also included additional functional diversity related to drought tolerance, where the existing PFTs were subdivided into drought tolerant and intolerant groups and were parameterized using the field experiment data. In essence, formulation 2 was designed to evaluate if increasing functional diversity alone while using a more simplistic water-stress function improves ED2 model predictions of ecosystem drought responses. Formulation 3 in contrast, evaluates if inclusion of both plant hydrodynamics and functional diversity related to drought tolerance improves ED2 predictions of the ecosystem drought responses.

In summary, this dissertation is designed to advance the science of tropical forest drought ecology. Chapter 2 is the first model inter-comparison of tropical ecosystem drought responses that tests the suitability of terrestrial biosphere models for predicting drought responses of tropical forests and identifies key areas for future research and model development. Chapter 3 aims to reveal how functional traits associated with tree water-use and transport efficiency varies with both successional type and drought tolerance. Chapter 4 is an evaluation of how both different soil water-stress formulations and representing varying levels of functional diversity in a dynamic vegetation model

(i.e. ED) affect predictions of ecosystem responses to chronic drought. Also, the analysis in Chapter 4 aims to reveal additional sources of model uncertainty, which brings the Research Framework cycle (Fig 1.1) full circle so that the next set of field experiments are informed by both model and theoretical uncertainty.

References

Anderegg WRL (2014) Spatial and temporal variation in plant hydraulic traits and their relevance for climate change impacts on vegetation. *New Phytologist*, 205, 1008-1014. doi: 10.1111/nph.12907.

Baker PA, Seltzer GO, Fritz SC, Dunbar RB, Grove MJ, Tapia PM, Cross SL, Rowe HD, Broda JP (2001) The history of South American tropical precipitation for the past 25,000 years. *Science* 291, 640-643. doi: 10.1126/science.291.5504.640

Baker TR, Phillips OL, Malhi Y, et al. (2004) Variation in wood density determines spatial patterns in Amazonian forest biomass. *Global Change Biology*, 10, 545–562, doi: 10.1111/j.1529-8817.2003.00751.x.

Baker IT, Prihodko L, Denning AS, Goulden M, Miller S, da Rocha HR (2008) Seasonal drought stress in the Amazon: Reconciling models and observations. *Journal of Geophysical Research* 113, G00B01. doi: 10.1029/2007JG000644

Baltzer JL, Davies SJ, Bunyavejchewin S, Noor NSM (2008) The role of desiccation tolerance in determining tree species distributions along the Malay–Thai Peninsula *Functional Ecology*, 22, 221–231 doi: 10.1111/j.1365-2435.2007.01374.x

Bonan GB (2008) Forests and climate change: Forcings, feedbacks, and the climate benefits of forests. *Science*, 320, 1444. doi: 10.1126/science.1155121.

Brando PM, Nepstad DC, Davidson EA, Trumbore SE, Ray D, Camargo P (2008) Drought effects on litterfall, wood production and belowground carbon cycling in an Amazon forest: results of a throughfall reduction experiment. *Philosophical Transactions of the Royal. Society B*, 363, 1839–1848. doi:10.1098/rstb.2007.0031

Breshears DD, Myers OB, Meyer CW, Barnes FJ, Zou CB, Allen CD, McDowell NG, Pockman WT (2009) Tree die-off in response to global change-type drought: mortality insights from a decade of plant water-potential measurements. *Frontiers in Ecology and the Environment*, 7. doi: 10.1890/080016.

Brodribb TJ, Holbrook NM (2003) Stomatal closure during leaf dehydration, correlation with other leaf physiological traits. Plant Physiology, 132, 2166-2173.

Brodribb TJ, Holbrook NM, Edwards EJ, Gutiérrez MV (2003) Relations between stomatal closure, leaf turgor and xylem vulnerability in eight tropical dry forest trees. *Plant, Cell and Environment*, 26, 443-450.

Bush MB, Miller MC, De Oliveira PE, Colinvaux PA (2002) Orbital-forcing signal in sediments of two Amazonian lakes. *Journal of Paleolimnology*, 27, 341-352.

Bush MB, Silman MR, Urrego DH (2004) 48,000 years of climate and forest change in a biodiversity hot spot. *Science*, 303, 827-829.

Campanello PI, Gatti MG, Goldstein G (2008) Coordination between water-transport efficiency and photosynthetic capacity in canopy tree species at different growth irradiances. *Tree Physiology*, 28, 85-94.

Castanho ADA, Coe MT, Costa MH, Malhi Y, Galbraith D, Quesada CA (2013) Improving simulated Amazon forest biomass and productivity by including spatial variation in biophysical parameters. *Biogeosciences*, 10, 2255-2272. doi: 10.5194/bg-10-2255-2013.

Čermák J, Kucera J, Bauerle WL, Phillips N, Hinckley TM (2007) Tree water storage and its diurnal dynamics related to sap flow and changes in stem volume in old-growth Douglas-fir trees. *Tree Physiology*, 27, 181-198. doi:10.1093/treephys/27.2.181.

Clark DB, Mercado LM, Sitch S, *et al.* (2011) The Joint UK Land Environment Simulator (JULES), model description—Part 2: carbon fluxes and vegetation dynamics. *Geoscientific Model Development* 4: 701-722. doi:10.5194/gmd-4-701-2011

Colinvaux PA, De Oliveira PE (2001) Amazon plant diversity and climate through the Cenozoic. *Palaeogeography, Palaeoclimatology, Palaeoecology*, 166, 51-63.

Cox PM (2001) Description of the TRIFFID Dynamic Global Vegetation Model. Hadley Centre Technical Note 24, Hadley Centre, Met Office, Bracknell, UK.

Cox PM, Betts RA, Jones CD, Spall SA, Totterdell IJ (2000) Acceleration of global warming due to carbon-cycle feedbacks in a coupled climate model. *Nature*, 408, 184-187.

da Costa ACL, Galbraith D, Almeida S, *et al.* (2010) Effect of 7 yr of experimental drought on vegetation dynamics and biomass storage of an eastern Amazonian rainforest. *New Phytologist* 187: 579–591. doi: 10.1111/j.1469-8137.2010.03309.x

Dirzo R, Raven PH (2003) Global state of biodiversity and loss. *Annual Review of Environment and Resources*, 28, 137–67. doi: 10.1146/annurev.energy.28.050302.105532

Engelbrecht BMJ, Comita LS, Condit R, Kursar TA, Tyree MT, Turner BL, Hubbell SP (2007) Drought sensitivity shapes species distribution patterns in tropical forests. *Nature*, 44, 80-83.

Farquhar GD, von Caemmerer S, Berry JA (1980) A biochemical model of photosynthetic CO_2 assimilation in leaves of C_3 species. *Planta*, 149, 78-90.

Field CB, Behrenfeld MJ, Randerson JT, Falkowski P (1998) Primary production of the biosphere: Integrating terrestrial and oceanic components. *Science*, 281, 237-240. doi: 10.1126/science.281.5374.237.

Fisher RA, Williams M, do Vale RL, da Costa AL, Meir P (2006) Evidence from Amazonian forests is consistent with isohydric control of leaf water potential. *Plant, Cell and Environment*, 29, 151–165.

Fisher RA, Williams M, da Costa AL, Malhi Y, da Costa RF, Almeida S, Meir P (2007) The response of an Eastern Amazonian rain forest to drought stress: results and modelling analyses from a throughfall exclusion experiment. *Global Change Biology*, 13, 2361–2378. doi: 10.1111/j.1365-2486.2007.01417.x.

Foley JA, Prentice IC, Ramankutty N, Levis S, Pollard D, Sitch S, Haxeltine A (1996) An integrated biosphere model of land surface processes, terrestrial carbon balance, and vegetation dynamics. *Global Biogeochemical Cycles* 10: 603–628.

Fonti P, von Arx G, García-González I, Eilmann B, Sass-Klaassen U, Gärtner H, Eckstein (2010) Studying global change through investigation of the plastic responses of xylem anatomy in tree rings. *New Phytologist*, 185, 42-53. doi: 10.1111/j.1469-8137.2009.03030.x.

Fyllas NM, Patiño S, Baker TR, *et al.* (2009) Basin-wide variations in foliar properties of Amazonian forests: phylogeny, soils and climate. *Biogeosciences*, 6, 2677-2708.

Haffer J (1969) Speciation in Amazonian forest birds. *Science*, 165, 131-137.

Haffer J, Prance GT (2001) Climate forcings of evolution in Amazonia during the Cenozoic: on the refuge theory of biotic differentiation. *Amazoniana*, 16, 579-607.

Huete AR, Didan K, Shimabukuro YE, *et al*. (2006) Amazon rainforests green-up with sunlight in dry season. *Geophysical Research Letters*, 33, L06405.doi: 10.1029/2005GL025583.

Huntingford C, Fisher RA, Mercado L, Booth BBB, Sitch S, Harris PP, Cox PM, Jones CD, Betts RA, Malhi Y, Harris GR, Collins M, Moorcroft P (2008) Towards quantifying uncertainty in predictions of Amazon 'dieback'. *Philosophical Transactions of the Royal Society, B*, 363, 1857-1864. doi: 10.1098/rstb.2007.0028

Huntingford C, Zelazowski P, Galbraith D, et al. (2013) Simulated resilience of tropical rainforests to CO_2-induced climate change. *Nature Geoscience*, 6, 268-273. doi: 10.1038/ngeo1741.

Hutyra LR, Munger W, Saleska SR *et al*. (2007) Seasonal controls on the exchange of carbon and water in an Amazonian rain forest . *Journal of Geophysical Research*, 112, G03008. doi:10.1029/2006JG000365.

IPCC (2014) *Climate Change 2014: Synthesis Report.* Contribution of Working Groups I, II and III to the Fifth Assessment Report of the Intergovernmental Panel on Climate Change [Core Writing Team, R.K. Pachauri and L.A. Meyer (eds.)]. IPCC, Geneva, Switzerland, 151 pp.

Jones PD, Briffa KR, Osborn TJ et al., (2009) High resolution palaeoclimatology of the last millennium: a review of current status and future prospects. *The Holocene*, 19, 3-49.

Kastner TP, Goñi MA (2003) Constancy in the vegetation of the Amazon Basin during the late Pleistocene: Evidence from the organic matter composition of the Amazon deep sea fan sediments. *Geology*, 31, 291-294.

Keenan TF, Hollinger DY, Bohrer G, Dragoni D, Munger JW, Schmid HP, Richardson AD (2013) Increase in forest water-use efficiency as atmospheric carbon dioxide concentrations rise. *Nature*, 499, 324-327. doi:10.1038/nature12291.

Kumagai T, Aoki S, Otsuki K, Utsumi Y (2009) Impact of stem water storage on diurnal estimates of whole-tree transpiration and canopy conductance from sap flow measurements in Japanese cedar and Japanese cypress trees. *Hydrological Processes*, 23, 2335-2344. doi: 10.1002/hyp.7338.

Lambers H, Chapin FS III, Pons TL (2008) *Plant Physiological Ecology,* 2nd Edn. Springer, New York. 610 pp.

Malhado ACM, Malhi Y, Whittaker RJ, *et al*. (2009) Spatial trends in leaf size of Amazonian rainforest trees. *Biogeosciences*, 6, 1563-1576.

Malhi Y, Aragão, Galbraith D, Huntingford C, Fisher R, Zelazowski P, Sitch S, McSweeney C, Meir P (2009) Exploring the likelihood and mechanism of a climate-change-induced dieback of the Amazon rainforest. *Proceedings of the National Academy of Sciences*, 106, 20610–20615. doi: 10.1073/pnas.0804619106.

Malhi Y, Roberts JT, Betts RA, Killeen TJ, Li W, Nobre CA (2008) Climate change, deforestation, and the fate of the Amazon. *Science,* 319, 169. doi: 10.1126/science.1146961

Markesteijn L, Poorter L (2009) Seedling root morphology and biomass allocation of 62 tropical tree species in relation to drought- and shade-tolerance. *Journal of Ecology*, 97, 311–325. doi: 10.1111/j.1365-2745.2008.01466.x.

Mayle FE, Beerling DJ, Gosling WD, Bush MB (2004) Responses of Amazonian ecosystems to climatic and atmospheric carbon dioxide changes since the last glacial maximum. *Philosophical Transactions of the Royal Society of London B*, 359, 499-514. doi: 10.1098/rstb.2003.1434

McDowell N, Pockman WT, Allen CD, Breshears DD, Cobb N, Kolb T, Plaut J, Sperry J, West A, Williams DG, Yepez EA (2008) Mechansims of plant survival and mortality during drought: why do some plants survive while other succumb to drought? *New Phytologist*, 178, 719-739. doi: 10.1111/j.1469-8137.2008.02436.x.

Medlyn BE, Zaehle S, De Kauwe MG, *et al*. (2015) Using ecosystem experiments to improve vegetation models. *Nature Climate Change*, 5, 528-534. doi:10:1038/nclimate2621.

Medvigy D, Wofsy SC, Munger JW, Hollinger DY, Moorcroft PR (2009), Mechanistic scaling of ecosystem function and dynamics in space and time: Ecosystem Demography model version 2. *Journal of Geophysical Research*, 114, G01002, doi:10.1029/2008JG000812.

Meinzer FC, Campanello PI, Domec JC, Gatti MG, Goldstein G, Villalobos-Vega R, Woodruff DR (2008) Constraints on physiological function associated with branch architecture and wood density in tropical forest trees. *Tree Physiology*, 28, 1609-1617.

Meinzer FC, Johnson DM, Lachenbruch B, McCulloh KA, Woodruff DR (2009) Xylem hydraulic safety margins in woody plants: coordination of stomatal control of xylem tension with hydraulic capacitance. *Functional Ecology*, 23, 922-930. doi: 10.1111/j.1365-2435.2009.01577.x

Metcalfe DB, Meir P, Aragão LEOC, *et al*. (2008) The effects of water availability on root growth and morphology in an Amazon rainforest. *Plant Soil*, 311, 189–199. doi: 10.1007/s11104-008-9670-9.

Monnin E, Indermühle A, Dällenbach A, Flückiger J, Stauffer B, Stocker TF, Raynaud D, Barnola J-M (2001) Atmospheric CO_2 concentrations over the last glacial termination. *Science*, 291, 112-114. doi: 10.1126/science.291.5501.112.

Moorcroft PR, Hurtt GC, Pacala SW (2001) A method for scaling vegetation dynamics: The Ecosystem Demography model (ED). *Ecological Monographs,* 71, 557-587.

Nemani R, Keeling C, Hashimoto H *et al*. (2003) Climate-driven increases in global terrestrial net primary production from 1982 to 1999. *Science* 300, 1560-1563.

Nepstad DC, Moutinho P, Dias-Filho MB, *et al*. (2002) The effects of partial throughfall exclusion on canopy processes, aboveground production, and biogeochemistry of an Amazon forest. *Journal of Geophysical Research*, 107(D20), 8085. doi:10.1029/2001JD000360.

Nepstad DC, Tohver IM, Ray D, Moutinho, Cardinot G (2007) Mortality of large trees and lianas following experimental drought in an Amazon forest. *Ecology*, 88, 2259-2269.

Oleson KW, Niu G-Y, Yang Z-L, *et al*. (2008) Improvements to the Community Land Model and their impact on the hydrological cycle. *Journal of Geophysical Research* 113: G01021. doi:10.1029/2007JG000563.

Pineda-García F, Paz H, Meinzer FC (2013) Drought resistance in early and late secondary successional species from a tropical dry forest: the interplay between xylem resistance to embolism, sapwood water storage and leaf shedding. *Plant Cell and Environment*, 36, 405-418. doi: 10.1111/j.1365-3040.2012.02582.x

Sakaguchi K, Zeng X, Christoffersen BJ, Restrepo-Coupe N, Saleska SR, Brando PM (2011) Natural and drought scenarios in an east central Amazon forest: Fidelity of the Community Land Model 3.5 with three biogeochemical models. *Journal of Geophysical Research*, 116, G01029. doi:10.1029/2010JG001477.

Saleska SR, Miller SD, Matross DM *et al.* (2003) Carbon in Amazon Forests: Unexpected seasonal fluxes and disturbance-induced losses. *Science*, 302, 1554-1557.

Schöngart J, Junk WJ, Piedade MTF, Ayres JM, Hüttermann A, Worbes M (2004) Teleconnection between tree growth in the Amazonian floodplains and the El Niño–

Southern Oscillation effect. *Global Change Biology*, 10, 683–692, doi: 10.1111/j.1529-8817.2003.00754.x.

Schuur EAG, Chadwick OA, Matson PA (2001) Carbon cycling and soil carbon storage in mesic to wet Hawaiian montane forests. *Ecology* 82, 3182–96.

Sellers PJ, Randall DA, Collatz GJ, Berry JA, Field CB, Dazlich DA, Zhang C, Collelo GD, Bounoua L (1996) A revised land surface parameterization (SiB2) for atmospheric GCMs. Part I: Model formulation. *Journal of Climate* 9: 676-705.

Stute M, Forster M, Frischkorn H, Serejo A, Clark JF, Schlosser P, Broecker WS, Bonani G (1995) Cooling of tropical Brazil (5°C) during the Last Glacial Maximum. *Science*, 269, 379-383.

Thompson LG, Mosley-Thompson E, Davis ME, Lin P-N, Henderson KA, Cole-Dai J, Bolzan JF, Liu K-B (1995) Late glacial stage and Holocene tropical ice core records from Huascarán, Peru. *Science,* 269, 46-50.

Thompson LG, Davis ME, Mosley-Thompson E, Sowers TA, Henderson KA, Zagorodnov VS, Lin P-N, Mikhalenko VN, Campen RK, Bolzan JF, Cole-Dai J, Francou B (1998) A 25,000-year tropical climate history from Bolivian ice cores. *Science,* 282, 1858-1864. doi: 10.1126/science.282.5395.1858.

Chapter 2

Confronting model predictions of carbon fluxes with measurements of Amazon forests subjected to experimental drought

(as published in New Phytologist)

Title: Confronting model predictions of carbon fluxes with measurements of Amazon forests subjected to experimental drought.

Thomas L. Powell[1], David R. Galbraith[2,3], Bradley O. Christoffersen[4], Anna Harper[5,6], Hewlley M. A. Imbuzeiro[7], Lucy Rowland[8], Samuel Almeida[9], Paulo M. Brando[10], Antonio Carlos Lola da Costa[11], Marcos Heil Costa[7], Naomi M. Levine[1], Yadvinder Malhi[3], Scott R. Saleska[4], Eleneide Sotta[12], Mathew Williams[8], Patrick Meir[8] and Paul R. Moorcroft[1*]

Affiliations:

1. Department of Organismic and Evolutionary Biology, Harvard University, Cambridge, Massachusetts, USA
2. School of Geography, University of Leeds, Leeds, United Kingdom
3. Environmental Change Institute, School of Geography and the Environment, University of Oxford, Oxford, United Kingdom
4. Department of Ecology and Evolutionary Biology, University of Arizona, Tucson, Arizona, USA
5. College of Engineering, Mathematics, and Physical Science, University of Exeter, Exeter, United Kingdom
6. Department of Atmospheric Science, Colorado State University, Fort Collins, Colorado, USA

7. Grupo de Pesquisas em Interação Atmosfera-Biosfera, Universidade Federal de Viçosa, Minas Gerias, Brazil

8. School of GeoSciences, University of Edinburgh, Edinburgh, United Kingdom

9. Museu Paraense Emilio Goeldi, Belém, Pará, Brazil

10. Instituto de Pesquisa Ambiental da Amazônia, Brasília, Brazil

11. Centro de Geociências, Universidade Federal do Pará, Belém, Pará, Brazil

12. Embrapa Amapá, Macapá, Amapá, Brazil

*corresponding author: paul_moorcroft@harvard.edu,

ph: +1-617-496-6744

New Phytologist (2013) 200:350-364. doi: 10.1111/nph/12390

Abstract:

- Considerable uncertainty surrounds the fate of Amazon rainforests in response to climate change.

- Carbon flux predictions of five terrestrial biosphere models (CLM3.5, ED2, IBIS, JULES and SiB3) and a hydrodynamic terrestrial ecosystem model (SPA) were evaluated against measurements from two large-scale Amazon drought experiments.

- Model predictions agreed with the observed carbon fluxes in the control plots of both experiments, but poorly replicated the responses to the drought treatments. Most notably, with the exception of ED2, the models predicted negligible reductions in aboveground biomass in response to the drought treatments, which was in contrast to an observed ~20% reduction at both sites. For ED2, the timing of the decline in aboveground biomass was accurate, but the magnitude was too high for one site and too low for the other.

- Three key findings indicate critical areas for future research and model development. First, the models predicted declines in autotrophic respiration under prolonged drought in contrast to measured increases at one of the sites. Second, models lacking a phenological response to drought introduced bias in the sensitivity of canopy productivity and respiration to drought. Third, the phenomenological water-stress functions used by the terrestrial biosphere models to represent the effects of soil moisture on stomatal conductance yielded unrealistic diurnal and seasonal responses to drought.

Keywords: Amazon, tropical rainforest, drought, terrestrial biosphere model, carbon cycle, throughfall exclusion,

Introduction:

Changes in precipitation patterns are projected to be one of the biggest consequences for the Amazon rainforest as global climate change intensifies over this century. Predicted shifts in precipitation include: an increase in the frequency of extremely wet or dry months (Lintner *et al.,* 2012), regional increases or decreases in dry season length and intensity (Malhi *et al.,* 2008; Costa & Pires, 2010, Good *et al*., 2013, Joetzjer *et al*., 2013), and either increased precipitation or chronic drying across large regions of the basin (Cox *et al.,* 2000, Li *et al*., 2006). Although the spatial and temporal patterns of predicted shifts in precipitation vary considerably between climate models (Jupp *et al*., 2010), there is increasing consensus toward drying and longer dry seasons (Joetzjer *et al*., 2013). However, it is presently unclear how resilient forests in different regions will be to a drier climate.

Process-based terrestrial biosphere models are key tools for assessing ecosystem resilience to climate change because of their ability to mechanistically predict ecosystem responses to novel environmental conditions. However, it is unclear whether current model formulations can accurately capture the impacts of chronic drought on Amazon forest ecosystems. Several modeling studies have been conducted to evaluate the importance of different ecosystem processes and physiological mechanisms that either modify Amazon carbon fluxes or confer tolerance during periods of water-stress (e.g. Baker *et al*., 2008; Fisher *et al*., 2007, 2010; Sakaguchi *et al*., 2011). However, these studies examined the predictions of single models using different meteorological forcing data and different representations of the soil properties; therefore, it is difficult to

understand how contrasting terrestrial biosphere formulations and parameterizations affect predictions of different Amazon forests to severe water limitation. In this analysis, we performed a detailed evaluation of five terrestrial biosphere models (CLM3.5, ED2, IBIS, JULES, SiB3) and a site-specific ecosystem model (SPA) to correctly capture the effects of water-limitation on carbon fluxes of two Amazon forests. Model predictions were compared against observations from the two throughfall exclusion (TFE) drought experiments located in the Caixuanã (CAX) and Tapajós (TNF) National Forests in the eastern Brazilian Amazon (Nepstad *et al*., 2002; Fisher *et al*., 2007; Meir *et al*., 2009). All model simulations used standardized initial spin-up conditions, soil physics, and local meteorological forcings.

The TFE drought experiments are ideal for evaluating the model specific soil water-stress responses since they prevented approximately 50% of the precipitation from entering the soil without altering atmospheric conditions (Nepstad *et al.,* 2002). Moreover, the TFEs serve as useful benchmarks for vegetation models since the simulated droughts cover a broader range of drying than is currently predicted by most climate models, thus ensuring conservative parameterizations. Also, unlike greenhouse-based drought manipulations, they evaluate ecosystem-level drought responses. Although soil type and water table depth are considerably different between the two sites (see Methods), both drought experiments had similar responses involving reductions in wood production and elevated mortality of dominant trees in the treatment plots (Nepstad *et al.,* 2007; Brando *et al.,* 2008; da Costa *et al.,* 2010).

In this study, the carbon dynamics of the TNF and CAX forests were simulated under observed precipitation (0% reduction), and three drought levels, classified as

substantial (30%), severe (50%, also TFE treatment level), and catastrophic (80%) reductions in precipitation. The six models were evaluated for their ability to predict reported carbon fluxes at the control and treatment levels. The models were compared to determine the level of agreement in the timing and magnitude of the response of ecosystem carbon fluxes to different levels of drought. Finally, the various formulations associated with soil water-stress were evaluated to determine the dominant mechanisms necessary for inclusion in terrestrial ecosystem models in order to provide useful information about the fate of the Amazon rainforest under future climate change.

Methods:

Study sites:

Two throughfall exclusion experiments were initiated in the Tapajós (2.897ºS, 54.952ºW) and Caxiuanã (1.737ºS, 51.458ºW) National Forests, Pará, Brazil, in 1999 and 2001, respectively, to assess whole ecosystem responses to drought. Mean annual precipitation at TNF is 2000 mm (Nepstad *et al.,* 2002) with a wet season from December to mid-June, while at CAX mean annual precipitation is 2272 mm (Fisher *et al.,* 2007) with a wet season from December to mid-July. Except for the below-average rainfall at TNF during the 2003 wet season, precipitation rates at the two sites during the experiments were typical (Fig. S2.1) (Rosolem *et al.,* 2008). The soils at both sites are Oxisols, but they differ in texture and depth: TNF is comprised of 60% clay and 38% sand with no hardpan layers in the top 12 m and a water table > 80 m (Nepstad *et al.,* 2002). CAX is 15% clay

and 78% sand with a stony/laterite layer 3-4 m deep, and a water table at approximately 10 m during the wet season (Fisher *et al.,* 2007).

Aboveground biomass at the beginning of the TNF drought experiment—estimated for trees ≥10cm diameter at breast height using allometric equations from Chambers *et al.,* (2001)—was ~15.0 kg C m^{-2} (Nepstad *et al.,* 2002). The TNF plot had a relatively rough canopy that ranged from 18 to 40 m in height with some emergent trees reaching 55 m. Aboveground biomass (trees ≥10cm dbh) at the beginning of the CAX drought experiment—estimated using the average of 8 published allometric equations—was ~21.4 kg C m^{-2} (see Table 1 in da Costa *et al.,* 2010). The CAX canopy was comparatively smooth with a mean height of 30 m.

A brief description of the experimental designs is given in Notes S3, and described in greater detail elsewhere (Nepstad *et al.,* 2002; Fisher *et al.,* 2007). The observations against which the models are evaluated are listed in Table 2.2 and descriptions of the measurement methodologies can be found in Notes S3.

Model descriptions:

Five terrestrial biosphere models and one terrestrial ecosystem model were analyzed in this study. All the models had been parameterized prior to this study. The five biosphere models CLM3.5, ED2, IBIS, JULES, and SiB3 used existing regional or global-scale parameterizations, while the SPA model had been parameterized for the CAX site as part of an earlier study (see references Tables 1, S2.3, S2.4). The definitions of model variables and parameters are given in Table S2.2. A brief description of the model formulations relevant for understanding how the modeled ecosystem responds to drought

is described below. The terrestrial biosphere models represented the biological response to water-stress with schemes relating to atmospheric demand and soil moisture supply. The former regulates carbon assimilation and evapotranspiration through biophysical processes that linked stomatal conductance to atmospheric humidity and the surface energy budget (Farquhar *et al.,* 1980, Farquhar & Sharky 1982, Collatz *et al.,* 1991), while the latter represented responses to soil water-stress and differed across all the models.

Table 2.1. Summary of the six models in this study.

Model name	Dynamic vegetation	Hydro-dynamic	Canopy layers	Reference
CLM3.5 Community Land Model version 3.5 Dynamic Global Vegetation Model	Yes	No	2: 1 sun and 1 shade	Bonan *et al.,*, (2003), Levis *et al.,* (2004), Oleson *et al.,* (2008)
ED2 Ecosystem Demography model version 2.1 (rv76)	Yes	No	Spatially variable	Medvigy *et al.,* (2009)

Table 2.1 continued.

Model name	Dynamic vegetation	Hydro-dynamic	Canopy layers	Reference
IBIS Integrated BIosphere Simulator version 2.6.4	Yes	No	2: 1 sun and 1 shade	Foley *et al.,* (1996), Kucharik *et al.,* (2000)
JULES Joint UK Land Environment Simulator version 2.1	Yes	No	10	Best *et al.,* (2011), Clark *et al.,* (2011)
SiB3 Simple Biosphere model version 3	No	No	1	Sellers *et al.,* (1996); Baker *et al.,* (2008)
SPA Soil-Plant-Atmosphere model	No	Yes	3 layers, each with sun and shade	Williams *et al.,* (1996), Williams *et al*., (2005)

Four of the terrestrial biosphere models, CLM3.5, IBIS, JULES, and SiB3, are so-called 'big leaf' models in which the plant canopy is horizontally aggregated (see references in Table 2.1). In SiB3, the composition of the plant canopy is prescribed as a

single plant functional type (PFT) with a single canopy layer parameterized for tropical trees. In CLM3.5, IBIS and JULES, the canopy is comprised of different PFTs competing for available resources within the grid cell and the relative success of each PFT determines its fractional coverage. CLM3.5 and IBIS have two canopy layers, parameterized for sun and shade leaves, while JULES has 10 canopy layers, each with its own nitrogen content that both increased with height and was used to scale V_{cmax} (i.e. the apparent maximum photosynthetic rate). In CLM3.5, IBIS, JULES and SiB3, leaf photosynthesis declines as soil water-stress increases through cumulative distribution functions of available soil moisture (see Table S2.3 and references therein). The specific functions vary between the models, yielding differing sensitivities of the plant canopy to decreasing soil moisture.

ED2 differs from the other models by being explicitly formulated at the scale of individual plants and using a system of size and age-structured partial differential equations to dynamically track the horizontally and vertically heterogeneous ensemble of individual trees growing within a grid cell (see references in Table 2.1). In addition, ED2 has three tropical forest PFTs (defined as early-, mid- and late-successional tree species) that differ in their photosynthesis, water-use, energy exchange, carbon allocation, and mortality (see Moorcroft *et al*. (2001), Medvigy *et al.* (2009) and M. Longo (unpublished)). Reflecting its individual-based nature, ED2 also explicitly represents mortality as a process distinct from other forms of tissue turnover, with per capita mortality rates varying as function of the carbon balance of the individual plants. Soil water-stress scales the maximum photosynthetic rate through a soil moisture supply

versus transpiration demand function (Table S2.3). The demand function includes a leaf biomass term that allows for leaf drop when soil moisture becomes limiting.

The SPA model (see references in Table 2.1) is a terrestrial ecosystem model that uses a hydrodynamic formulation to mechanistically simulate changes in water potential and storage from the soil, through the stem, to leaves in each canopy layer. SPA simulated a single tropical PFT with three canopy layers, each partitioned into an average sun or shade leaf fraction. Compared to the terrestrial biosphere models, SPA's hydrodynamic formulation more mechanistically represents the genesis of plant water-stress. However, it has a much simpler formulation of carbon fluxes, assuming for example, that autotrophic respiration (R_a) was a fixed fraction of gross primary production (*GPP*) (Table S2.4). To facilitate comparison with the other models, SPA's R_a was subdivided into leaf (R_{lf}), root (R_r) and wood (R_w) respiration components by using the C:N ratios reported in Williams *et al.* (2002) to estimate the relative size of each respiring pool, with 10% of the wood pool assumed to be actively respiring.

Simulation protocol and meteorological drivers:

In order to isolate modeled biological responses to drought, the physical representation of the soil was standardized across all the models (Appendix A; Appendix B, Notes S4). The models were run off-line using site-level meteorological measurements made above the forest canopy at nearby weather stations. The TNF meteorological measurements covered 2002 to 2004 (N. Restrepo-Coupe, unpublished data) and were recycled sequentially over the eight-year simulation period from 1999 to 2006. The CAX meteorological measurements covered the entire 2001 to 2008 simulation period (da

Costa *et al*., 2010). Shortwave radiation was split into 68% direct and 32% diffuse and then further split into 43% visible and 57% near-IR for direct, and 52% visible and 48% near-IR for diffuse (Goudriaan, 1977).

All model simulations followed a standardized initialization, spin-up, and drought simulation protocol (Appendix A). The models were initialized with a near-bare-ground initial condition and then forced with sequentially recycled site-level meteorological drivers until aboveground biomass and soil carbon pools reached equilibrium under preindustrial atmospheric CO_2 concentrations (278 ppm). The models were then brought up to present day atmospheric CO_2 concentrations (380 ppm) following the exponential increase in CO_2 since 1750. The drought simulations were initialized from these spin-ups. The simulations were run with one baseline year followed by seven years of reduced precipitation for each site, (TNF: baseline1999, TFE 2000-2006 and CAX: baseline 2001, TFE 2002-2008). The site years were selected to coincide with the actual TFE experiments. During the experimental periods, precipitation was reduced by either 30%, 50%, or 80%. These are denoted throughout this paper as d30, d50 and d80, and with d0 identifying the control simulation. Consistent with the field experiment protocols, precipitation in the TNF simulations was reduced only during the wet season, while CAX precipitation was reduced all year, and the other meteorological variables (e.g. humidity) were not manipulated.

Data Analysis and Presentation:

The most detailed carbon accounting for either experiment is reported for the fourth year (2005) at CAX (see Table 2 of Metcalfe *et al.,* 2010b), and so modeled ecosystem (R_e)

and component respiratory (R) fluxes were evaluated against these reported values. Similar data was not available for TNF; however, soil respiration (R_s) (Davidson *et al*., 2008) and net ecosystem production (*NEP*), *GPP* and R_e from a neighboring flux tower site (Hutyra *et al.,* 2007) were available for the fourth (2003) year.

In the plots, the effect of drought on carbon fluxes is presented as the change (Δ) in magnitude with respect to the control (d0) simulation with negative Δ values indicating reductions in flux caused by drought. The ensemble median values of the model simulations were calculated rather than mean values so as not to over-weight individual model outliers. In the time series plots, 95% confidence intervals (CI) are shown for the ensemble means of the models and are a measure of model agreement about the associated flux. The 95% CI is not, however, a measure of whether or not the process is represented correctly; the latter is evaluated through the data-model comparison. Observations are given as within plot means with 95% CIs indicating spatial variability. Errors were propagated by summing in quadrature absolute errors for addition and subtraction and relative errors for products and quotients (Taylor, 1997), assuming that reported observation errors were independent and random.

Table 2.2 List of observations and associated references.

Definition	**Symbol**	**Units**	**Site and source**
Aboveground biomass	*AGB*	kg C m^{-2}	CAX: da Costa *et al*., 2010 TNF: Brando *et al*., 2008
Gross primary production of carbon	*GPP*	kg C m^{-2} yr^{-1}	TNF: Hutyra *et al*., 2007

Table 2.2 continued.

Definition	Symbol	Units	Site and source
Litter production		kg C m^{-2} yr^{-1}	TNF: Brando *et al*., 2008
Net ecosystem production of carbon	*NEP*	kg C m^{-2} yr^{-1}	TNF: Hutyra *et al*., 2007
Net primary production of carbon in wood	NPP_w	kg C m^{-2} yr^{-1}	CAX: da Costa *et al*., 2010 TNF: Brando *et al*., 2008
Autotrophic respiration	R_a	kg C m^{-2} yr^{-1}	CAX: Metcalfe *et al*., 2010b
Whole ecosystems respiration	R_e	kg C m^{-2} yr^{-1}	CAX: Metcalfe *et al*., 2010b TNF: Hutyra *et al*., 2007
Heterotrophic respiration	R_h	kg C m^{-2} yr^{-1}	CAX: Metcalfe *et al*., 2010b
Leaf respiration	R_{lf}	kg C m^{-2} yr^{-1}	CAX: Metcalfe *et al*., 2010a,b
Root respiration	R_r	kg C m^{-2} yr^{-1}	CAX: Metcalfe *et al*., 2010
Soil respiration	R_s	kg C m^{-2} yr^{-1}	CAX: Sotta *et* al., 2007, Metcalfe *et al*., 2010b, TNF: Davidson *et al*., 2008
Wood respiration	R_w	kg C m^{-2} yr^{-1}	CAX: Metcalfe *et al*., 2010b

Results:

Since this analysis is principally concerned with agreement between the predictions of the individual models and the observations at the two drought experiments, model ensemble median and mean predictions with 95% CIs are shown, but are not emphasized. The

overall ecosystem responses predicted by the models in response to the two drought treatments are summarized in Figure 2.1, which shows the dynamics of aboveground biomass (*AGB*) (see also Table S2.1). As indicated by the *AGB* dynamics of the control (d0) simulations, the CLM3.5, ED2, IBIS and JULES terrestrial biosphere models predicted equilibrium *AGB* values similar to the observed value of 14.2 kg C m^2 at TNF (Fig. 2.1a). At CAX, the terrestrial biosphere models had comparatively higher *AGB* predictions, yet all were lower than an observed value of 21.4 kg C m^2 (Fig. 2.1b). SiB3 did not track *AGB*. In contrast, the SPA ecosystem model prediction for the CAX control plot was close to observed value, but at TNF it was more than double the observed value.

The models exhibited divergent predictions of *AGB* under increasing drought treatment levels (Figs. 2.1c,d, S2.2a,b, Table S2.1). The observed reductions in *AGB* at the treatment (d50) level at TNF and CAX were -3.2 kg C m^2 and -3.8 kg C m^2; however, CLM3.5, IBIS, JULES and SPA all exhibited little or no response at either site (Fig. 2.1c,d, Table S2.1). In contrast, ED2 predicted a marked reduction in *AGB* at TNF (-5.4 kg C m^2), and a small reduction at CAX (-1.4 kg C m^2). Although, the magnitude of ED2's predicted decrease in *AGB* at TNF was too large, the timing of its predicted decrease in the third year of the drought treatment agreed with the observations. At the d80 treatment level, both CLM3.5 and ED2 predicted almost a complete loss of *AGB*, while IBIS, JULES and SPA still predicted only marginal losses in *AGB* by the end of the experiment (Fig. S2.2a,b).

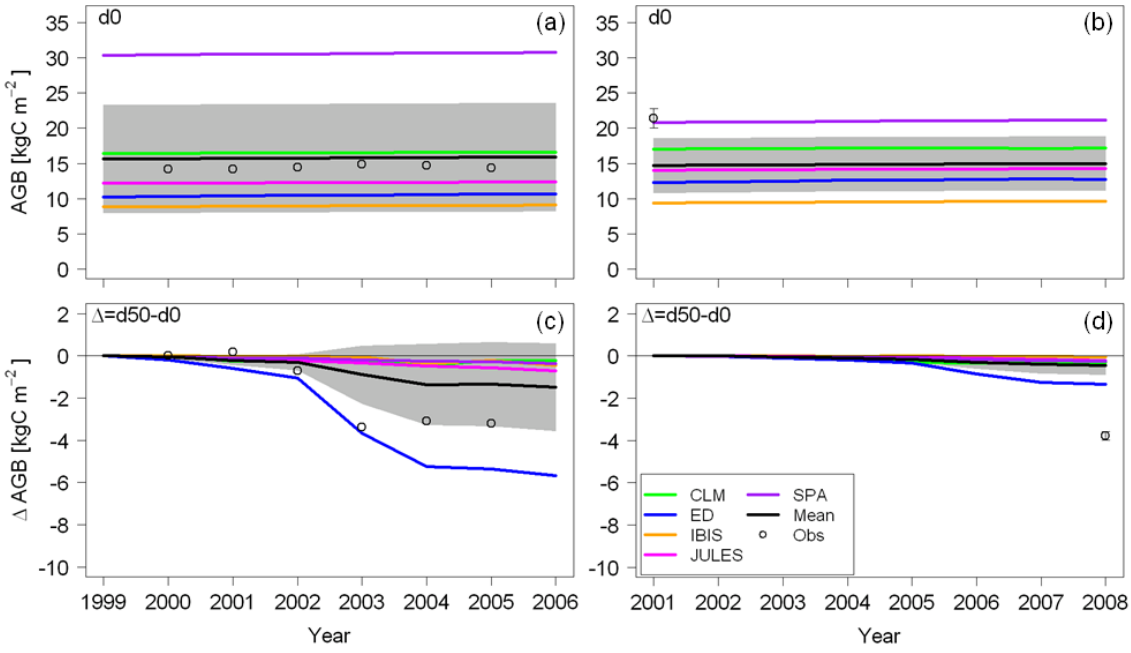

Figure 2.1. Annual aboveground biomass (*AGB*, kg C m^{-2}) predicted for Tapajós (TNF, left side) and Caxiuanã (CAX, right side) National Forests. Colored lines are individual model predictions and black line is the 5 model ensemble mean. Shaded area is the 95% CI of the models. Open symbols are published observations (Mean ± 95% CI (when reported), TNF: Brando *et al.,* 2008, CAX: da Costa *et al.,* 2010). d0 and d50 are drought levels indicating a 0% and 50% reduction in precipitation. The *Δ* plots (c, d) show the amount the control (a, b) *AGB* was altered by the 50% drought treatment.

Net Ecosystem Productivity and its Constituents:

Individual model predictions of control plot *NEP* ranged between a small carbon source and a moderately strong carbon sink at both sites (Fig. 2.2a,c, Table S2.1). JULES and SiB3 simulations of *NEP* agreed with the flux tower measurements at TNF in year four (-0.09 ± 0.05 kg C m^{-2} yr^{-1}), predicting the control plot to be a weak carbon source (Fig. 2.2a, Table S2.1). On the other hand, CLM3.5, ED2, IBIS, and SPA predicted TNF control plot *NEP* to be a carbon sink (Fig. 2.2a, Table S2.1).. At CAX, CLM3.5 predicted the control plot *NEP* to be a weak carbon source, while ED2, IBIS, JULES, SiB3 and SPA predicted a carbon sink (Fig. 2.2c, Table S2.1).

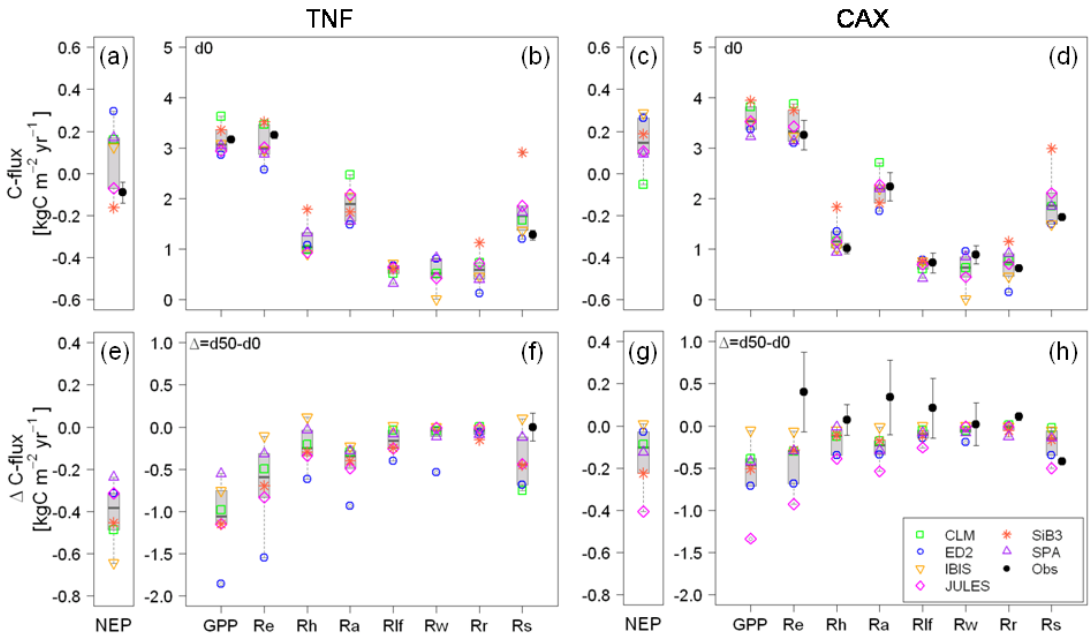

Figure 2.2. Net and component ecosystem carbon fluxes (kg C m^{-2} yr^{-1}) in the fourth year of the experiment for TNF (left side) and CAX (right side). Carbon flux definitions and observation sources are given in Table 2.2. Colored symbols are model predictions and black symbols are observations (mean ± 95% CI). d0 and d50 are drought levels indicating a 0% and 50% reduction in precipitation. The Δ indicates the amount the control (d0) fluxes were altered by the 50% drought treatment.

At both sites, model predictions of *GPP* and component *R* fluxes in the control plots generally agreed well with the available measurements (Fig. 2.2b,d, Table S2.1). All models except SiB3 correctly predicted that autotrophic respiration (R_a) should exceed heterotrophic respiration (R_h) as observed at CAX.

When precipitation was reduced by 50%, all models, except IBIS at CAX, predicted considerable reductions in *NEP* at both sites (Fig. 2.2e,g, Table S2.1). Although measurements of overall *NEP* were unavailable for comparison, model predictions of the annual component *R* fluxes compared poorly with observations from CAX (Fig. 2.2h, Table S2.1). The response of individual model predictions of annual R_e and its components to d50 ranged from neutral to negative, while the observed responses

were neutral to positive. Almost the entire mismatch between observed R_e and model predictions arose from the disagreement within the components of R_a, in particular R_{lf} (Fig. 2.2h, Table S2.1). For comparative purposes, the TNF component R fluxes for the fourth year are also provided in Figure 2.2f and Table S2.1 despite absence of validation data at this site. The patterns and magnitudes of the model predictions for TNF (Fig. 2.2f) were generally similar to those at CAX except for ED2 whose predictions changed substantially, reflecting the predicted reduction in *AGB* at this site (Fig. 2.1c, Table S2.1).

Soil Respiration:

A direct comparison in the magnitude of observed and modeled R_s was only possible for CAX because the meteorological drivers for the simulations were concurrent with the R_s measurements between November 2001 and 2003 (Fig. S2.3). In the control plot, predictions of R_s by CLM3.5, IBIS, and SPA were consistently in agreement with the magnitude and seasonality of the observations, while the magnitude of JULES and seasonal dynamics of ED2 and SiB3 exceeded the observations (Fig. S2.3a). At the treatment level, however, there was good agreement between model predictions and measurements of the R_s response to d50 only during the wet season, but not the dry season (Fig. S2.3b).

The sensitivity of R_s to θ_s in the observations was significantly different at the two sites, where a dependency was only observed at CAX (Fig. 2.3). Accordingly, the absence of a θ_s dependency in the IBIS and SPA formulas were more realistic at TNF (Fig. 2.3a); while the approximately parabolic relationship between R_s versus θ_s found in JULES was more realistic for CAX, but incorrectly parameterized to match the

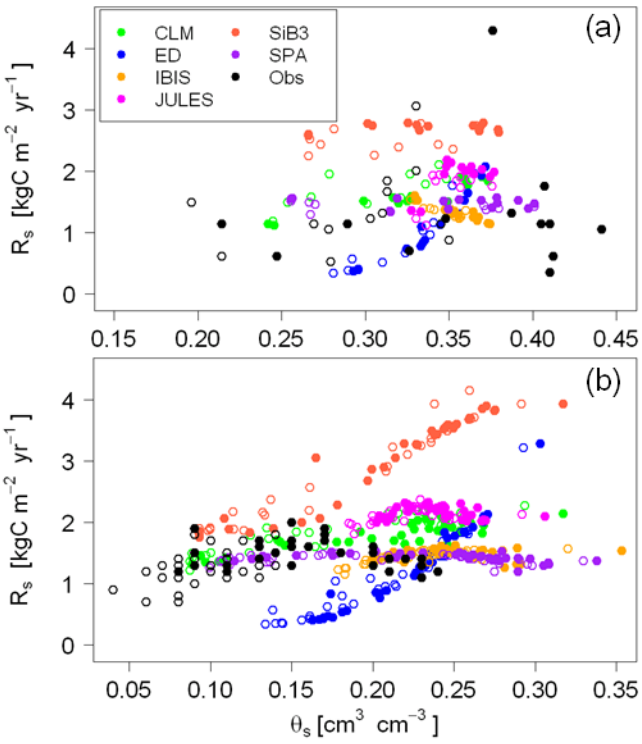

Figure 2.3. Periodic measurements of soil respiration (R_s, mean± 95%CI, kg C m^{-2} yr^{-1}, black symbols) as a function of volumetric soil water content (θ_s, cm^3 cm^{-3}) for (a) TNF (Davidson *et al.,* 2008) and (b) CAX (Sotta *et al.,* 2007). Concurrent R_s predictions are given for each model (colored symbols). Closed symbols are for the control plots (d0), open symbols are for the treatment plots (d50).

observations (Fig. 2.3b). Predictions of R_s by ED2 and SiB3 were excessively sensitive to soil moisture, but in contrasting directions relative to the observations. For ED2, R_s declined well below the observations at low θ_s, but rapidly exceeded them at high θ_s (Fig. 2.3). Interestingly, at the annual time scale, the low R_s predictions by ED2 for the control plots were caused by relatively low R_r rather than R_h (Fig. 2.2b,d, Table S2.1). On the other hand, the parameterization of R_s in SiB3 produced fluxes equal to the observations at low θ_s, which then increased linearly to an optimal θ_s level (Fig. 2.3). Hence, SiB3's R_s was generally higher than the other models, particularly at TNF where θ_s was often

above the prescribed optimal level (~.25 m^3 m^{-3}) (Figs. 2.2b,d, 2.3, Table S2.1). Moreover, SiB3's over-estimation of R_s in both control plots (e.g. Fig. 2.2b,d) was also due to its R_r formulation. Unlike CLM3.5, ED2, IBIS, and JULES, growth respiration (R_g) is not explicitly modeled in SiB3; rather, a relatively high, non-dimensional scalar (0.5) is used in its R_r calculation to achieve plant carbon-balance closure (Table S2.4).

Net Primary Production and Litter Fluxes:

Model predictions of annual woody biomass increment (NPP_w) in the control plots of both sites were systematically higher than the observations, with the exception of JULES at TNF (Fig. 2.4a,b, Table S2.1). The model predictions of NPP_w under the drought treatment at TNF were however, realistic in the sense that the models generally captured the observed decline in NPP_w and the accompanying pattern of interannual variability (Fig. 2.4c,d). In contrast, NPP_w was poorly captured under the drought treatment at CAX, where CLM3.5, ED2 and JULES all systematically over-predicted the changes in observed NPP_w; while IBIS and SPA under-predicted the observed reductions in NPP_w in 2003, 2007 and 2008 (Fig. 2.4d, Table S2.1).

The predictions of litter fluxes for the control plots of both sites had a very large range (Fig. 2.5a,b, Table S2.1). IBIS's litterfall predictions for the TNF control plot agreed well with the observations (~0.30 kg Cm^{-2} yr^{-1}), while ED and CLM3.5 both under-predicted observations, and JULES and SPA had litter fluxes that were significantly lower and higher, respectively, than the observations. At CAX, each model's prediction of annual litterfall in the control plots was of a similar magnitude as its TNF prediction, except for a 35% lower prediction by SPA. Except for JULES, the

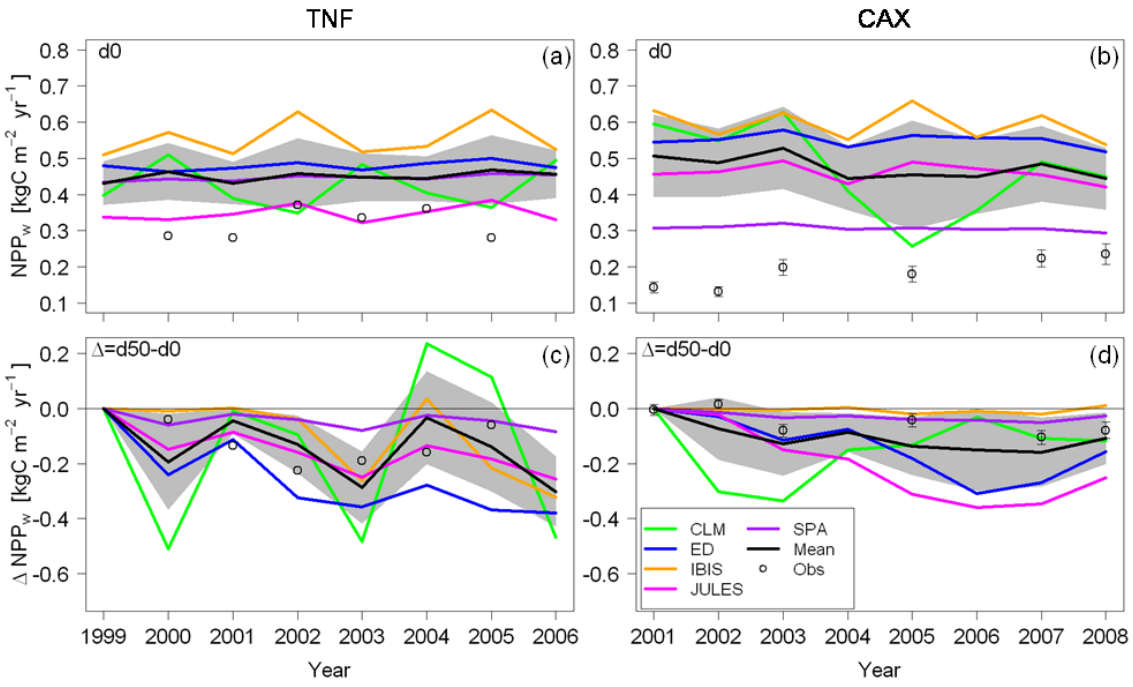

Figure 2.4. Annual NPP_w (kg C m^{-2} yr^{-1}) for TNF (left side) and CAX (right side). Colored lines are individual model predictions and black line is the 5 model ensemble mean. Shaded area is the 95% CI of the models. Open symbols are published observations (mean ± 95% CI (when reported), TNF: Brando *et al.,* 2008, CAX: da Costa *et al.,* 2010). d0 and d50 are drought levels indicating a 0% and 50% reduction in precipitation. The Δ plots (c, d) show the amount the control (a, b) NPP_w was altered by the 50% drought treatment.

models generally predicted a long-term decline in litterfall, which contrasted the initial increase and then subsequent decline found in the observations at TNF (Fig. 2.5c,d).

Leaf area index (*LAI)* predictions for the control simulations at both sites varied significantly between models (Fig. 2.6a,b). The *LAI* predictions of JULES, SIB3 and SPA were in agreement with observed *LAI* values of 6 m^2 m^{-2} measured at TNF (Fig. 2.6a). In contrast, CLM3.5 and IBIS over-predicted TNF *LAI* by 4 and 2 m^2 m^{-2}, respectively, while ED2 under-predicted it by 3 m^2 m^{-2}. The *LAI* observations for the control plot at CAX were intermediate between the ED2 prediction of 4 m^2 m^{-2} and the JULES, SIB3 and SPA predictions around 7 m^2 m^{-2} (Fig. 2.6b). In both treatment plots

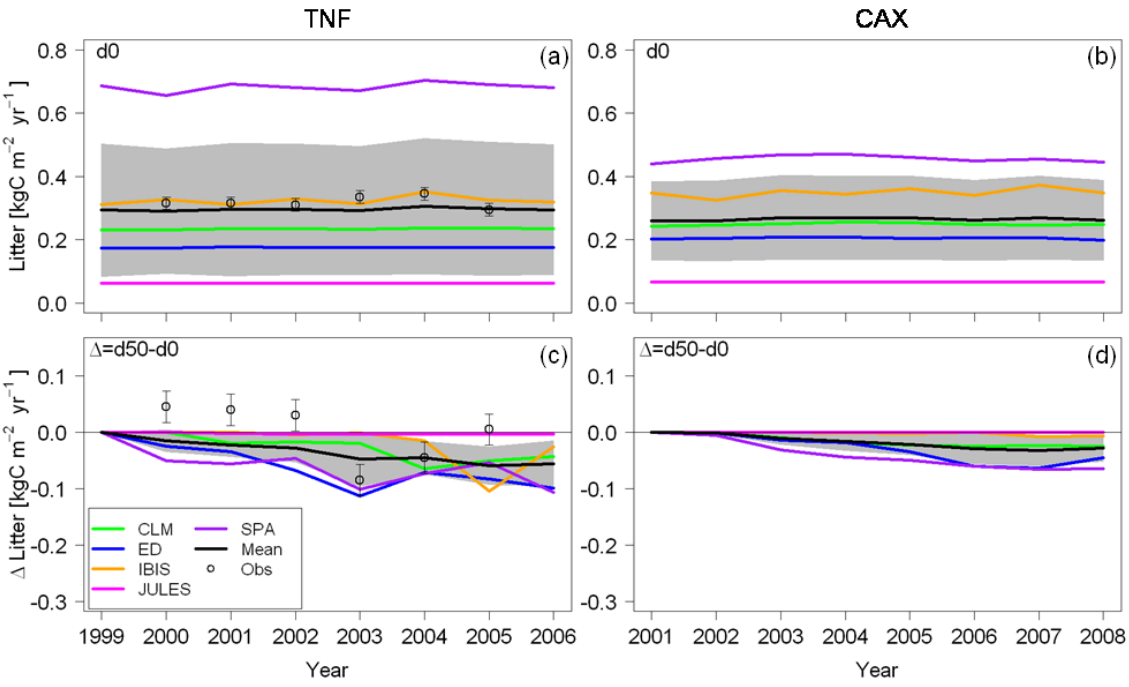

Figure 2.5. Annual litter production (kg C m^{-2} yr^{-1}) for TNF (left side) and CAX (right side). Colored lines are individual model predictions and black line is the 5 model ensemble mean. Shaded area is the 95% CI of the models. Open symbols are published observations (mean ± 95% CI, TNF: Brando *et al.,* 2008). d0 and d50 are drought levels indicating a 0% and 50% reduction in precipitation. The *Δ* plots (c, d) show the amount the control (a, b) litter production was altered by the 50% drought treatment.

there was an overall decline in *LAI* by 20 to 30% over the first four years (Fig. 2.6c,d), and at TNF, the observed seasonality of *LAI* increased markedly (Fig. 2.6c). At CAX, observed *LAI* in the treatment plot remained suppressed by ~20% in the sixth year (Metcalfe *et al*., 2010). Although, the leaf area formulations of CLM3.5, ED2, IBIS and SPA all contained soil moisture dependencies, their predictions of *LAI* displayed contrasting sensitivities to the d50 treatment (Fig. 2.6c,d). ED2 and SPA replicated the observed trends of *LAI* in the treatment plots. However, by the third year, the leaf-drop formulation in ED2 resulted in a recurring 90% loss of canopy foliage each dry season; whereas SPA predicted a 20% relative reduction in *LAI*. In CLM3.5, *LAI* declined in a

stepwise fashion that was similar in magnitude to the observations, but only half the relative reduction. IBIS predicted a 30% reduction in *LAI* in the fourth year for the TNF treatment plot (not shown, as TNF *LAI* was not measured after 2003), but no response at all in the CAX treatment plot. The leaf area formulations for JULES and SiB3 were not dependent on soil moisture, and thus *LAI* did not display a significant drought response over the seven year experimental period.

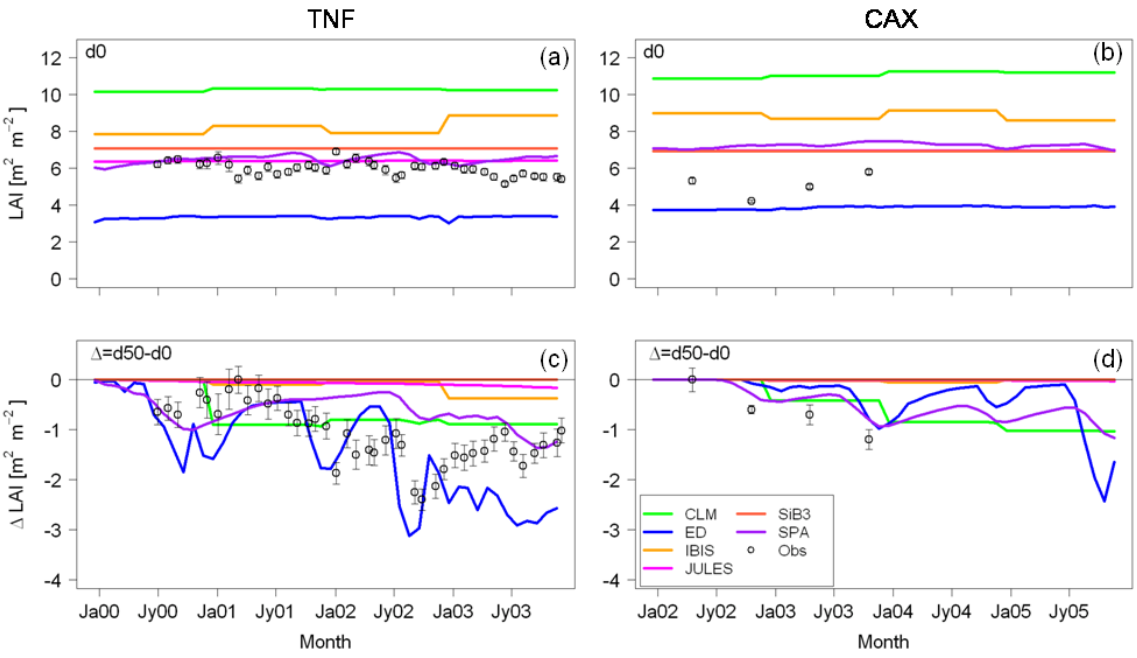

Figure 2.6. Leaf area index (*LAI*, m^2 m^{-2}) for TNF (left side) and CAX (right side) over years 1 to 4 of experiment. Colored lines are individual model predictions. Open symbols are published observations (Mean ± 95% CI, TNF: Nepstad & Moutinho, 2008; CAX: Fisher *et al*., 2007). d0 and d50 are drought levels indicating a 0% and 50% reduction in precipitation. The *Δ* plots (c, d) show the amount the control (a, b) *LAI* was altered by the 50% drought treatment.

Carbon fluxes as a Function of Drought Level:

To better understand the drought sensitivities of the models, we examined their responses to three levels of drought: 30%, 50% and 80% reductions in precipitation. The range between the six models in cumulative *NEP* after seven years was large at the control level, with SiB3 on one end predicting both sites to be carbon neutral, and ED2 on the other end predicting both sites to be strong carbon sinks (data not shown). There was also considerable disagreement between models about the interannual variation of *NEP* where the magnitudes and signs were often opposing (Fig. 2.7a,b). As drought severity increased from d30 to d80, model agreement about the magnitude and interannual variability of *ΔNEP* decreased (Figs. 2.7c-h, 2.8).

The contrasting trends in *NEP* under ambient and drought conditions reflected differences between the six models in their hypotheses about the balance between *GPP* and *R* for the two ecosystems. After seven years under the control simulation, modeled *GPP* ranged between 20.4 and 24.9 kg C m^{-2} $7yrs^{-1}$ at TNF and 22.5 and 27.4 kg C m^{-2} $7yrs^{-1}$ at CAX. CLM3.5 and SiB3 occupied the higher end of the range of *GPP* at both sites, while ED2, IBIS, JULES and SPA occupied the lower end. As drought intensity increased, there was increasing disagreement in both the cumulative magnitude (Fig. 2.8) and interannual variation (Fig. S2.4) of the model *GPP* predictions at both sites. Among the biosphere models, IBIS's predictions of *GPP* were generally the least sensitive to the increasing levels of drought at both sites, while the greatest reductions were predicted by ED2 at the d30 and d50 levels for TNF (Figs. 2.8b,f, S2.4c,e), by CLM3.5 at the d30 and d80 levels at CAX and TNF, respectively (Figs. 2.8d,j), and by JULES at the d50 and d80 levels at CAX (Figs. 2.8h,i, S2.4f,h). The reductions in *GPP* predicted by the SPA

ecosystem model under the d50 and d80 drought levels at both sites were also comparatively small (Fig. 2.8f,h,j,l).

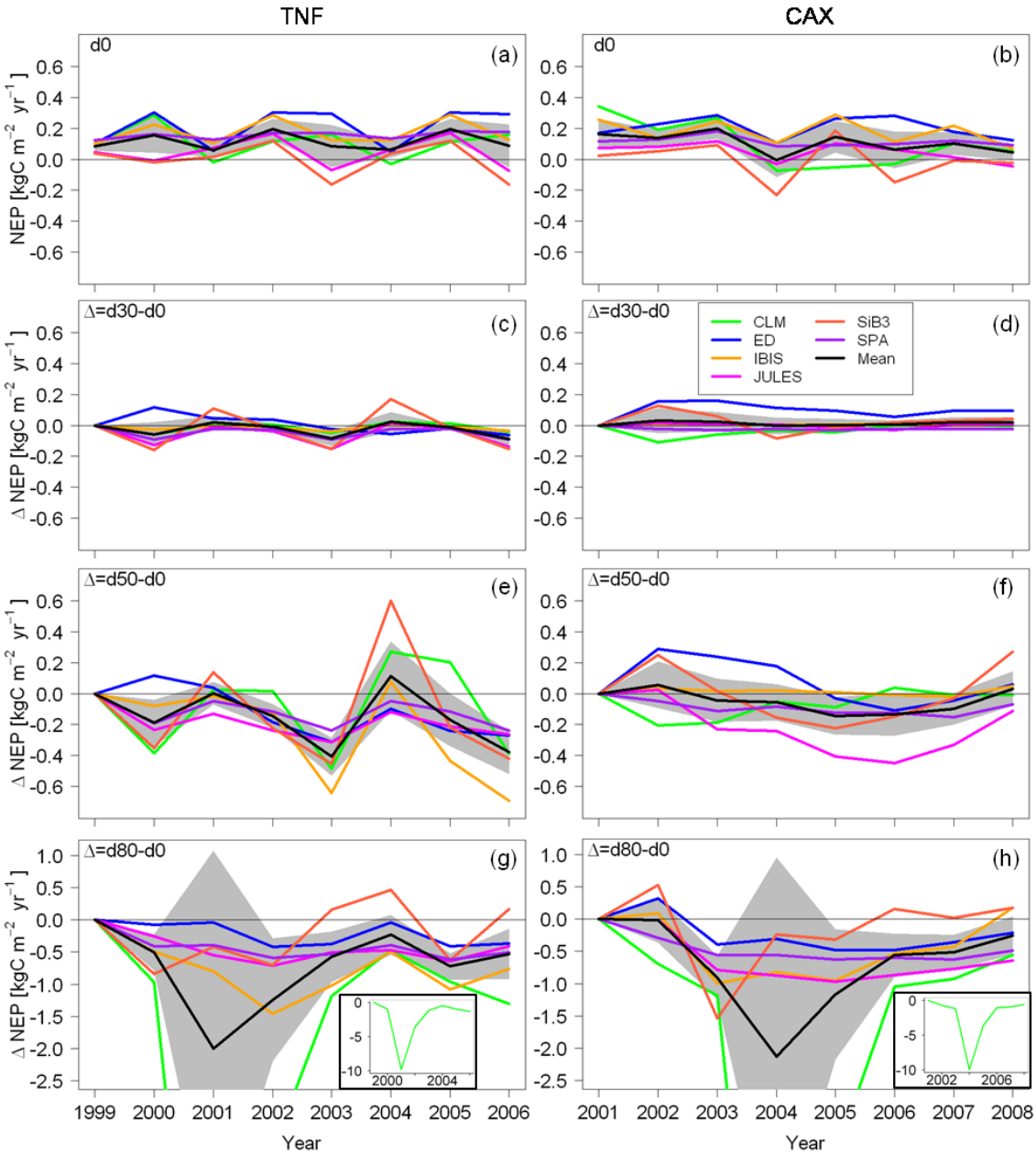

Figure 2.7. Annual net ecosystem production of carbon (*NEP*, kg C m^{-2} yr^{-1}) for TNF (left side) and CAX (right side). Colored lines are individual model predictions and black line is the 6 model ensemble mean. Shaded area is the 95% CI of the models. Drought levels are indicated by d30, d50 and d80, which are respectively 30%, 50% and 80% reductions in precipitation. The Δ indicates the amount the d0 carbon fluxes were altered by the indicated drought level. Insets in (g) and (h) show full range for CLM3.5.

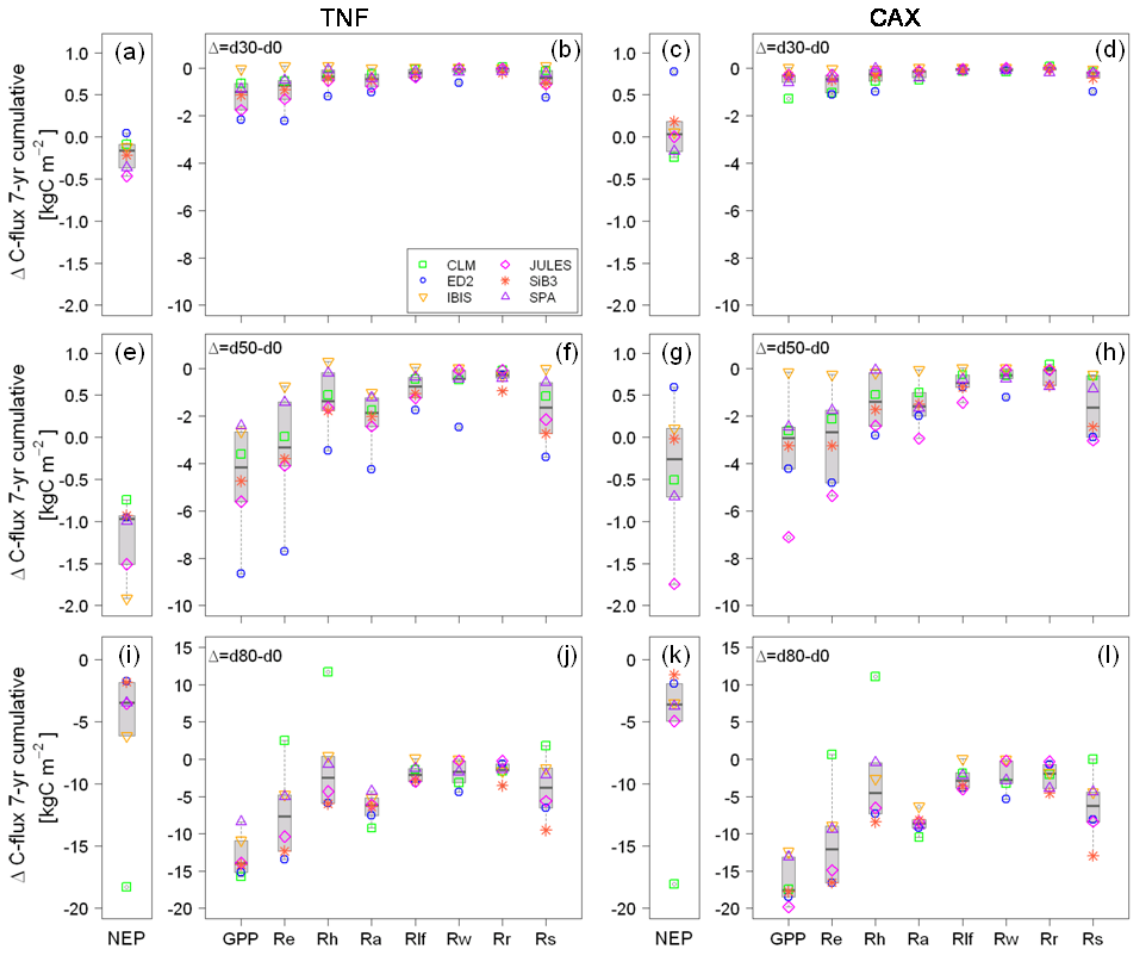

Figure 2.8. Change in the 7-yr cumulative net and component ecosystem carbon fluxes (kg C m^{-2} yr^{-1}) predicted by each model for TNF (left side) and CAX (right side). The line in the box is the median value for the models. Carbon flux definitions are given in Table 2.2. Drought levels are indicated by d30, d50 and d80, which are respectively 30%, 50% and 80% reductions in precipitation. The *Δ* indicates the amount the d0 carbon fluxes were altered by the indicated drought level.

These differences in predicted *GPP* could in part be accounted for by the contrasting formulations associated with soil water-stress. Canopy aggregated *GPP* declines under soil water deficits through a combination of two sets of mechanisms, each operating differently among all six models. The first set modifies canopy leaf area. The substantially lower predictions of *GPP* by ED2 at the d30 and d50 levels at TNF (Fig.

2.8b,f) were predominately caused by a reduction in *LAI*, first through leaf-shedding (Fig. 2.6c), then through a loss of *AGB* (Fig. 2.1a).

GPP also decreases through plant responses to atmospheric demand, i.e. vapor pressure deficit (*VPD*), and reductions in soil-water supply. In the terrestrial biosphere models, the photosynthesis routine accounts for the effects of *VPD* on stomatal conductance. The effects of supply are incorporated via a phenomenological function (β) that down-regulates stomatal conductance (g_s) and as a consequence *GPP,* with decreasing soil moisture. (Throughout this paper the symbol g_s includes β.) β varies between 0 and 1, where 1 implies stomata are only *VPD* regulated and 0 causes full stomatal closure (Fig. 2.9, Notes S1). Across all models, β increasingly trended toward 0 with increasing drought intensity and duration over the seven year simulation (Fig. S2.5). β was also generally lower at each drought level at TNF compared to CAX (Fig. S2.5). Examination of diurnal-scale variation of β revealed contrasting dynamics between the models (Fig. 2.10a-e): β had a diurnal cycle in ED2, while in CLM3.5, IBIS, JULES and SiB3 it did not (Fig 2.10a-e). In addition, β in CLM3.5 and ED2 was responsive to individual rain events (Fig. 2.10a,b,f), whereas in IBIS, JULES and SiB3 changes in β were more gradual and occurred over seasonal timescales (Fig. 2.10c-f, S2.5e-j). Finally in ED2, IBIS, and JULES, β directly scaled net photosynthesis, while in CLM3.5 and SiB3 β scaled v_{cmax} (Table S2.3), dampening the effect of β on *GPP* following rain events (Fig. 2.10a,e). In contrast to the biosphere models, in SPA stomatal function is mechanistically linked to both the supply of soil moisture and atmospheric demand through a porous medium pipe-model formulation.

Figure 2.11 shows the predicted distributions of hourly midday (11:00-14:00) g_s values at both sites that spans a six month period between the wet and dry seasons (May to November, during 2000 at TNF and during 2003 at CAX). In the control simulations at both sites, JULES had very broad distributions of g_s that peaked around 400 mmol CO_2 m^{-2} leaf s^{-1}, while the distributions of g_s in ED2 and IBIS were intermediate and peaked around 250 and 500 mmol CO_2 m^{-2} leaf s^{-1}, respectively, and the distributions of g_s in CLM3.5 and SiB3 were relatively narrow and peaked around 150 and 300 mmol CO_2 m^{-2}

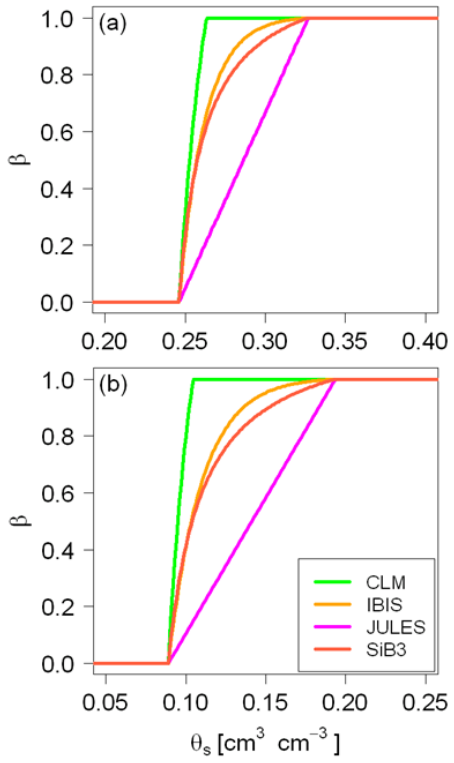

Figure 2.9. Relationships between the soil water-stress factors (β) and volumetric soil moisture (θ_s, cm^3 cm^{-3}) for CLM3.5, IBIS, JULES and SiB3 for (a) TNF and (b) CAX. The function for each model is given in Table S2.3 and the parameter values used for each model are given in Table S2.2.

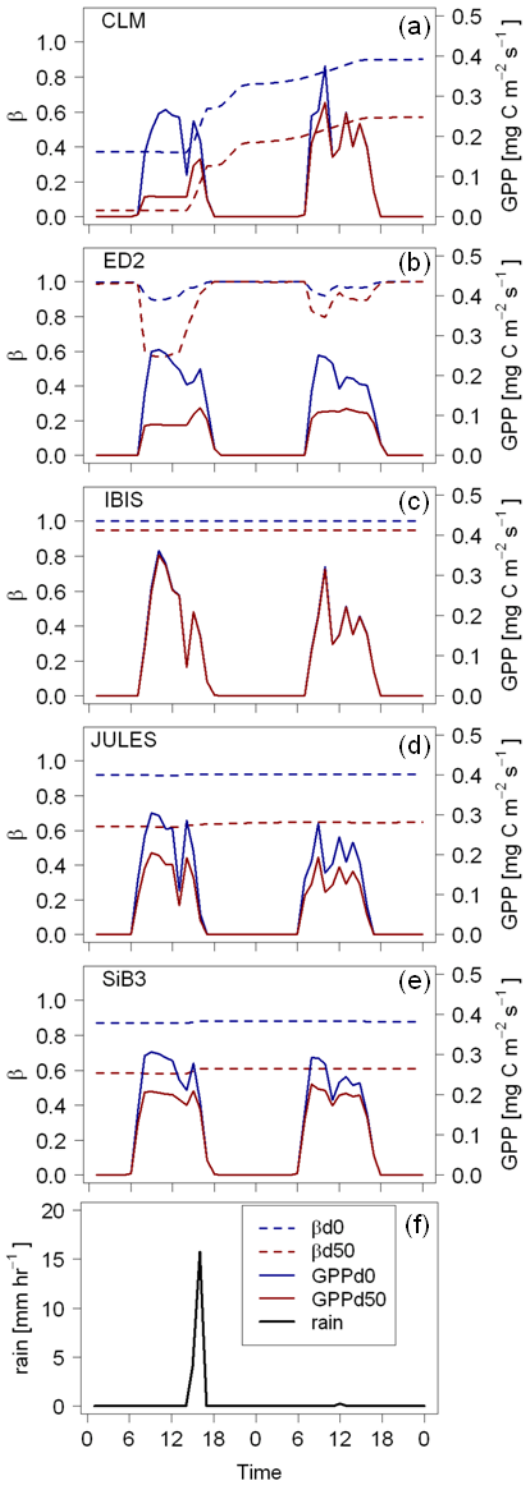

Figure 2.10. Diurnal trends of hourly ecosystem water-stress factor (β) and ecosystem gross primary production (*GPP*, mg C m^{-2} s^{-1}) at the TNF for (a) CLM3.5, (b) ED2, (c) IBIS, (d) JULES, and (e) SiB3 for two days, October 13-14, 2000. (f) Bottom panel shows a concurrent rain (mm hr^{-1}) event. d0 and d50 indicate 0% and 50% reductions in precipitation.

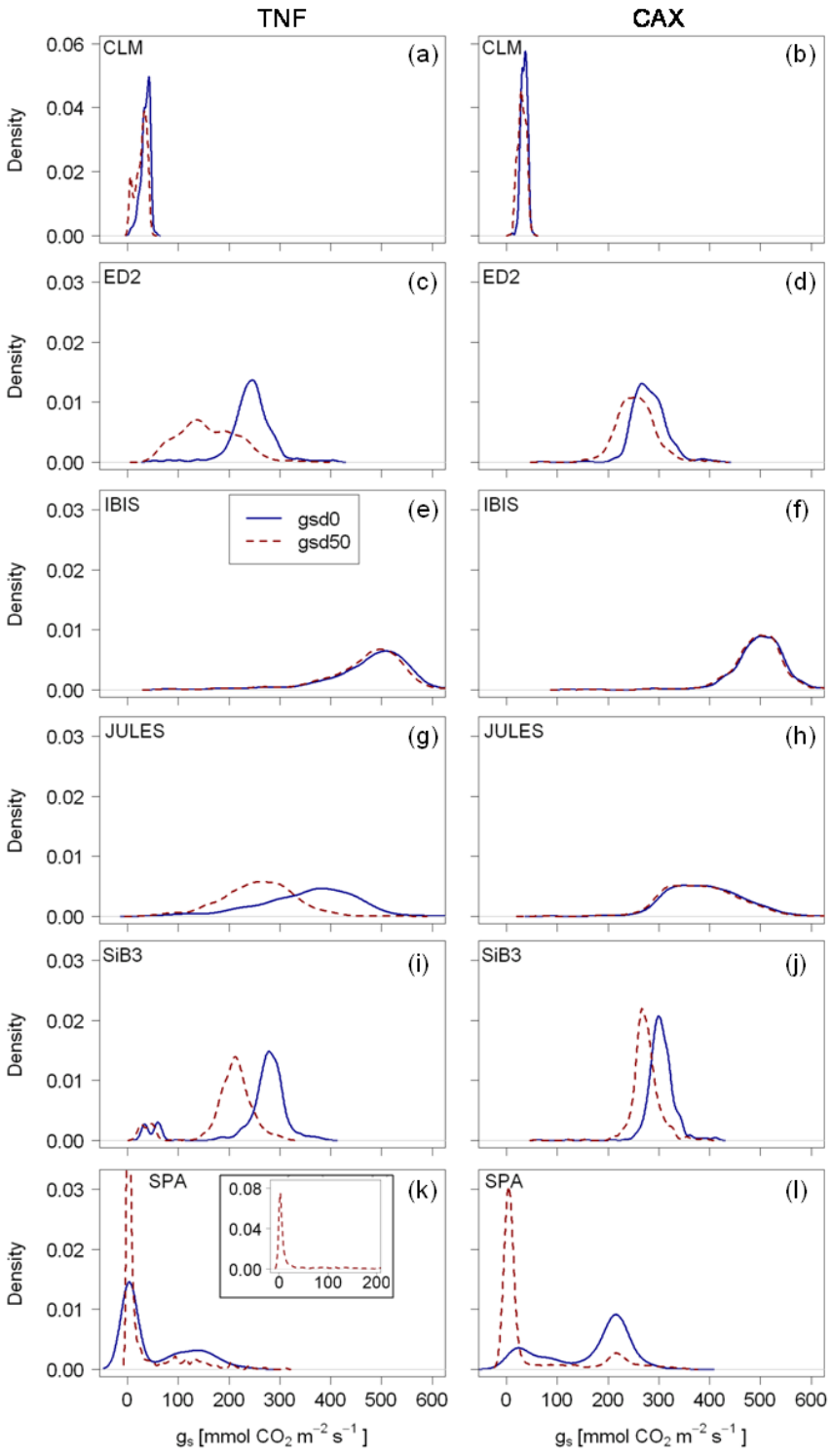

Figure 2.11. Density plots of modeled hourly stomatal conductance (g_s) during the midday (11:00 -14:00) over a 6 month period, May to November, in 2000 for TNF (left side) and 2003 for CAX (right side). d0 (solid) and d50 (dashed) indicate 0% and 50% reductions in precipitation. Inset in (k) shows full range of g_s at the d50 level for the SPA model.

leaf s^{-1}, respectively (Fig. 2.11a-j). SPA, on the other hand, predicted a bimodal distribution, with the larger of the two peaks switching between TNF and CAX (Fig. 2.11k,l). Under the drought treatment, the β–correction caused a downward shift by 50 to 100 mmol CO_2 m^{-2} leaf s^{-1} in the distributions of g_s in CLM3.5, ED2, JULES at TNF, and SiB3, but not in JULES at CAX or IBIS at either site (Fig. 2.11a-j). The distributions of g_s in CLM3.5 also became bimodal under drought. In SPA, the drought treatment at both sites resulted in a very narrow concentration of g_s values just above 0 mmol CO_2 m^{-2} leaf $s^{-1}$with a long positive tail, which was a substantially greater change compared to CLM3.5, ED2 and SiB3 (Fig. 2.11a-d,i,j).

There were considerable differences between the six models about the relative contribution of each constituent flux to R_e in the control simulations for both sites. For all models except SiB3, R_a was the dominant component of R_e, but by varying magnitudes (Figs. S2.6a,b, S2.7a,b). Accordingly, CLM3.5 was on one end of the range by estimating R_a to be more than double R_h, and SiB3 was on the other end with R_a and R_h contributing equally to R_e. Also, the patterns of interannual variation of R_h and R_a were often opposing between models (Figs. S2.6a,b, S2.7a,b). Of the constituent fluxes of R_a, there was generally strong agreement about model predictions of R_{lf} and R_w, and considerable uncertainty in R_r, which accounted for most of the uncertainty in R_a (not shown, but similar pattern visible in Fig. 2.2b,d). One notable exception was IBIS's significantly low predictions of R_w (see also Fig. 2.2b.d).

Variation between model predictions of respiration fluxes also increased substantially with drought intensity, yet some clear patterns of individual models emerged (Fig. 2.8). ED2, JULES and SiB3 predicted increasingly the highest reductions

in R_h as drought levels intensified owing to their decomposition formulations including a soil moisture factor. In ED2, the soil moisture factor regulating R_h was so influential that it resulted in ΔNEP being positive at the d30 and d50 drought levels (Figs. 2.7c-f, 2.8a,c,g). IBIS was the least sensitive to all drought levels, predicting only small increases in R_h and reductions in R_a at TNF (Fig. 2.8b,f,j), and virtually no response of its respiratory fluxes at CAX (Fig. 2.8d,h,l). While the cumulative seven year response of IBIS was small, its prediction of d50 R_a at TNF comes into alignment with the other models by the seventh year (Fig. S2.7e), implying its respiration does eventually respond to the drought treatment. At the d80 level, the R_h prediction of CLM3.5 was a significant positive outlier (Fig. 2.8j,l), thus reflecting the respiration of the additional dead biomass, which was not captured by ED2 even though it too experienced a high mortality flux (Fig. S2.2). These substantial increases in R_h predicted by CLM3.5 occurred only in the second and third years at TNF and the third and fourth years at CAX; otherwise the R_h predictions were in alignment with the other models (Fig. S2.6). Finally, for CLM3.5 at the d80 level, its predictions of R_a had much more interannual variation relative to the similar behavior of the other models (Fig. S2.7).

Discussion:

Under current climate conditions, the six models analyzed here have a reasonably high degree of skill in replicating ecosystem carbon fluxes (Fig. 2.2a,b,d, Table S2.1). The models also had some success in capturing the responses to the experimental drought, as

generally capturing the observed reductions in NPP_w (Fig. 2.4c,d), and ED2 correctly predicted the timing of the reduction in *AGB* (Fig. 2.1c), but the models failed to accurately predict the magnitude of the drought-induced reductions in *AGB* and accompanying component carbon fluxes (R_e, R_a, R_r, and R_s at CAX and R_s at TNF) (Figs. 2.1c,d, 2.2f,h, Table S2.1).

One explanation for this pattern of having high skill under current climate and poor skill under drier climate is that the models are poorly parameterized because they have been developed to replicate past observations of rainforests, which are rarely limited by water (Huete *et al.,* 2006, Hutyra *et al.,* 2007). Data-model assimilation using the observations from the two drought experiments may help to correct this problem. However, the results of this analysis more strongly suggest that the models require more realistic representations of key photosynthetic and respiratory drought response mechanisms. These are discussed in more detail below.

Photosynthesis & soil water-stress.

In all models except SPA, the stomatal response to decreasing soil moisture is represented by down-regulation imposed through a phenomenological function (β). The nature of the β-function differs across these models (Fig. 2.9, Table S2.3), and thus, each represents a contrasting hypothesis about how plant productivity is affected by available soil moisture. Any bias associated with β translates directly into a corresponding bias in the magnitude and timing of the decline in *GPP* as θ_s declines. For IBIS, JULES and SiB3, β changed gradually as available soil moisture was drawn down or replenished (Fig. S2.5), but was effectively static over diurnal periods (Fig. 2.10c,d,e,). In CLM3.5,

β was very responsive to rain events (Figures 2.10a,f) since it was parameterized based on ψ_s instead of θ_s (Table S2.3), but was static during dry days. In contrast, in ED2 β had a clear diurnal cycle (Fig. 2.10b) because its value is affected by evaporative demand at the leaf, which changes significantly over the daily photoperiod. It is also important to note that in CLM3.5, ED2, IBIS and SPA the level of soil water supply is impacted by the changes in demand that are modulated through leaf area dynamics (Fig. 2.6). We return to this issue below.

The mechanistic hydrodynamic formulation in SPA has been shown to be effective in capturing both the seasonal and diurnal dynamics of stomatal control over *GPP* (Fisher *et al*., 2006) and thus, obviates the need for a β-type correction factor. However, the reduction in the mean density of ecosystem-averaged leaf-level g_s predicted by SPA for CAX in this study is considerably greater than the reduction of ~40 mmol CO_2 m^{-2} leaf s^{-1} reported for four canopy trees, and simulated by SPA in a local CAX parameterization using detailed soil hydraulic measurements (Fisher *et al*., 2006). In this study, using generic soil hydraulics parameters, the sensitivity of g_s to drought predicted by SPA increased. On the other hand, the drought induced reduction in g_s predicted by CLM3.5, ED2, and SiB3 was similar in magnitude to the individual level measurements reported by Fisher *et al*. (2006). These results indicate the challenge of generating at a regional scale the local hydraulic parameters required for a SPA-style mechanistic formulation of plant water-use. Therefore, for regional applications, where soil hydraulics data are limited, the β-formulations of CLM3.5, ED2 and SiB3 are relatively robust in terms of down-regulating g_s.

Autotrophic respiration.

After the drought treatment was initiated, leaf dark respiration at CAX increased both in terms of unit leaf area and unit mass (Metcalfe *et al.,* 2010a). At the same time, LAI decreased, but the decline did not offset the increase in dark leaf respiration rate, resulting in an overall increase in R_{lf} (Fig. 2.2h). The predicted reductions in R_{lf} under the experimental drought directly conflict with these observations (Fig. 2.2h, Table S2.1). Of particular note, JULES and SiB3 explicitly down-regulate R_{lf} by β (Table S2.4) with this effect being stronger in JULES (Fig. 2.8h) since its decrease in β begins at a higher θ_s relative to SiB3 (Fig. 2.9).

The results of this study suggest that respiration formulations need to be modified to test hypotheses about increases in maintenance respiration when soil moisture becomes severely limiting. For example, it is possible that R_{lf} increases under drought due to futile respiratory cycles or because of demand for additional energy to maintain solute gradients, repair damaged tissue (Würth *et al*., 2005; Meir *et al*., 2008; Metcalfe *et al*., 2008), or repair leaf embolisms (Brodribb & Holbrook, 2003). Furthermore, all six models evaluated in this study follow the paradigm, either explicitly (SPA only) or heuristically, that growth declines when drought induces stomatal closure and down-regulates *GPP*. However, many studies across a range of plant forms have shown that under water-stress growth declines before photosynthesis, such that they become uncoupled and carbon accumulates within the plant (Würth *et al*., 2005; reviewed by Muller *et al.,* 2011). In many cases, the excess carbon is converted to carbon rich compounds that require extra energy to generate. Inclusion in future model iterations of formulations that up-regulate respiration during water-stress to account for all of these

discussed processes is critical for correctly computing the plant carbon balance during drought.

Changes in plant carbon pools.

Another critical component of capturing how *GPP* and R_a respond to soil water-stress, is correctly characterizing how carbon stocks change under drought. Accordingly, properly constraining seasonal leaf-area dynamics is imperative for reducing substantial biases in predicted *GPP* and R_a (Richardson *et al.,* 2012). Yet, all of the models failed to capture both the initial increase in litter production observed in the drought treatment plots at TNF (Fig. 2.5a) and, except for CLM3.5, ED2, and SPA, the reductions in LAI observed at both sites (Fig. 2.6c,d). While the mechanisms controlling leaf-shedding and flushing by tropical trees are not well understood (Kim *et al*., 2012), they appear to be related to seasonal cumulative soil water deficit (Nepstad *et al.,* 2007, Brando *et al*., 2010). The seasonally static leaf-area of CLM3.5, IBIS, and JULES and SiB3 introduced additional biases in their predictions of *GPP* and R_{lf} (Fig. 2.6), while the phenological formulations of ED2 and SPA that are dependent on soil moisture appear to be more reasonable approximations for canopy leaf-area dynamics.

Similarly, correctly predicting R_a under drought conditions requires not only the per unit tissue R_a to be accurate, but also the changes in the plant's carbon stocks. In this regard, the insensitivity of plant biomass to increasing water stress seen in Figure 2.1 is particularly problematic for the dynamic vegetation models. For IBIS, JULES, SPA and also SiB3 in terms of *LAI*, even the d80 drought level did not trigger a reduction in biomass (Fig. S2.2), which implies that even though they contain mechanisms to modify

plant carbon balance under extreme drought, they still do not contain a mechanism that translates a carbon *imbalance* into a loss of biomass (D. Galbraith, unpublished). Without a drought related mortality mechanism, these models will not be able to accurately predict carbon fluxes under drought because the fluxes will be derived from incorrect levels of biomass or leaf area. In CLM3.5 and ED2, significant changes in carbon stocks occurred (Figs. 2.1, 2.6) after chronically negative plant carbon balance occurred. Accordingly for ED2, the 50% reduction in *AGB* and 90% reduction in *LAI* at the d50 level at TNF cause the reductions in *GPP* and the component *R* fluxes (except R_r) to be considerably greater than predicted by the other models (Fig. 2.8f). Also, even for CLM3.5 and ED2, mortality due to negative carbon balance was incorrectly tuned to replicate the observed losses in *AGB* in the treatment plots (Figs. 2.1, S2.2).

Net ecosystem carbon balance

Changes in *NEP* are dependent not only on correctly quantifying changes in plant carbon stocks, but also on how rates of decomposition change in response to drought. Accordingly, CLM3.5 and ED2 reflect contrasting hypotheses about the rate soil carbon is respired under drought, which becomes evident in their contrasting predictions of R_h (Fig. S2.6) and resulting *NEP* (Figs. 2.7, 2.8) following their predicted *AGB* declines (Figs. 2.1c and S2.2). CLM3.5 predicted R_h to dramatically increase for the two years following its predicted *AGB* loss (Fig. S2.6g,h). Meanwhile, ED2 predicted a general decline in R_h under all drought levels (Fig. S2.6c-h), even though there was an increase in its soil carbon pool (not shown) following its predicted *AGB* loss (Fig 2.1c, S2.2). As a result, CLM3.5's predicted *NEP* was significantly lower than the other models (Figs

2.7g,h, 2.8i,k); whereas ED2's *NEP* prediction was similar to the other models (Figs 2.7e,h, 2.8e,k).

Overall the models compared well to the site specific empirically derived R_s annual estimates (Davidson *et al.,* 2008, Sotta *et al.,* 2007) at the d0 level (Fig. 2.2b,d), but poorly under the d50 conditions (Fig. 2.2f,h, Table S2.1). The inability of the models to correctly capture drought effects on R_s stems from the compounding effect of two related problems. First, in an adjacent forest at CAX, measurements of R_r accounted for 42 and 61% of R_s during the wet and dry seasons, respectively (Metcalfe *et al*., 2007), while all models except SPA predicted R_h to be the dominant component of in R_s (Fig 2.2d). Second, inaccurate soil moisture dependencies of R_h are apparent from the poor agreement between the modeled dependencies of R_s on θ_s compared to the observations (Fig. 2.3). In particular, the dependencies in ED2 and SiB3 resulted in extreme excursions from the R_s observations at high (ED2 and SiB3) and low (ED2) θ_s values (Fig. 2.3). While no direct measurements of *NEP* for the drought plots were available for evaluation, the predictions of R_h (Fig. S2.6c-h), and consequently *NEP* (Fig. 2.7c-h), under drought by ED2 and SiB3 were likely unrealistic given the mismatch between their predictions and the observations of R_s (Fig S2.3). In order to make correct estimates of *NEP* under drought, future model development must focus on correcting both the relative contribution of R_h to R_s and the parameterization of the dependency of R_h on θ_s.

Conclusions:

To our knowledge, this is the first time a series of terrestrial biosphere models run under a standardized protocol have been evaluated for their ability to predict how chronic drought affects plant and ecosystem carbon balances. This study demonstrates that terrestrial biosphere models are competent at predicting plant and ecosystem carbon fluxes under the present climate, but still require substantial development for predicting the consequences of severe drought scenarios. Model development should be focused on testing hypotheses associated with enhanced R_a under severe water-stress, controls over leaf phenology, and drought induced mortality.

Acknowledgements:

This research was funded by a grant from the Andes-Amazon Initiative of The Gordon and Betty Moore Foundation. T.L. Powell, B.O. Christoffersen, and S.R. Saleska gratefully acknowledge support from the National Science Foundation Partnership for International Research and Education in Amazon Climate Interactions grant (NSF award #OISE-0730305). Patrick Meir was supported by NERC award NE/J011002/1 and ARC award FT110100457. The LBA-DMIP project (NASA award #NNX09AL52G) provided the TNF meteorological data. We are grateful to the Museu Paraense Emilio Goeldi, the LBA office in Santarém, and the dedicated researchers who collected the data that made this model evaluation possible. We thank Eric Davidson for furnishing us with their published original TNF R_s data.

References:

Baker IT, Prihodko L, Denning AS, Goulden M, Miller S, da Rocha HR. 2008. Seasonal drought stress in the Amazon: Reconciling models and observations. *Journal of Geophysical Research* 113, G00B01. doi: 10.1029/2007JG000644

Best MJ, Pryor M, Clark DB, Rooney GG, Essery RLH, Ménard CB, Edwards JM, Hendry MA, Porson A, Gedney N *et al.* 2011. The Joint UK Land Environment Simulator (JULES), Model description-Part I: Energy and water fluxes. *Geoscientific Model Development* 4: 677-699. doi:10.5194/gmd-4-677-2011

Bonan GB, Levis S, Sitch S, Vertenstein M, Oleson KW. 2003. A dynamic global vegetation model for use with climate models: concepts and description of simulated vegetation dynamics. *Global Change Biology* 9: 1543-1566.

Brando PM, Nepstad DC, Davidson EA, Trumbore SE, Ray D, Camargo P. 2008. Drought effects on litterfall, wood production and belowground carbon cycling in an Amazon forest: results of a throughfall reduction experiment. *Philosophical Transactions of the Royal Society, B* 363: 1839–1848. doi:10.1098/rstb.2007.0031

Brando PM, Goetz SJ, Baccini A, Nepstad DC, Beck PSA, Christman MC. 2010. Seasonal and interannual variability of climate and vegetation indices across the Amazon. *Proceedings of the National Academy of Sciences* 107:14685-14690. doi/10.1073/pnas.0908741107

Brodribb TJ, Holbrook NM. 2003. Stomatal closure during leaf dehydration, correlation with other leaf physiological traits. *Plant Physiology* 132: 2166-2173.

Chambers JQ, dos Santos J, Ribeiro RJ, Higuchi N. 2001. Tree damage, allometric relationships, and above-ground net primary production in central Amazon forest. Forest Ecology and Management 152:73-84.

Clapp RB, Hornberger GM. 1978. Empirical equation for some soil hydraulic properties. *Water Resources Research* 14:601-604.

Clark DB, Mercado LM, Sitch S, Jones CD, Gedney N, Best MJ, Pryor M, Rooney GG, Essery RLH, Blyth E *et al.* 2011. The Joint UK Land Environment Simulator (JULES), model description—Part 2: carbon fluxes and vegetation dynamics. *Geoscientific Model Development* 4: 701-722. doi:10.5194/gmd-4-701-2011

Collatz GJ, Ball JT, Grivet C, Berry JA. 1991. Physiological and environmental regulation of stomatal conductance, photosynthesis and transpiration: a model that includes a laminar boundary layer. *Agricultural and Forest Meteorology* 54: 107-136.

Costa MH, Pires GF. 2010. Effects of Amazon and Central Brazil deforestation scenarios on the duration of the dry season in the arc of deforestation. *International Journal of Climatology* 30: 1970-1979.

Cosby BJ, Hornberger GM, Clapp RB, Ginn TR. 1984. A statistical exploration of the relationships of soil moisture characteristics to the physical properties of soils. *Water Resources Research* 20: 682-690.

Cox PM, Betts RA, Jones CD, Spall SA, Totterdell IJ. 2000. Acceleration of global warming due to carbon-cycle feedbacks in a coupled climate model. *Nature* 408: 184-187.

Cox PM. 2001. Description of the TRIFFID Dynamic Global Vegetation Model. Hadley Centre Technical Note 24, Hadley Centre, Met Office, Bracknell, UK.

da Costa ACL, Galbraith D, Almeida S, Portela BTT, da Costa M, de Athaydes Silva Junior J, Braga AP, de Gonçalves PHL, de Oliveira AAR, Fisher R, Phillips OL *et al.* 2010. Effect of 7 yr of experimental drought on vegetation dynamics and biomass storage of an eastern Amazonian rainforest. *New Phytologist* 187: 579–591. doi: 10.1111/j.1469-8137.2010.03309.x

Davidson EA, Nepstad DC, Ishida FY, Brando PM. 2008. Effects of an experimental drought and recovery on soil emissions of carbon dioxide, methane, nitrous oxide, and nitric oxide in a moist tropical forest. *Global Change Biology* 14: 2582–2590. doi: 10.1111/j.1365-2486.2008.01694.x

Farquhar GD, Sharkey TD. 1982. Stomatal conductance and photosynthesis. *Annual Review of Plant Physiology* 33: 317-345.

Farquhar GD, von Caemmerer S, Berry JA. 1980. A biochemical model of photosynthetic CO_2 assimilation in leaves of C_3 species. *Planta* 149: 78-90.

Fisher RA, Williams M, Lobo do Vale, da Costa AL, Meir P. 2006. Evidence from Amazonian forest is consistent with isohydric control of leaf water potential. *Plant, Cell and Environment* 29: 151-165.

Fisher RA, Williams M, da Costa AL, Malhi Y, da Costa RF, Almeida S, Meir P. 2007. The response of an Eastern Amazonian rain forest to drought stress: results and modelling analyses from a throughfall exclusion experiment. *Global Change Biology* 13: 2361-2378.

Fisher R, McDowell N, Purves D, Moorcroft P, Sitch S, Cox P, Huntingford C, Meir P, Woodward FI. 2010. Assessing uncertainties in a second-generation dynamic vegetation model caused by ecological scale limitations. *New Phytologist* 187: 666-681. doi: 10.1111/j.1469-8137.2010.03340.x

Foley JA, Prentice IC, Ramankutty N, Levis S, Pollard D, Sitch S, Haxeltine A. 1996. An integrated biosphere model of land surface processes, terrestrial carbon balance, and vegetation dynamics. *Global Biogeochemical Cycles* 10: 603–628.

Good P, Jones C, Lowe J, Betts R, Gedney N 2013. Comparing tropical forest projections from two generations of Hadley Centre Earth System models, HadGEM2-ES and HadCM3LC. *Journal of Climate*, 26, 495–511. doi: 10.1175/JCLI-D-11-00366.1

Goudriaan J. 1977. Crop micrometeorology: A simulation study. Center for Agricultural Publishing and Documentation, Wageningen, The Netherlands. 249pp.

Huete AR, Didan K, Shimabukuro YE, Ratana P, Saleska SR, Hutyra LR, Yang W, Nemani RR, Myneni R. 2006. Amazon rainforests green-up with sunlight in dry season. *Geophysical Research Letters* 33: L06405.doi: 10.1029/2005GL025583.

Hutyra LR, Munger W, Saleska SR, Gottlieb E, Daube BC, Dunn AL, Amaral DF, de Camargo PB, Wofsy SC. 2007. Seasonal controls on the exchange of carbon and water in an Amazonian rain forest . *Journal of Geophysical Research* 112: G03008. doi:10.1029/2006JG000365.

Joetzjer E, Douville H, Delire C, Ciais P. 2013. Present-day and future Amazonian precipitation in global climate models: CMIP5 versus CMIP3. *Climate Dynamics*, 41, 2921-2936. doi: 10.1007/s00382-012-1644-1

Jupp TE, Cox PM, Rammig A, Thonicke K, Lucht W, Cramer W. 2010. Development of probability density functions for future South American rainfall. *New Phytologist* 187: 682–693. doi: 10.1111/j.1469-8137.2010.03368.x

Kim Y, Knox RG, Longo M, Medvigy D, Hutyra LR, Pyle EH, Wofsy SC, Bras RL, Moorcroft PR. 2012. Seasonal carbon dynamics and water fluxes in an Amazon rainforest. *Global Change Biology* 18: 1322–1334. doi: 10.1111/j.1365-2486.2011.02629.x

Kucharik CJ, Foley JA, Delire C, Fisher VA, Coe MT, Lenters JD, Young-Molling C, Ramankutty N, Norman JM, Gower ST. 2000. Testing the performance of a Dynamic Global Ecosystem Model: Water balance, carbon balance, and vegetation structure. *Global Biogeochemical Cycles* 14: 795-825.

Levis S, Bonan GB, Vertenstein M, Oleson KW. 2004. The Community Land Model Dynamic Global Vegetation Model (CLM-DGVM): technical description and user's guide. 50 pp, Boulder, CO, USA, National Center for Atmospheric Research.

Li W, Fu R, Dickinson RE. 2006. Rainfall and its seasonality over the Amazon in the 21st century as assessed by the coupled models for the IPCC AR4, Journal of Geophysical Research, 111, D02111, doi:10.1029/2005JD006355.

Lintner B, Biasutti M, Diffenbaugh NS, Lee J-E, Niznik MJ, Findell KL. 2012. Amplification of wet and dry month occurrence over tropical land regions in response to global warming, *Journal of Geophysical Research,* 117, D11106, doi:10.1029/2012JD017499.

Malhi Y, Roberts JT, Betts RA, Killeen TJ, Li W, Nobre CA. 2008. Climate change, deforestation, and the fate of the Amazon. *Science* 319: 169. doi: 10.1126/science.1146961

Medvigy D, Wofsy SC, Munger JW, Hollinger DY, Moorcroft PR. 2009. Mechanistic scaling of ecosystem function and dynamics in space and time: Ecosystem Demography model version 2. *Journal of Geophysical Research* 114: G01002, doi:10.1029/2008JG000812.

Meir P, Metcalfe DB, Costa ACL, Fisher RA. 2008. The fate of assimilated carbon during drought: impacts on respiration in Amazon rain forests. *Philosophical Transactions of the Royal Society, London B* 363:1849-55. doi: 10.1098/rstb.2007.0021

Meir P, Brando PM, Nepstad D, Vasconcelos S, Costa ACL, Davidson E, Almeida S, Fisher RA, Sotta ED, Zarin D, Cardinot G. 2009. The effects of drought on Amazonian rain forests. In: Keller M, Bustamante M, Gash J, Silva Dias P, eds. *Amazonia and Global Change, Geophysical Monograph Series* 186: 429-449.

Metcalfe DB, Meir P, Aragão LEOC, Malhi Y, da Costa ACL, Braga A, Gonçalves PHL, de Athaydes J, de Almeida SS, Williams M. 2007. Factors controlling spatio-temporal variation in carbon dioxide efflux from surface litter, roots, and soil organic matter at four rain forest sites in the eastern Amazon. *Journal of Geophysical Research – Biogeosciences* 112: G04001. doi: 10.1029/2007JG000443.

Metcalfe DB, Meir P, Aragão LEOC, Da Costa ACL, Braga AP, Gonçalves PHL, De Athaydes Silva J Jr, de Almeida SS, Dawson LA, Malhi Y, *et al.* 2008. The effects

of water availability on root growth and morphology in an Amazon rainforest. *Plant and Soil* 311: 189–199. doi:10.1007/s11104-008-9670-9

Metcalfe DB, Lobo-do-Vale R, Chaves MM, Maroco JP, Aragão LEOC, Malhi Y, Da Costa AL, Braga A, Gonçalves PL, De Athaydes J, *et al.* 2010a. Impacts of experimentally imposed drought on leaf respiration and morphology in an Amazon rainforest. *Functional Ecology* 24: 524-533. doi: 10.1111/j.1365-2435.2009.01683.x

Metcalfe DB, Meir P, Aragão LEOC, Lobo-do-Vale R, Galbraith D, Fisher RA, Chaves MM, Maroco JP, da Costa ACL, de Almeida SS, *et al.* 2010b. Shifts in plant respiration and carbon use efficiency at a large-scale drought experiment in the eastern Amazon. *New Phytologist* 187: 608–621. doi: 10.1111/j.1469-8137.2010.03319.x

Moorcroft PR, Hurtt GC, Pacala SW. 2001. A method for scaling vegetation dynamics: The Ecosystem Demography model (ED). *Ecological Monographs* 71: 557-587.

Muller B, Pantin F, Génard M, Turc O, Freixes S, Piques M, Gibon Y. 2011. Water deficits uncouple growth from photosynthesis, increase C content, and modify the relationship between C and sink organs. *Journal of Experimental Botany* 62: 1715-1729. doi: 10.1093/jxb/erq438

Nepstad DC, Moutinho PR. 2008. LBA-ECO LC-14 Rainfall Exclusion Experiment, LAI, Gap Fraction, TNF, Brazil: 2000-05. Data set. Available on-line [http://lba.cptec.inpe.br/] from LBA Data and Information System, National Institute for Space Research (INPE/CPTEC), Cachoeira Paulista, Sao Paulo, Brazil [accessed 17 November 2012].

Nepstad DC, Moutinho P, Dias-Filho MB, Davidson E, Cardinot G, Markewitz D, Figueiredo R, Vianna N, Chambers J, Ray D, *et al.* 2002. The effects of partial throughfall exclusion on canopy processes, aboveground production, and biogeochemistry of an Amazon forest. *Journal of Geophysical Research* 107(D20): 8085. doi:10.1029/2001JD000360.

Nepstad DC, Tohver IM, Ray D, Moutinho P, Cardinot G. 2007. Mortality of large trees and lianas following experimental drought in an Amazon forest. *Ecology* 88:2259-2269.

Oleson KW, Niu G-Y, Yang Z-L, Lawrence DM, Thornton PE, Lawrence PJ, Stöckli R, Dickinson RE, Bonan GB, Levis S, *et al*. 2008. Improvements to the Community Land Model and their impact on the hydrological cycle. *Journal of Geophysical Research* 113: G01021. doi:10.1029/2007JG000563.

Richardson AD, Anderson RS, Altafarain M, Barr AG, Bohrer G, Chen G, Chen JM, Ciais P, Davis KJ, Desai A, *et al.* 2011. Terrestrial biosphere models need better representation of vegetation phenology: results from the North American Carbon Program Site Synthesis. *Global Change Biology* 18: 566-584. doi: 10.1111/j.1365-2486.2011.02562.x

Rosolem R, Shuttleworth WJ, Gonçalves LGG. 2008. Is the data collection period of the Large-Scale Biosphere-Atmosphere Experiment in Amazonia representative of long-term climatology? *Journal of Geophysical Research* 113: G00B09, doi:10.1029/2007JG000628.

Sakaguchi K, Zeng X, Christoffersen BJ, Restrepo-Coupe N, Saleska SR, Brando PM. 2011. Natural and drought scenarios in an east central Amazon forest: Fidelity of

the Community Land Model 3.5 with three biogeochemical models. *Journal of Geophysical Research* 116: G01029. doi:10.1029/2010JG001477.

Sellers PJ, Randall DA, Collatz GJ, Berry JA, Field CB, Dazlich DA, Zhang C, Collelo GD, Bounoua L. 1996. A revised land surface parameterization (SiB2) for atmospheric GCMs. Part I: Model formulation. *Journal of Climate* 9: 676-705.

Sotta ED, Veldkamp E, Schwendenmann L, Guimarães BR, Paixão RK, Ruivo MLP, da Costa ACL, Meir P. 2007. Effects of an induced drought on soil carbon dioxide (CO_2) efflux and soil CO2 production in an eastern Amazonian rainforest, Brazil. *Global Change Biology* 13: 2218–2229. doi: 10.1111/j.1365-2486.2007.01416.x

Taylor JR. 1997. *An Introduction to Error Analysis: The Study of Uncertainties in Physical Measurements, 2nd Edition*, pp. 49-61. University Science Books, Sausalito, CA.

Williams M, Rastetter EB, Fernandes DN, Goulden ML, Wofsy SC, Shaver GR, Melillo JM, Munger JW, Fan S-M, Nadelhoffer KJ. 1996. Modelling the soil-plant-atmosphere continuum in a *Quercus-Acer* stand at Harvard Forest: the regulation of stomatal conductance by light, nitrogen and soil/plant hydraulic properties. *Plant, Cell and Environment* 19: 911–927.

Williams M, Shimabukuro YE, Herbert DA, Pardi Lacruz S, Renno C, Rastetter EB. 2002. Heterogeneity of soils and vegetation in an eastern Amazonian rain forest: Implications for scaling up biomass and production. *Ecosystems* 5: 692-704. doi: 10.1007/s10021-002-0165-x.

Williams M, Schwarz PA, Law BE, Irvine J, Kurpius MR. 2005. An improved analysis of forest carbon dynamics using data assimilation. *Global Change Biology* 11: 89-105. doi: 10.1111/j.1365-2486.2004.00891.x

Würth MKR, Peláe-Riedl S, Wright SJ, Körner C. 2005 Non-structural carbohydrate pools in a tropical forest. *Oecologia* 143: 11-24. doi: 10.1007/s00442-004-1773-2

Chapter 3

Do differences in xylem cavitation resistance and leaf hydraulic traits explain differences in drought tolerance among mature tropical rainforest trees?

Abstract

Considerable uncertainty surrounds the fate of Amazon rainforests due to predicted reductions in precipitation resulting from climate change and deforestation. Two long-term large-scale ecosystem drought experiments established in the eastern Brazilian Amazon observed an increase in mortality rates among some species while others had no change; yet a mechanistic cause for these differences was not implicated. In this study, xylem pressure at 50% conductivity (xylem-P_{50}), leaf turgor loss point (*TLP*), cellular osmotic potential (π_o) and cellular bulk modulus of elasticity (ε), all traits thought to confer drought tolerance, were measured on upper canopy branches and leaves of four genera found at both experimental sites. Each genus was placed *a priori* into one of four functional type categories: drought-tolerant versus intolerant based on the drought experiment results and subdivided into early versus late-successional based on wood density. We tested the hypotheses that these measured traits would be significantly different between each of the plant functional types and that they would be spatially conserved across sites. Xylem-P50, *TLP*, and π_o, but not ε, occurred at significantly higher water potentials for the drought-intolerant type compared to the tolerant type; however, there were no significant differences between the early- and late-successional types. These results suggest that these three traits are important for defining trade-offs associated with drought tolerance, but appear to be orthogonal to traits associated with succession. Differences in these hydraulic traits that occurred between the drought-tolerant and intolerant types was conserved between the two research sites, even though

they were separated by 400 km, and had contrasting soil types and meteorology. This more detailed understanding of how xylem and leaf hydraulic traits vary between drought-tolerant and intolerant tropical tree species will facilitate a much needed improvement in the representation of plant hydrology in terrestrial biosphere models, which will enhance our ability to make robust predictions of tropical ecosystem responses to drought.

Introduction

Climate model predictions are converging toward longer dry seasons across much of the Amazon basin and considerable overall drying in the eastern region by the end of this century (Malhi *et al.,* 2008; Joetzjer *et al*., 2013). Widespread deforestation is also predicted to cause lower precipitation through an extensive central corridor of the basin (Coe *et al*., 2013). Dynamic vegetation models are one of our most promising tools for assessing the consequences of these predicted changes in precipitation. However, it is unclear how resistant different species, and thus forests, across the Amazon basin might be to chronic drought because at present these models are poorly formulated to represent the physiological responses of different tree species (Gailbraith *et al*., 2010; Sakaguchi *et al*., 2011; Powell *et al*., 2013). The resolution to this problem requires a more detailed understanding of the mechanisms that cause mature trees to succumb to drought and the time dimension over which these mechanisms induce mortality in different species (McDowell *et al*., 2008; Hartman, 2011; McDowell *et al*., 2013).

Two in-situ ecosystem scale drought experiments were established in the eastern Brazilian Amazon—Tapajos (TNF) and Caxiuana (CAX) National forests—to directly assess the ecological impact of a chronic 50% reduction in precipitation (Nepstad *et al*. 2007; da Costa *et al*., 2010). Two key and consistent findings emerged from both experiments despite being separated by 400 km. First, mortality rates of the largest trees increased by 3.0 to 4.5-fold in the drought plots, while mortality of the subdominant trees (<10 cm DBH) was unchanged, thus resulting in a 20% reduction in aboveground biomass (Nepstad *et al*., 2007; da Costa *et al*., 2010). Second, the increase in mortality rates was not equal between genera (da Costa et al. 2010). A mechanistic cause for the

differential mortality rates was not implicated; yet, the results from the earlier studies now make it possible to test for differences in hydraulic traits between species identified as drought-tolerant and intolerant.

Maintaining connectivity of water through the soil-plant-atmosphere continuum is essential for vascular plants to maintain photosynthesis. Plants manage the risk of caviation both anatomically and through stomatal regulation of transpiration. Anatomically, wider xylem elements, larger pit membrane pores, and a higher density of pit membranes between vessel elements can increase the efficiency of water transport and hence carbon gain, but also increase the vulnerability for embolisms to form in the xylem as tension builds (Wheeler *et al*., 2005, Choat *et al*., 2008; Poorter *et al*., 2010). The xylem pressure when 50% of conductivity is lost (xylem -P_{50}) is a key trait that can be used to directly compare how different species balance this trade-off between maximizing water transport and minimizing risk of cavitation. More negative xylem-P_{50} values have been associated with trees growing in drier climates in the tropics (Choat *et al*., 2007). However, species-wise differences in xylem vulnerability has not been experimentally linked to differences in mortality rates of *in situ* mature trees experimentally exposed to chronically dry soils.

Plants also minimize the risk of cavitation through stomatal closure. Turgor loss point (*TLP*) is an easily measured, higher order trait that is the point when the leaf becomes so dehydrated its cells lose turgor. *TLP* correlates with the leaf water potential when the stomata are 50% closed (Brodribb *et al*. 2003). Cellular osmotic potential at full hydration (π_o) and bulk modulus of elasticity of leaf cell walls (ε) are two first order traits that contribute to *TLP*. π_o is the amount leaf water potential is lowered by solutes in

the cells. ε determines the volumetric change in the leaf cell as turgor declines and represents the amount of water available from cellular storage between full hydration and *TLP*. Species with lower *TLP* and π_o were found to be more prominent in the drier climates across the tropics (Choat *et al*., 2007; Baltzer *et al*. 2008), which is also general pattern that occurs between dry versus wet biomes (Bartlett *et al*., 2012). Conclusive patterns for ε are more variable between these same studies.

It is also not known if the resistance of the drought-tolerant species was a result of plasticity in their hydraulic efficiency or stomatal sensitivity to drier soils as affected by *TLP*, π_o or ε. Plasticity of hydraulic traits of tropical species has been poorly studied in general, but a few studies indicate that it may be important (e.g. Campanello *et al*., 2008; Fonti *et al*., 2010), but see also Bartlett *et al*. (2014). For example, when light environment in the understory increases after a disturbance, xylem conductivity increased in early-successional species but remained the same in late-successional species (Campanello *et al*., 2008). This result suggests an important interaction between traits that select for drought tolerance and successional status.

Wood density may be a useful trait for using as a proxy for drought tolerance since it has been measured for many tropical species (Fearnside, 1997) and is negatively correlated with precipitation gradient that exists across the Amazon basin (Baker *et al*., 2004, but see also ter Steege et al., 2006). Wood density correlates with successional type, where species with lower density tend to be early-successional and species with higher density tend to be late-successional (Poorter *et al*., 2010). However, it has not been experimentally determine on mature trees if traits that define successional type covary or are orthogonal to traits that confer drought tolerance.

Hydraulic resistance increases with tree height (Ryan *et al*., 2006), which implies that as precipitation patterns change in the future, the trade-off between growth versus hydraulic safety will become increasingly important for mature trees. Measurements of how these hydraulic traits differ in mature trees growing in the same ecosystem and experimentally treated with a severe and chronic drought has never been done. Accordingly, we tested four hypotheses. The first two hypotheses concern how *TLP*, π_o, ε and xylem-P_{50} varied between PFTs. *TLP*, π_o, and ε were predicted to occur at a lower leaf water potential, and xylem-P_{50} was predicted to occur at a lower stem water potential in canopy trees that are characterized as drought-tolerant relative to intolerant (H1), and late relative to early-successional (H2). The second two hypotheses tested spatial and temporal variation in the hydraulic traits. When variation in a hydraulic trait occurs between PFTs it was predicted to be conserved geographically (H3) due to the similarity in observed mortality rates between the two drought experiments. Temporally, trees characterized as both drought-tolerant and early-successional were predicted to have greater plasticity in *TLP*, π_o, ε and xylem-P_{50} compared those characterized as either drought-intolerant or late-successional (H4).

Materials and Methods

Study Sites

The study was conducted in the two Amazon rainforest throughfall exclusion experiments (TFE) located in the Caxiuanã (CAX; 1.737ºS, 51.458ºW) and Tapajós (TNF; 2.897ºS, 54.952ºW) National Forests, Pará, Brazil. The TFEs were established to directly measure whole ecosystem responses to severe and chronic drought (Nepstad *et*

al., 2002, 2007; Brando *et al*.; 2008, da Costa *et al*., 2010). The Tapajós TFE experiment ran from 2000 to 2004 (Nepstad *et al*., 2007); therefore *post hoc* measurements were made on the four selected species in the forest adjacent to the TFE plots. The Caxiuanã TFE experiment commenced in January 2002 was still running at the time of this study. Physical and biological characteristics of each site are summarized in Table 3.1.

Table 3.1. Physical and biological characteristics of the Caxiuanã and Tapajós National Forest throughfall exclusion sites.

Characteristic	Caxiuanã	Tapajós	Reference
Mean annual precipitation	2272 mm	2000 mm	Fisher *et al*., 2007, Nepstad *et al*., 2002
Wet season (>100 mm mo^{-1})	Dec. to mid-Jul.	Dec. to mid-Jun.	Rosolem *et al.,* 2008
Soil type	clay: 15% sand: 78%	clay: 60% sand: 38%	Fisher *et al*., 2007, Nepstad *et al*., 2002
Water table depth	10 m	>80 m	Fisher *et al*., 2007, Nepstad *et al*., 2002
Aboveground biomass of trees >10 cm dbh	214 t C ha^{-1}	150 t C ha^{-1}	da Costa *et al.,* 2010, Nepstad *et al*., 2002

A brief description of the TFE experimental design is given here; more detailed descriptions are provided in Nepstad *et al*., (2002) and Fisher *et al*., (2007). Two 1-ha plots, one control and one treatment plot, were established in each of the CAX and TNF forests. Both plots in each forest were selected to be structurally and floristically similar. A 1-2 m high leaky plastic septum was constructed over the entire understory of the treatment plot. The septum prevented approximately 50% of the rainfall from reaching the soil (Nepstad *et al*., 2002). The remaining rainfall was diverted off site through a

system of gutters and drainage ditches. The drainage ditches were 1 x 1 m and encircled each plot to also prevent lateral roots from accessing soil moisture from outside the plots (Nepstad *et al*., 2002).

Species selection and sampling

The four genera selected for this study were classified *a priori* into one of four categories: drought-tolerant versus intolerant and early- versus late-successional (Table 3.2). First, the genera were selected from those listed in Table 3.2 of da Costa *et al*. (2010), which lists changes in mortality rates of several genera tracked in the drought experiments. Genera that exhibited a change in mortality were designated drought-intolerant and those that exhibited no change were designated drought-tolerant. Second, the two species within each *drought* category were then designated as either early-successional or late-successional based on wood density being either low (<0.6 kg cm3) or high (>0.8 kg m3), respectively (Poorter *et al*., 2010). At each site, samples were collected from mature individuals belonging to single species (or two *Ingas* at CAX) representing each of the four selected genera and hence, functional groups (Table 3.2).

Table 3.2. Species selected to represent each plant functional group. Sites are noted by CAX for Caxiuanã and TNF for Tapajós National Forests.

Drought Sensitivity	**Succession**	
	Early	**Late**
Intolerant	**Genus: *Inga***	**Genus: *Eschweilera***
	CAX: *I. alba, I. gracilifolia*	CAX: *E. coriacea*
	TNF: *I. alba*	TNF: *E. coriacea*
Tolerant	**Genus: *Protium***	**Genus: *Licania***
	CAX: *P.tenuifolium*	CAX: *L. octandra*
	TNF: *P. robustum*	TNF: *L. canescens*

One or two branches approximately 3 cm in diameter, 2.5 m in length, containing several branchlets and >100 leaves were harvested from each individual at a height of 14 – 25 m. All branches were located in the upper crown and in full sunlight during the afternoon. The branches were harvested between 6:30 and 7:30 am local time, and the canopy was generally wet from rain or condensation from the night before, thus indicating minimal transpiration had yet occurred. After harvest, the branches were wrapped in plastic and the distal end was placed in water and transported for 30 to 60 minutes to the lab. The whole branches were stored in the lab in large plastic bags with the distal ends submerged in water until the leaves or branches could be prepared for measurements on the morning of the harvest. The exact number of trees, leaves and branches sampled from each species at each site is provided in Table S3.1.

A total of three measurement campaigns were carried out at each site. Each campaign was over a 2-4 week period, with at least one campaign in each of the wet and dry seasons. Seasonality in the data was not detected and therefore the data were pooled. Measurements for CAX were made in May 2011, November 2011, and October 2012. Measurements for TNF were made in January 2011, July 2011, and October 2012.

Leaf hydraulic traits

Dawn and midday leaf water potentials (ψ_{lf}) were measured in the forest immediately following the branch harvest using a PMS model 600 pressure chamber (PMS Instrument Co., Albany, OR). Pressure-volume (p-v) curves were constructed for each species to estimate *TLP*, π_o and ε. The p-v curves were composites of all of the leaves sampled for each species. Only fully expanded healthy leaves either second or third from the tip were

used. Initial rehydration of the leaves was not necessary since the leaves were often wet from rain or morning dew at the time of harvest (this was also confirmed by the initial chamber balance pressure being consistently < 0.2 MPa). Each leaf was patted dry, excised from its branch, weighed to 0.0001g and then pressurized in the pressure chamber to measure the leaf water potential. The leaves were allowed to desiccate on the bench between each set of mass and pressure measurements.

Xylem vulnerability

Xylem vulnerability was measured using the air-injection method (Sperry & Saliendra, 1994) on 11 to 13 cm branch segments that were approximately 0.6 cm in diameter. The branch segments were inserted in a pressure chamber where the xylem's ability to resist cavitation from the positive pressure pushing through the pit membranes was assumed to be equivalent to the xylem's ability to resist air seeding through pit membrane pores as tension within the vessel builds. The pressure chamber was constructed from a stainless steel, union tee, pipe adapter for 0.5 in OD inline tubes. Rubber plugs held in place with washers were used to make a seal between the branch segments and the chamber. Once inside the chamber, 0.5 cm of bark was removed from the distal end of the branch segment, the tip was shaved with a razor and then attached to the plumbing system using a 4 cm silicon coupling. The plumbing system consisted of a 1 l lactated ringer and Tygon® tubing. De-ionzed water was unavailable at the remote locations of both field stations. Filtered (0.2 μm) well water was used rather than the weak solution of KCl in de-ionized water commonly used in other studies (e.g. Choat *et al*., 2010). We assumed

that the well water and rooting zone water contained similar chemical constituents and therefore the xylem was reacting similarly to both.

Flow rates were measured for 10 minutes from the proximal end of the branch segment for each measurement period. On each branch segment, the native flow rate was measured first followed by a 10 minute flushing with water under ~0.1 MPa to refill extremely weak vessels that may have cavitated. The flow rate measured after flushing was taken as the maximum flow rate. Subsequent flow rates were measured after each incremental increase in air pressure in the pressure chamber. The stem segments were disconnected from the plumbing system, pressurized for 10 minutes and then depressurized before being reconnected to the plumbing system and resuming flow. It was found on a subset of stem segments for each species that flow rates equilibrated after approximately 15 minutes after the plumbing system was reconnected. Therefore, water was allowed to flow through the stem segments for 30 minutes prior to commencing each measurement. The pressure head was between 15 and 20 cm when water was flowing through the branch.

Statistics and Analysis

The *TLP* was calculated using a change-point detection algorithm on composite p-v curves containing all data points for each species (Barr *et al*., 2013). A 95% CI was established for each *TLP* estimate from a 10000 iteration bootstrap sampling. Once the *TLP* was established, π_o and ε were calculated for each species using the relationship between [100 – RWC (%)] and $1/\psi_{lf}$ (MPa) where π_o equals $1/\psi_{lf}$ when [100 – RWC] equals 0 (i.e. the y-intercept) and ε equals the slope of the relationship between [100 –

RWC] and ψ_{lf} in the linear portion of the curve prior to *TLP*. RWC is the water content of the leaf relative to being fully saturated and equals 100% when ψ_{lf} is 0.

A Weibull function was fit to the relationship between xylem pressure and percent loss of conductance (PLC) relative to maximum conductance of the branch segment (Meinzer *et al*., 2009). The point where PLC reached 50% was defined as the xylem-P_{50}. The error estimate for xylem-P_{50} was calculated using the maximum and minimum P_{50} values that could be established from the error on the parameter estimates of the Weibull functions.

Soil moisture was consistently lower throughout the rooting zone in the drought treatment plots (Fig. S3.1, see also Fisher et al. 2007 and Brando et al. 2008). For all four species measured at CAX, no significant differences were detected between the composite pressure-volume curves (Fig. S3.2) or xylem vulnerability curves (Fig. S3.3) constructed for each species measured in the control versus drought plots. Therefore, at CAX both the pressure-volume data and xylem vulnerability data collected from individuals growing in the control and drought plots were combined for each species.

Results

Leaf traits

Median *TLPs* $\pm$ CIs (95% confidence interval) of the two drought-intolerant species (*Inga* and *Eschweilera*) were significantly higher (range: -1.51 to -1.64 MPa) than the two drought-tolerant species (*Protium* and *Licania*, range: -2.33 to -2.46) at both TNF and CAX (Table 3.3, Fig. 3.1). In contrast, median *TLPs* $\pm$ CIs of the measured species

did not differentiate between the early- versus late-successional functional types. In this study, the CIs mark the boundaries within which 95% of the bootstrapped *TLP* estimates fall, since the bootstrapped estimates of *TLP* were not normally distributed around the mean (Fig. S3.4).

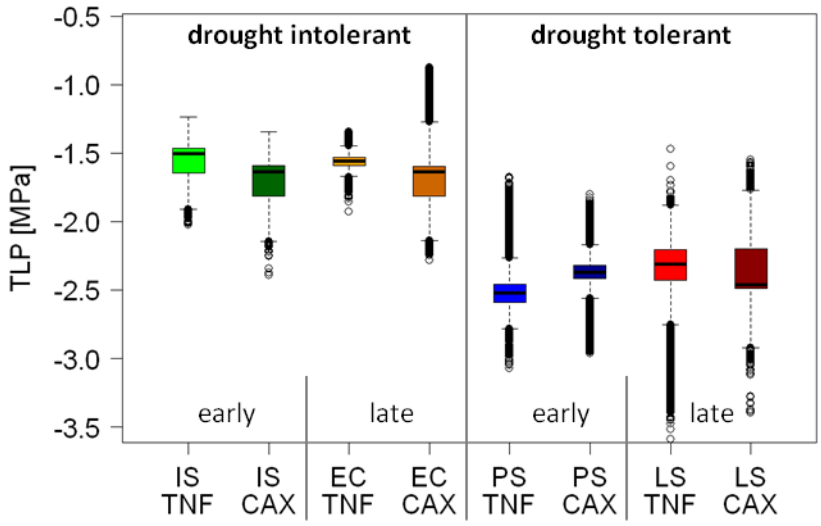

Figure 3.1. Boxplots showing the distribution of turgor loss point (TLP, MPa) estimates for each plant functional type measured at the Tapajós (open symbols) and Caxiuanã (closed symbols) National Forests. (a) *Inga* species (IS) represent early-successional drought-intolerant. (b) *Eschweilera coriacea* (EC) represent late-successional drought-intolerant. (c) *Protium* species (PS) represents early-successional drought-tolerant. (d) *Licania* species (LS) represent late-successional drought-tolerant.

At both sites median π_o of the two drought-intolerant species were significantly higher (range: -1.56 to -1.82 MPa) than the two drought-tolerant species (range: -2.35 to -2.51 MPa); but no significant difference was detected between the early versus late-successional species (Table 3.3, Fig. 3.2). In contrast, differences in median ε between the four species were not organized according to either of the drought tolerance or successional plant functional types (Fig. 3.3).

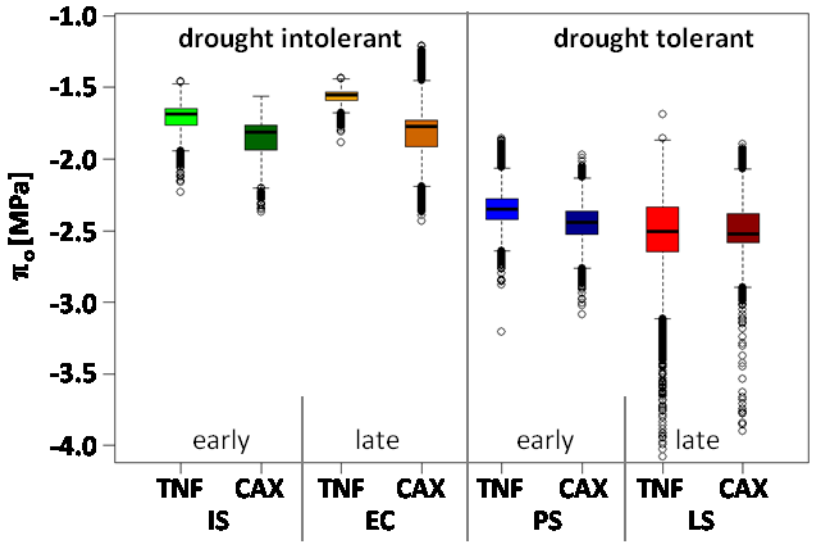

Figure 3.2. Boxplots showing the distribution of leaf osmotic potentials (π_o, MPa) for each plant functional type measured at the Tapajós (TNF) and Caxiuanã (CAX) National Forests. IS: *Inga* species represent early-successional drought-intolerant. EC: *Eschweilera coriacea* represent late-successional drought-intolerant. PS: *Protium* species represents early-successional drought-tolerant. LS: *Licania* species represents late-successional drought-tolerant.

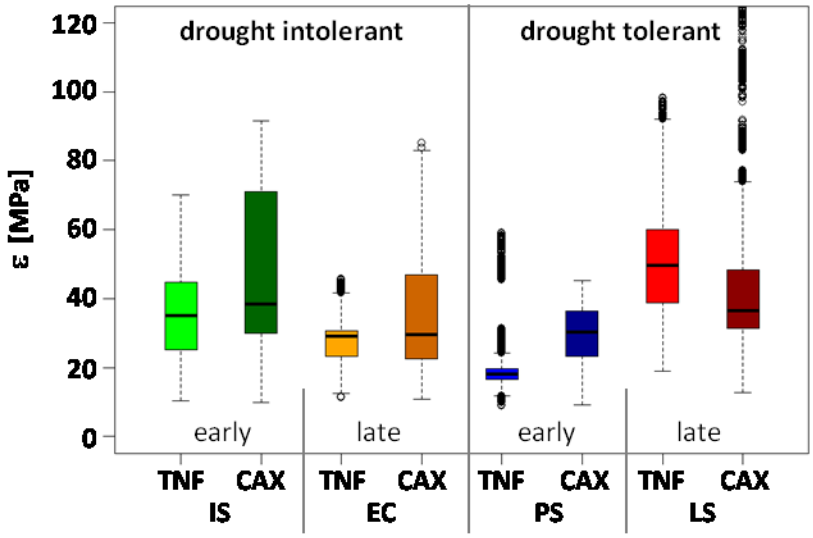

Figure 3.3. Boxplots showing the distribution of the leaf bulk modulus of elasticity (ε, MPa) for each plant functional type measured at the Tapajós (TNF) and Caxiuanã (CAX) National Forests. IS: *Inga* species represent early-successional drought-intolerant. EC: *Eschweilera coriacea* represent late-successional drought-intolerant. PS: *Protium* species represents early-successional drought-tolerant. LS: *Licania* species represents late-successional drought-tolerant. Note: outliers for LS at CAX extend to 186 MPa.

Table 3.3. Median estimates with 95% confidence intervals of measured leaf and xylem traits for the species at the Tapajós (TNF) and Caxiuanã (CAX) National Forests, which are representative of each of the four plant functional types. IS: *Inga* species. EC: *Eschweilera coriacea*. PS: *Protium* species. LS: *Licania* species. TLP: leaf tugor loss point. π_o: leaf osmotic potential. Xylem-P_{50}: water potential when 50% of conductance is lost.

Drought sensitivity	Successional type (Species ID)	Trait:	TLP		π_o		Xylem-P_{50}	
		Site:	CAX	TNF	CAX	TNF	CAX	TNF
Intolerant	Early (IS)		−1.64 +0.15,−0.32	−1.51 +0.11,−0.33	−1.82 +0.12,−0.25	−1.69 +0.11,−0.18	−1.4±0.1	−1.1±0.1
	Late (EC)		−1.64 +0.62,−0.45	−1.56 +0.15,−0.13	−1.78 +0.39,−0.43	−1.56 +0.07,−0.11	−1.2±0.1	−2.0±0.1
Tolerant	Early (PS)		−2.38 +0.29,−0.33	−2.53 +0.62,−0.19	−2.44 +0.21,−0.25	−2.35 +0.35,−0.22	−2.3±0.1	−1.8±0.1
	Late (LS)		−2.46 +0.66,−0.45	−2.31 +0.38,−0.79	−2.52 +0.40,−0.30	−2.51 +0.42,−0.67	−2.2±0.2	−1.4±0.2

Dawn and midday ψ_{lf} estimates for the four CAX species are reported for both the control and drought treatment plots in Table 3.4. Differences in both dawn and midday ψ_{lf} were not organized according to the four PFT classifications. Dawn ψ_{lf} for all four species were near zero in the control plots and only *Protium* was considerably (and significantly) more negative than zero (-1.15 MPa) in the drought plot (Table 3.4). The control plot *Inga* and *Licania* midday ψ_{lf} were considerably higher (-0.38 and -0.14 MPa, respectively) than *Eschweilera* and *Protium* ψ_{lf} (-0.74 and -1.42 MPa, respectively). There was also a significant reduction in midday ψ_{lf} of *Eschweilera*, *Protium* and *Licania* (Table 3.4) growing in the drought plots.

Table 3.4. Dawn and midday leaf water potential (Y_{lf}, MPa) measured at Caxiuanã in the control and treatment plots on 11/18/2011. Each species represents one of the four plant functional types evaluated in this study: drought tolerant versus intolerant and early versus late successional.

Drought Tolerance	Succession	Species	Midday ψ_{lf} (MPa)		Dawn ψ_{lf} (MPa)	
			Control	Treatment	Control	Treatment
Intolerant	Early	*Inga alba*	0.38±0.06	0.44±0.17	0.04±0.01	0.03±0.01
	Late	*Eschweilera coriacea*	0.74±0.08*	1.95±0.13*	0.08±0.01*	0.04±0.01*
Tolerant	Early	*Protium tenuifolium*	1.42±0.03*	1.91±0.04*	0.18±0.04*	1.15±0.10*
	Late	*Licania octandra*	0.14±0.02*	0.35±0.04*	0.07±0.01	0.06±0.01

Xylem vulnerability

With the exception of the late-successional species (*Eschweilera* and *Licania*) at TNF, the drought-intolerant species (*Inga* and *Eschweilera*) were more vulnerable to xylem cavitation under decreasing xylem pressure compared to the drought-tolerant species (*Protium* and *Licania*) (Fig. 3.4). Xylem-P_{50} of the drought-intolerant species ranged between -1.1 and -1.4 MPa, and between -1.8 to -2.3 MPa for the drought-tolerant

species. However, this pattern was reversed for the two late-successional species at TNF, where the xylem-P_{50} of drought-tolerant species (*Licania*) was -1.4 MPa and -2.0 MPa for the drought-intolerant species (*Eschweilera*). The xylem vulnerability curves were steeper for the drought-intolerant species compared to the drought-tolerant species (Fig. 3.4).

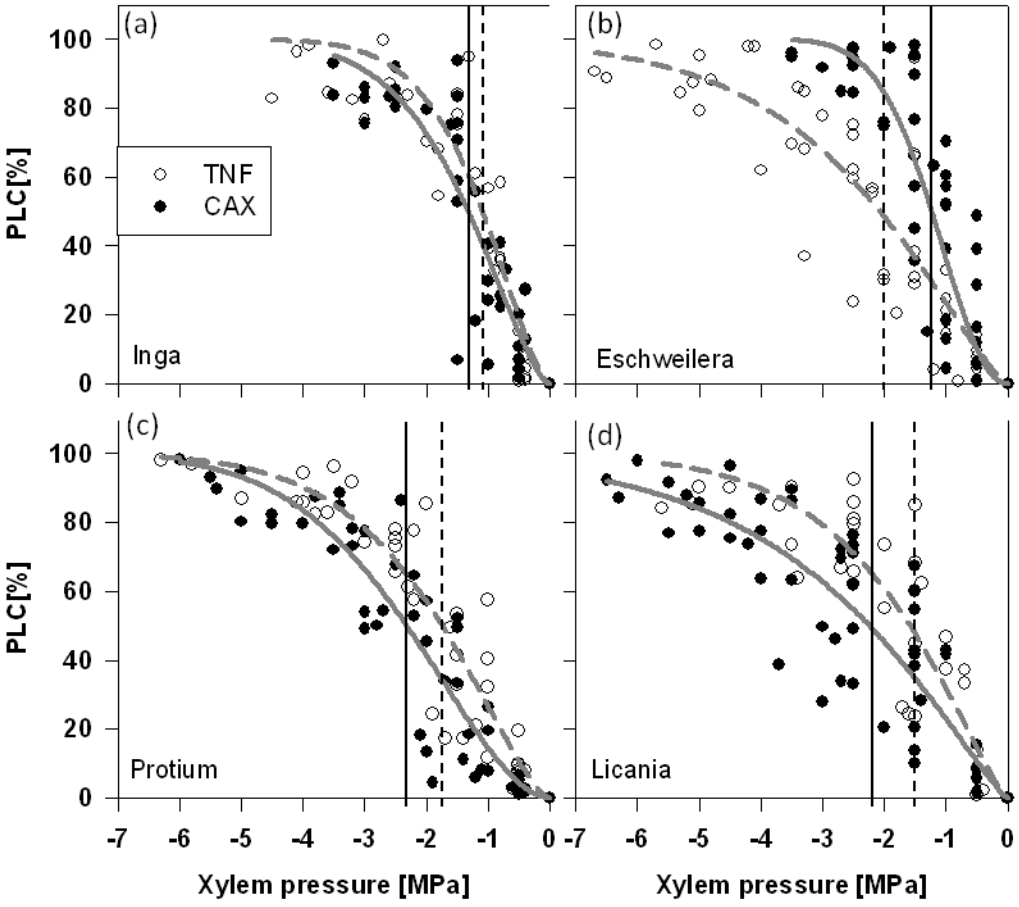

Figure 3.4. Xylem vulnerablity curves showing the percent loss of conductivity (PLC) with decreasing xylem pressure (MPa) of the selected species representing the four plant functional types measured at the Tapajós (TNF, open symbols) and Caxiuanã (CAX, closed symbols) National Forests. (a) *Inga*: early-successional drought-intolerant. (b) *Eschweilera*: late-successional drought-intolerant. (c) *Protium* early-successional drought-tolerant. (d) *Licania*: late-successional drought-tolerant. Vertical lines indicate point when 50% loss of conductance (P_{50}) was reached for the TNF (dashed) and CAX (solid) species.

Geographic and genus level conservation of traits

Eschweilera coriacea and *Inga alba* were found at both research sites with a sufficient number of canopy-sized individuals to construct robust p-v and xylem vulnerability curves. Because only two canopy sized individuals of *I. alba* occurred in the drought plots at CAX in 2011, *I. gracilifolia* was measured to supplement the *Inga* TLP data. No significant differences were detected between the *I. alba* and *I. gracilifolia* p-v curves (data not shown). There were no common species for *Protium* and *Licania* between the two research sites, thus two different species were selected for each genus.

Although the sites were separated by 400 km and soil properties differed markedly, *TLP*, π_o, and xylem-P_{50} were generally conserved at the genus level across the two sites for all plant functional types, with the exception of xylem-P_{50} of *Eschweilera* and *Licania* (Table 3.3, Figs. 3.1, 3.2, 3.4). Moreover, the pattern and magnitude of how the traits differed between drought-tolerant versus intolerant plant functional types was also conserved for all three traits, with the exception of *Eschweilera* and *Licania* xylem-P_{50} at TNF. Hence, at each site the *TLP*, π_o and xylem-P_{50} of the drought-intolerant plant functional type was always 0.7 to 0.9 MPa higher than the drought-tolerant type (Table 3.3).

Discussion

In this study, we investigated how variations in leaf hydraulic traits (*TLP*, π_0, ε) and xylem vulnerability (xylem-P_{50}) correlate with drought tolerance and successional type of

mature tropical trees growing across the eastern Amazon rainforest. Tree species from four genera were selected, each representing one of four different plant functional types (summarized in Table 3.2). Variations in these traits have been evaluated between global biomes, within the tropical forest biome, and between differing climate regions within the tropics (Choat *et al*., 2007, Baltzer *et al*., 2008; Bartlett *et al*., 2012; Anderegg, 2014). Results from these previous studies implied that differences in hydraulic traits confer drought tolerance. However, our study is the first to explicitly link measured differences in hydraulic traits to differential mortality rates of mature tropical tree species that were experimentally exposed to chronic drought.

Our results supported hypothesis one (H1) that drought adapted species can tolerate more negative water pressures before *TLP* (Fig. 3.1), π_o (Fig. 2) and xylem-P_{50} (Fig. 3.4) are reached (Table 3.3). The drought-tolerant PFTs gained lower *TLPs* through π_0 adjustments (Fig. 3.2) and not through ε adjustments (Fig. 3.3). Our within-ecosystem result supports a more general hypothesis about π_o being the dominant control over *TLP* across biomes (Bartlett *et al*., 2012). Gaining a lower *TLP* through π_o requires active transport of solutes into the cell, which provides a physiological explanation for the observed increases in foliar respiration in the drought treatment plots at CAX (Metcalfe *et al*., 2010). At present, this *cost* for being drought-tolerant is poorly represented in dynamic vegetation models (Powell *et al*., 2013). Therefore, future research is needed to constrain the theoretical linkage between active solute transport for regulating turgor and total plant carbon balance.

The second hypothesis (H2), leaf hydraulic traits (*TLP*, π_o and ε) and xylem-P_{50} would differ between early and late-successional species, was not supported by this

study. Our results suggest that variation in wood density is not necessarily a useful proxy for establishing a growth versus drought-tolerance axis of competition for mature trees. At the sapling stage, however, a strong relationship between wood density and cavitation resistance has been found for tropical trees (Markesteijn *et al*., 2011). Indeed, wood density reflects life-history strategies related to succession where slower-growing, shade-tolerant species tend to have denser wood (Poorter *et al*. 2010). Furthermore, variation in rainforest wood density seems to be better explained by the density of fiber cells and fiber cell-wall thickness than by vessel cross-sectional area (Poorter *et al*., 2010).

The spatial separation between the sites includes contrasting soil types, soil depths, water table depths, and meteorological conditions (Table 3.1), which leads to the surprising result that the observed increase in mortality rates and losses in aboveground biomass were similar (Nepstad *et al*., 2007; da Costa *et al*., 2010). However, given the similar ecosystem responses, it was predicted that the plant hydraulic traits would be spatially conserve (H3), which was supported with the only exception being *Licania* and *Eschweilera* xylem-P_{50} (Figs 1-4, Table 3.1). CAX and TNF are separated by approximately 400 km. It should be noted that our two study sites were confined to *terra firme* forests in the eastern portion of the Amazon basin. It is still unclear if these traits will be similarly conserved among these PFTs growing in seasonally inundated forests or forests along the eastern flank of the Andes where on average precipitation is higher and wood density is lower (Baker *et al*., 2004, ter Steege *et al*., 2006).

This study helps to clarify the resistance of the standing population of mature trees to reductions in precipitation. Our results did not support the fourth research hypothesis (H4) that there would be plasticity in the hydraulic traits of the early-

successional and drought-tolerant PFTs. Both the p-v curves and xylem vulnerability curves of the control and drought plots at CAX almost completely overlapped (Figs. S3.2, S3.3). Therefore, our results imply that the hydraulic systems of these *terra firma* tropical trees have a low capacity to acclimate to a drier climate. Plasticity in the measured plant hydraulic traits during the initial years of the drought experiment could not be ruled out; as our measurements were made in the 8th year of the drought experiment at CAX and after the study concluded at TNF. It is possible that a competitive release for water may have caused these traits to reverted back to pretreatment values after the 20% reduction in aboveground biomass occurred in the third year (Nepstad *et al*., 2007, da Costa *et al*., 2010). For example, the reduction in biomass may have partially alleviated the water stress in the drought plots by increasing per capita available soil moisture. However, any plasticity that occurred in the drought treatment plots likely would have been minor since the mean seasonal adjustment in *TLP* across all tropical species is <15% (Bartlett et al., 2014).

At longer ecological and evolutionary time scales, trait differences that occur during the seedling and sapling stage and during ontogeny may be critical for determining the long-term composition and resilience of tropical forests after a drought induced dieback. Plastisticy has been demonstrated to occur in xylem conductivity of early-successional saplings when its light environment increases (Campanello *et al*., 2008). Also, species distribution patterns across the Isthmus of Panama are determined by niche differentiation along soil moisture gradients where selection occurs during both the seedling and adult stages (Engelbrecht *et al*., 2007).

The leaf water potential measurements were taken near the end of the 2011 dry season at CAX (Table 3.4); a period when the ecosystem approaches its lowest available soil moisture (da Costa *et al*. 2010). Soil moisture measurements during this period indicated significantly less available soil water in the drought plots through at least a 2 m rooting depth (Fig. S3.1). *Protium tenuifolium* (early-successional drought-tolerant) was the only species measured in the treatment plot that began the day with its leaves under water stress (Table 3.2). Fisher *et al*. (2006) also measured leaf water potentials on 7 tree species growing the CAX experimental plots and found that all 7 species used an isohydric strategy to protect themselves from drought. An isohydric strategy is one where the stomata close at a set water potential threshold, which is typically well below the xylem-P_{50}, in order to maintain a relatively large safety margin. In this study, *Eschweilera* and *Protium* in the drought plots had significant decreases in their midday leaf water potentials (Table 3.2), which decreased their safety margins with respect to their xylem-P_{50}; hence, indicating that an anisohydric strategy may also be common.

Variation in the hydraulic traits exists among tropical tree species (Anderegg, 2014). However, prior to this study it was not clear if this variation in hydraulic traits correlated with differential mortality rates during droughts, or if it was related to a separate ecological process such as successional dynamics (Campanello *et al*., 2008, Markesteijn *et al*., 2011). Our results provide strong evidence that hydraulic traits determine drought-tolerance plant functional type and that these traits are orthogonal to the axis of variation for traits that determine successional type.

There is a critical need for improving the representation of functional diversity in dynamic vegetation models used for predicting how forests across the Amazon basin will

respond to severe and chronic drought (Anderegg, 2014). These models currently use a single water-stress parameterization for the moist tropical rainforest PFT (Sakaguchi *et al*., 2011; Powell *et al*., 2013). This study emphasizes the need to establish additional PFTs with contrasting water-stress parameterizations in dynamic vegetation models when these models are used to evaluate the effects of severe drought on forest ecosystems. There is not yet strong support for representing spatial (Figs. 3.1-3.4) and temporal (Figs. S3.2, S3.3) variation in hydraulic traits within each new tropical PFT. This study also provides critical information about the distributions of the error associated with *TLP* (Table 3.3, Figs. 3.1, S3.4) and xylem-P_{50} (Table 3.3) which can be used to constrain the different water-stress formulations the models. Finally, representing the variation in both xylem vulnerability and stomatal sensitivity to decreasing water pressure allows for testing the evolutionary stability of contrasting strategies during past episodes of extreme drought.

The air injection method only tests xylem vulnerability to cavitation that arises from the air seeding hypothesis, where air is drawn into vessels under tension through pit membrane pores (Tyree and Zimmerman, 2002). The air injection method does not test xylem vulnerability to the nucleation of voids developing either spontaneously in xylem water under tension or from seeding by hydrophobic imperfections on the vessel walls. However, the negative xylem pressure required to induce spontaneous nucleation is well beyond the injection pressures that eliminated flow in this study. Air seeding arising from defects on vessel walls cannot be entirely ruled out; however defects do not confer a known beneficial trade-off unlike *weaker* pit membranes. In fact, pit membranes can account for >50% of the xylem hydraulic resistance (Choat et al. 2008), which would be

reduced by more porous (i.e. weaker) membranes. Therefore, it is difficult to invoke a selective pressure that allows for the persistence of a vessel-wall-defect gene in relatively high abundances (Tyree and Zimmerman, 2002).

Conclusions

This study provides valuable insight into the traits controlling drought tolerance of tropical rainforest trees and provides much needed information for parameterizing more realistic water-stress functions in terrestrial biosphere models. Evidence from this study supports H1 and rejects H2 thereby suggesting that traits associated with drought tolerance are orthogonal to wood density, which is an important life history trait associated with succession. The evidence also supports H3 and rejects H4, thus suggesting that hydraulic traits of *terra firma* trees are largely conserved spatially and temporally. However, lack of plasticity in hydraulic traits indicates that mature trees belonging to the drought-intolerant functional type are vulnerable to reductions in precipitation because of their limited ability to adjust. Finally, variability in plant hydraulic traits does exist between tropical tree species, and this variability may have been and will be critical in determining the fate of the Amazon rainforest if precipitation patterns change.

Acknowledgments

This research was funded by a National Science Foundation Doctoral Dissertation Improvement Grant (NSF award # DEB-1110540), the National Science Foundation Partnership for International Research and Education in Amazon Climate Interactions grant (NSF award #OISE-0730305), and graduate research funding provided by the Department of Organismic and Evolutionary Biology, Harvard University. I thanko the Museu Paraense Emilio Goeldi, the LBA office in Santarém, and the many dedicated field technicians who provided logistical support and assistance collecting samples. I am extremely grateful to Jim Wheeler, Tony Rockwell, and Missy Holbrook for providing me with their time and expertise in training me on the measurement techniques. I am also grateful to Kathy Ran and Alex Oliveira for assisting me in the field.

References

Anderegg WRL (2014) Spatial and temporal variation in plant hydraulic traits and their relevance for climate change impacts on vegetation. *New Phytologist*, 205, 1008-1014. doi: 10.1111/nph.12907.

Baker TR, Phillips OL, Malhi Y, et al. (2004) Variation in wood density determines spatial patterns in Amazonian forest biomass. *Global Change Biology*, 10, 545–562, doi: 10.1111/j.1529-8817.2003.00751.x.

Baltzer JL, Davies SJ, Bunyavejchewin S, Noor NSM (2008) The role of desiccation tolerance in determining tree species distributions along the Malay–Thai Peninsula *Functional Ecology*, 22, 221–231 doi: 10.1111/j.1365-2435.2007.01374.x

Barr AG, Richardson AD, Hollinger DY, *et al.* (2013) Ude of change-point detection for friction-velocity threshold evaluation in eddy-covariance studies. *Agricultural and Forest Meteorology*, 171-172, 31-45. doi: 10.1016/j.agrformet.2012.11.023.

Bartlett MK, Scoffoni C, Sack L (2012) The determinants of leaf tugor loss point and prediction of drought tolerance of species and biomes: a global meta-analysis. *Ecology Letters*: 15, 393-405. dio: 10:1111/j.1461-0248.2012.01751.x.

Bartlett MK, Zhang Ya, Kreidler N, Sun S, Ardy R, Cao K, Sack L (2014) Global analysis of plasticity in turgor loss point, a key drought tolerance trait. *Ecology Letters*, 17: 1580-1590. doi: 10.1111/ele.12374

Brando PM, Nepstad DC, Davidson EA, Trumbore SE, Ray D, Camargo P (2008) Drought effects on litterfall, wood production and belowground carbon cycling in an Amazon forest: results of a throughfall reduction experiment Phil. Trans. R. Soc. B (2008) 363, 1839–1848. doi:10.1098/rstb.2007.0031

Brodribb TJ, Holbrook NM, Edwards EJ, Gutiérrez MV (2003) Relations between stomatal closure, leaf tugor and xylem vulnerability in eight tropical dry forest trees. *Plant, Cell and Environment,* 26, 433-450.

Campanello PI, Gatti MG, Goldstein G (2008) Coordination between water-transport efficiency and photosynthetic capacity in canopy tree species at different growth irradiances. *Tree Physiology*, 28, 85-94.

Choat B, Sack L, Holbrook NM (2007) Diversity of hydraulic traits in nine *Cordia* species growing in tropical forests with contrasting precipitation. *New Phytologist*, 175, 686-698. doi: 10.1111/j.1469-8137.2007.02137.x

Choat B, Cobb AR, Jansen S (2008) Structure and function of bordered pits: new discoveries and impacts on whole-plant hydraulic function. *New Phytologist*, 177, 608-626. doi: 10.1111/j.1469-8137.2007.02317.x

Coe MT, Marthews TR, Costa MH, *et al*. (2013) Deforestation and climate feedbacks threaten the ecological integrity of south southeastern Amazonia. Phil Trans R Soc B 368: 20120155. doi.org/10.1098/rstb.2012.0155

da Costa ACL, Galbraith D, Almeida S, *et al.* (2010) Effect of 7 yr of experimental drought on vegetation dynamics and biomass storage of an eastern Amazonian rainforest. *New Phytologist* 187: 579–591. doi: 10.1111/j.1469-8137.2010.03309.x

Engelbrecht BMJ, Comita LS, Condit R, Kursar TA, Tyree MT, Turner BL, Hubbell SP (2007) Drought sensitivity shapes species distribution patterns in tropical forests. *Nature*, 44, 80-83.

Fearnside PM (1997) Wood density for estimating forest biomass in Brazilian Amazonia. *Forest Ecology and Management*, 90, 59-87.

Fisher RA, Williams M, Lobo do Vale, da Costa AL, Meir P (2006) Evidence from Amazonian forest is consistent with isohydric control of leaf water potential. *Plant, Cell and Environment* 29: 151-165.

Fisher RA, Williams M, da Costa AL, Malhi Y, da Costa RF, Almeida S, Meir P (2007) The response of an Eastern Amazonian rain forest to drought stress: results and modelling analyses from a throughfall exclusion experiment. *Global Change Biology* 13: 2361-2378.

Fonti P, von Arx G, García-González I, Eilmann B, Sass-Klaassen U, Gärtner H, Eckstein (2010) Studying global change through investigation of the plastic responses of xylem anatomy in tree rings. *New Phytologist*, 185, 42-53. doi: 10.1111/j.1469-8137.2009.03030.x.

Galbraith D, Levy PE, Sitch S, Huntingford C, Cox P, Williams M, Meir P (2010) Multiple mechanisms of Amazonian forest biomass losses in three dynamic global vegetation models under climate change. *New Phytologist*, 187, 647-665. doi: 10.1111/j.1469-8137.2010.03350.x

Hartmann H (2011) Will a 385 million year-struggle for light become a struggle for water and for carbon? – How trees may cope with more frequent climate change-type drought events. *Global Change Biology*, 17, 642-655. doi: 10.1111/j.1365-2486.2010.02248.x

Joetzjer E, Douville H, Delire C, Ciais P (2013) Present-day and future Amazonian precipitation in global climate models: CMIP5 versus CMIP3. *Climate Dynamics*. doi: 10.1007/s00382-012-1644-1

Malhi Y, Roberts JT, Betts RA, Killeen TJ, Li W, Nobre CA (2008) Climate change, deforestation, and the fate of the Amazon. *Science* 319: 169. doi: 10.1126/science.1146961

Markesteijn L, Poorter L, Bongers F, Paz, H, Sack L (2011) Hydrualics and life history of tropical dry forest tree species: coordination of species' drought and shade tolerance. *New Phytologist*, 191, 480-495. doi: 10.1111/j.1469-8137.2011.03708.x

McDowell N, Pockman WT, Allen CD, *et al*. (2008) Mechansims of plant survival and mortality during drought: why do some plants survive while other succumb to drought? *New Phytologist*, 178, 719-739. doi: 10.1111/j.1469-8137.2008.02436.x.

McDowell N, Ryan MG, Zeppel MJB, Tissue D (2013) Improving our knowledge of drought-induced forest mortality through experiments, observations, and modeling *New Phytologist*, 200,289-293.

Meinzer FC, Johnson DM, Lachenbruch B, McCulloh KA, Woodruff DR (2009) Xylem hydraulic safety margins in woody plants: coordination of stomatal control of xylem tension with hydraulic capacitance. *Functional Ecology*, 23, 922-930. doi: 10.1111/j.1365-2435.2009.01588.x.

Metcalfe DB, Meir P, Aragão LEOC, *et al* .(2010) Shifts in plant respiration and carbon use efficiency at a large-scale drought experiment in the eastern Amazon. *New Phytologist* 187: 608–621. doi: 10.1111/j.1469-8137.2010.03319.x

Nepstad DC, Moutinho P, Dias-Filho MB, *et al.* (2002) The effects of partial throughfall exclusion on canopy processes, aboveground production, and biogeochemistry of an Amazon forest. *Journal of Geophysical Research* 107(D20): 8085. doi:10.1029/2001JD000360.

Nepstad DC, Tohver IM, Ray D, Moutinho P, Cardinot G (2007) Mortality of large trees and lianas following experimental drought in an Amazon forest. *Ecology* 88:2259-2269.

Poorter L, McDonald I, Alarcon A, *et al*. (2010) The importance of wood traits and hydraulic conductance for the performance and life history strategies of 42 rainforest tree species. *New Phytologist* 185: 81-492. doi: 10.1111/j.1469-8137.2009.03092.x.

Powell TL, Galbraith DR, Christoffersen BO, *et al*. (2013) Confronting model predictions of carbon fluxes with measurements of Amazon forests subjected to experimental drought. *New Phytologist*, 200, 350-364. doi: 10.1111/nph.12390

Rosolem R, Shuttleworth WJ, Gonçalves LGG (2008) Is the data collection period of the Large-Scale Biosphere-Atmosphere Experiment in Amazonia representative of long-term climatology? *Journal of Geophysical Research* 113: G00B09, doi:10.1029/2007JG000628.

Ryan MG, Phillips N, Bond BJ (2006) The hydraulic limitation hypothesis revisited. *Plant, Cell and Environment*, 29, 367-381. doi: 10.1111/j.1365-3040.2005.01478.x.

Sperry JS, Saliendra NZ (1994) Intra- and inter-plant variation in xylem cavitation in *Betula occidentalis*. *Plant, Cell and Environment*, 17, 1233-1241.

Sakaguchi K, Zeng X, Christoffersen BJ, Restrepo-Coupe N, Saleska SR, Brando PM (2011) Natural and drought scenarios in an east central Amazon forest: Fidelity of the Community Land Model 3.5 with three biogeochemical models. *Journal of Geophysical Research* 116: G01029. doi:10.1029/2010JG001477.

ter Steege H, Pitman NCA, Phillips OL, *et al*. (2006) Continental-scale patterns of canopy tree composition and function across Amazonia. *Nature*, 443, 444-447. doi:10.1038/nature05134.

Tyree MT, Zimmermann MH (2002) *Xylem Structure and the Ascent of Sap*. Second Edition. Springer-Verlag, New York, USA.

Wheeler JK, Sperry JS, Hacke UG, Hoang N (2005) Inter-vessel pitting and cavitation in woody Rosaceae and other vesselled plants: a basis for a safety versus efficiency trade-off in xylem transport. *Plant, Cell and Environment*, 28, 800-812.

Chapter 4

Improving tropical forest drought responses in dynamic vegetation models: are drought-tolerance plant functional types or a mechanistic representation of plant water movement required?

Abstract

There is a critical need to understand the ecological implications of the predicted drying in many regions of the Amazon basin that may occur by end of this century. Dynamic vegetation models (DVM) have great potential for conducting this evaluation, but they are not currently formulated to make robust predictions about ecosystem drought responses. In this study, two potentially important mechanisms were evaluated for the first time within the framework of the Ecosystem Demography model, a DVM that is formulated to represent fine-scale competition between individuals belonging to different plant functional types with alternative drought tolerance strategies. The following research hypotheses were tested: (a) competition arising from drought-tolerant and intolerant functional diversity, (b) mechanistic plant water transport, or (c) both, are fundamental ecological controls and therefore, must be included in DVMs when used for making drought response predictions of tropical forests. The third hypothesis was confirmed that both greater functional diversity and plant hydrodynamics are required. Plant hydrodynamics capture the size-dependent physiological processes, which in turn enable DVMs to more correctly capture the observed structural shifts associated with size-dependent mortality. Increased functional diversity captures the observed compositional shifts in tropical forest tree species that occurs during extreme droughts. But, including functional diversity alone without the accompanying plant hydrodynamics predicts that the forests will be considerably more resistant to drought than has been observed.

Introduction

Climate models are converging toward a drier climate over significant portions of Amazonia as global climate change intensifies over this century (Joetzjer *et al*., 2013). The drying may occur as intensified wet and dry seasons (Lintner *et al*., 2012) or as increases in dry season length and intensity (Malhi *et al*. 2008, Costa and Pires 2010; Boisier *et al*., 2015). There is a critical need to understand the implications of these potential changes in precipitation on the different forest ecosystems across the Amazon basin because of the numerous and important ecosystem services they provide (Bonan, 2008). Dynamic vegetation models (DVMs) are one of our leading tools for assessing the effects of future perturbations on forested landscapes because of their ability to link biological responses that occur at multiple scales of organization. Early model predictions of the Amazon rainforest forecasted widespread reductions in biomass (Cox *et al*. 2004) and significant compositional shifts toward seasonal forests (Malhi *et al*., 2009). Then, later model predictions suggested changes in precipitation would likely have minor effects on vegetation (Huntingford *et al*., 2013; Powell *et al*., 2013). These contrasting results underscore the need for proper benchmarking to evaluate if DVMs are appropriately formulated for making these predictions.

Two ecosystem scale drought experiments located in the eastern Brazilian Amazon have great potential to serve as one set of benchmarks to test the ability of DVMs to capture ecosystem drought responses (Nepstad *et al*., 2007; Fisher *et al*., 2007; Brando *et al*., 2008; da Costa *et al*., 2010). In these two experiments, 50% of the incoming precipitation was intercepted over a 1-ha plot and diverted off-site. Although separated by 400 km and having contrasting soil types (clay vs. sand), there was

remarkable consistency in the drought responses of the two ecosystems. At both sites, aboveground biomass (*AGB*) was reduced by approximately 22% after three years of sustained drought (Brando *et al*., 2008; da Costa *et al*., 2010). The large upper canopy trees (diameter at breast height (dbh) > 40 cm) were the most vulnerable to the experimental drought, while the subdominant trees (dbh < 20 cm) were marginally affected (Nepstad *et al*., 2007; da Costa *et al*., 2010). There were also differential mortality rates between species, with some showing no increase under the drought treatment (da Costa *et al*., 2010). Finally, autotrophic respiration, most notably in the leaves, increased in trees exposed to the drought (Metcalfe *et al*., 2010b). A detailed evaluation of six land surface models, four of which were DVMs, revealed a limited ability by all to capture many or all of these key results (Powell *et al*., 2013).

Under present climate conditions, DVMs are able to reasonably capture the spatial variability of *AGB* across the Amazon basin (Zhang *et al*., 2015). This result in part arises because water is not typically a limiting resource in the Amazon rainforest (Nemani *et al*., 2003; Huytra *et al*., 2007); and therefore under well-watered conditions, only temperature, humidity deficit and CO_2 concentration near the leaf surface are needed to represent stomatal conductance (Leuning, 1995). However, during droughts, the soil moisture deficit must be accounted for in the calculation of stomatal conductance (Baldocchi, 1997).

It is not clear how sophisticated soil water-stress formulations need to be within DVMs. Two modifications to the biological representations of water-stress and water-transport in DVMs are proposed here for improving model predictions of tropical forest drought responses. The first proposal requires additional functional diversity to more

accurately reflect the range of drought tolerance adaptations. For example, DVMs currently use a single parameterization to represent the wide variation in xylem vulnerablility to cavitation (Anderegg, 2014). An alternative proposal is that the mechanism of water-transport through the soil-plant-atmosphere continuum must be represented with considerably more detail (Fisher *et al*., 2007; Sakaguchi *et al*., 2011; Sperry and Love, 2015). These two proposals are not necessarily mutually exclusive. These formulations are incorporated into the Ecosystem Demography model, a DVM that is formulated to represent fine-scale competition between individuals that belong to different plant functional types with alternative drought tolerance strategies. This analysis tests the hypothesis that (a) drought-tolerant and intolerant functional diversity, (b) mechanistic plant water transport, or (c) both, may be fundamental ecological controls during episodes of severe soil moisture deficits and therefore, must be included in DVMs when used for making drought response predictions of tropical forests.

Model development

The Ecosystem Demography model

The Ecosystem Demography model, version 2 (ED2, Medvigy *et al*., 2009) is a state of the art dynamic vegetation model (DVM) ideally formulated to evaluate the research hypotheses of this analysis. ED2 simultaneously tracks hydrology, land-surface biophysics, soil carbon and biogeochemistry for multiple tropical plant functional types (PFTs) (Moorcroft *et al*., 2001). One important innovation of ED2 relevant to this study is that it bridges the gap between fine-scale (sub-grid) and landscape level processes by

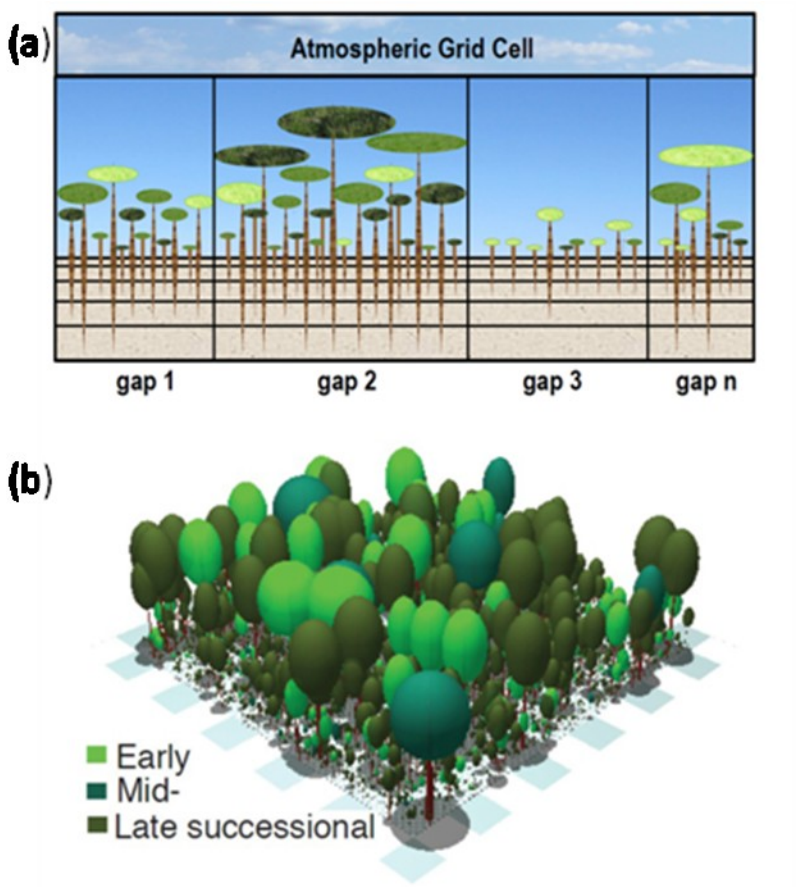

Figure 4.1. Panel (a) graphically illustrates how ED2 represents the structure and composition of a simulated forest within one atmospheric grid cell. Sub-grid scale gaps are defined by age since disturbance and canopy structure and have independent soil layers. Gap areas are defined by parcels with similar properties; yet are not equal in size or necessarily contiguous in space. Panel (b) shows the mosaic canopy structure of a potential forest in one grid cell that results from the dynamics of competition.

representing competition between discrete demographic groups (Fig. 4.1). Competition is tracked through sub-grid scale mortality and subsequent reproduction and growth of similarly aged cohorts and PFTs. This unique feature can be adapted to also evaluate the competitive advantages of differing drought tolerance strategies within and between PFTs. ED2 incorporates a complete representation of land-surface biophysics that explicitly solves for the carbon, water and energy fluxes of the land surface including a

multilayer soil model that better represents soil moisture dynamics. As a result, ED2 can either be run off-line using six standard meteorological forcing variables—precipitation, pressure, radiation, wind-speed, temperature, and humidity, or coupled to the Regional Atmospheric Modeling System, which allows for biophysical feedbacks to the atmosphere during regional runs.

Table 4.1. Explanation of model variables and parameters

Symbol	Definition	Value	Units
model variables:			
B_{ri}	Root biomass a soil layer *i*		Unitless
C_s	Stem capacitance		kg H_2O m^{-3}
D	Total canopy demand for soil water (EDor)		kg H_2O m^{-2} s^{-1}
gx	Xylem conductance		kg H_2O m^{-2} s^{-1} MPa^{-1}
h_t	Tree height		m
i	Index of vertical layer		
P_g	Leaf-level gross photosynthesis		μmol CO_2 m^{-2} s^{-1}
P_n	Leaf-level net photosynthesis		μmol CO_2 m^{-2} s^{-1}
S_i	Supply of available water in layer i (EDor)		kg H_2O m^{-2} s^{-1}
T_{leaf}	Leaf temperature		°C
T_{max}	Maximum evapotranspiration		kg H_2O m^{-2} s^{-1}
TLP	Turgor loss point of leaf		MPa
V_s	Volume of stem wood		m^3
z	Conductive path length		m
β_i	Soil water-stress factor a for soil layer *i*	0-1	Unitless
β_t	Total soil water-stress factor integrated over the soil column	0-1	Unitless
θ_i	Volumetric soil water content in soil layer *i*		m^3 m^{-3}

Table 4.1 continued.

Symbol	Definition	Value	Units
Ψ_l	Leaf water potential		MPa
Ψ_s	Soil water potential		MPa
model parameters:			
a1	Curve fitting parameter	DT: 3.00 DI: 1.15	
a2	Curve fitting parameter	DT: 2.00 DI: 2.50	
c1	Empirical vulnerability curve fitting parameter	DT: 2.55 DI: 2.45	
c2	Empirical vulnerability curve fitting parameter	DT: 1.47 DI: 1.80	
c3	Empirical curve fitting parameter	DT: 2.83 DI: 1.67	
c4	Empirical curve fitting parameter	DT: 3.00 DI: 3.50	
g	Acceleration of gravity	9.8	$m\ s^{-2}$
hp	Height penalty parameter	1.0-1.04	Unitless
K_w	Soil-plant conductivity parameter	1.4260×10^{-5}	$m^3\ s^{-1}$ (kg C root)$^{-1}$
$K_{x,max}$	Maximum xylem conductivity parameter	DT: 3.0 DI: 3.3	kg H_2O m^{-3} s^{-1} MPa^{-1}
SLA	Specific leaf area. See Model Development	Variable	m^{-2} kg
ρ_{water}	Density of water	1000	kg H_2O m^{-3}
ρ_{wood}	Wood density. See Model Development	Variable	g cm^{-3}
θ_f	Volumetric soil water content at field capacity	CAX: 0.193 TNF: 0.327	$m^3\ m^{-3}$
θ_w	Volumetric soil water content at the wilting point	CAX: 0.089 TNF: 0.246	$m^3\ m^{-3}$
θ_{wood}	Wood water content coefficient	2.0	kg H_2O m^{-5}
Ψ_w	Soil matrix potential at wilting point	-153	m

For this analysis, the original ED2 formulation (denoted as EDor) was configured to represent competition between two successional (early and late) tropical tree PFTs through inherent differences in photosynthesis, growth and mortality. For parameter derivations, see Moorcroft *et al*., (2001) and Medvigy *et al*., (2009). PFTs with higher wood density (ρ_{wood}) have lower mortality rates compared to PFTs with lower wood density. PFTs initially designated as 'early', 'mid' and 'late' successional were used during the bare-ground spin-up (see protocol below). At both study sites, only two of the three PFTs became established in the equilibrium forests from the bare-ground spin-up. At both sites the 'late' PFT (ρ_{wood} = 0.90 g cm^{-3}) became established and is designated as the late-successional type here. The 'early' (ρ_{wood} = 0.53 g cm^{-3}) PFT became established at CAX and the 'mid' (ρ_{wood} = 0.71 g cm^{-3}) became established at TNF; but here both are designated as the early-successional type for their respective sites. Specific leaf area (*SLA*) also varied between the three spin-up PFTs: both sites late-successional *SLA* = 9.66, CAX early *SLA* = 16.02, TNF early *SLA* = 11.64 m^2 kg^{-1}-C. EDor includes a tunable parameter that encompasses the conductivity of the entire soil-to-leaf system (K_W, m^3 kg-C^{-1} yr^{-1}). K_W is the same across PFTs and remains static as water-stress builds.

Leaf level photosynthesis (*P*) and transpiration (*T*) are calculated using the Farquhar *et al*. (1980) model (von Caemmerer and Farquhar, 1981; Ball *et al*., 1986) and scaled to the canopy following Leuning (1995), which accounts for the effect of vapor pressure deficit on stomatal conductance. Then, a scaling variable, β (dimensionless), is used to down-regulate *P* (kg CO_2, m^{-2} s^{-1}) and *T* (kg H_2O, m^{-2} s^{-1}) to account for the effect of soil moisture limitation on stomatal conductance:

$$P_n = P_g\beta - (1-\beta)R_l \qquad \text{Eqn. 1a.}$$

$$T_n = T_{max}\beta - (1-\beta)T_{min} \qquad \text{Eqn. 1b.}$$

Subscripts *n* and *g* indicate *net* and *gross* photosynthesis or transpiration, respectively, and R_l is leaf respiration. Subscripts *max* and *min* indicate hydraulically unlimited potential transpiration and cuticular transpiration, respectively.

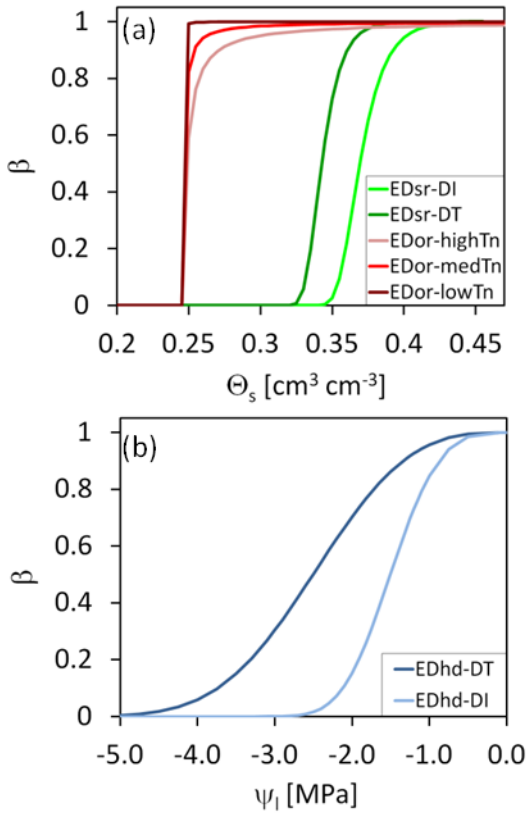

Figure 4.2. Curves representing the β scaling function for the original (EDor, Eqn. 2a), simple resistor (EDsr, Eqn. 3), and hydrodynamic (EDhd, Eqn. 8) formulations. (a) β is a function of soil water content (θ, $cm^3\ cm^{-3}$) as in the *or* and *sr* formulations. The *or* formulation also includes water demand and therefore, diurnally β moves between the upper boundary curve when transpiration T_n is low (0.01 mm hr^{-1}) and the lower boundary curve when T_n is high (0.72 mm hr^{-1}). (b) β is a function of leaf water potential (Ψ_l, MPa) as in the *hd* formulation. *DT* indicates drought-tolerant. *DI* indicates drought-intolerant.

Soil water-stress in EDor uses a phenomenological relationship between soil moisture supply (S) and transpirational demand (D):

$$\beta_t = \sum_i \frac{1}{1+\frac{D}{S_i}} \quad \text{Eqn. 2a}$$

$$S_i = K_w \, \theta_i \, B_{ri} \quad \text{Eqn. 2b}$$

$$D = T_{max} \, LAI \quad \text{Eqn. 2c}$$

Soil moisture supply is a function of K_w, volumetric soil moisture (θ, $m^3\ m^{-3}$) and root biomass (B_r, kg-C). The niche space for S operates at the gap scale and therefore, leaf-level D of each cohort is scaled by leaf area index (LAI, $m^2\ m^{-2}$) to calculate the demand of all cohorts growing in the gap. The subscript t is the total of β integrated over all soil layers (i). Because this formulation includes both supply and demand, the soil moisture dependent curve along which β operates falls within a range that is dependent on transpiration rates (Fig. 2a). For EDor, the β function is parameterized the same for all tropical PFTs, thus precluding an explicit hydraulic axis of diversity.

Two alternative water-stress formulas were tested. Both formulations also down regulate P and T through the application of β in Eqn. 1. The second formulation (referred to here as EDsr), tests a single-resistor formulation that is a Weibull function of soil water potential (Ψ_s):

$$\beta = \left[-\left(\frac{-\Psi_s}{a_1}\right)^{a_2}\right] \quad \text{Eqn. 3}$$

where a_1 and a_2 are fitting parameters. This is the most parsimonious of the three soil water-stress formulas tested and is common among land surface models (e.g. CLM3.5 (Oleson *et al.,* 2008), IBIS (Foley *et al*., 1996), JULES (Cox, 2001; Clark *et al*., 2011), SiB3 (Sellers *et al.,* 1996)) used to predict drought effects on the Amazon basin (e.g. Cox

et al., 2004; Baker *et al.,* 2008; Harper *et al*., 2010; Sakaguchi *et al*., 2011). EDsr β is different from EDor β in two key ways. First, the β function was parameterized to represent drought-tolerant and intolerant PFTs using the xylem vulnerability curves in Chapter 3 of this dissertation. The early- and late-successional PFTs of EDor were each divided into a drought-tolerant and intolerant PFT, thus increasing the functional diversity to 4 PFTs that explicitly operate along light and soil moisture axes of competition. Second, each PFT-wise parameterization for β in EDsr operates along a single curve that is dependent only on soil moisture *supply* (Fig. 2a), which makes it diurnally static during rain free days (e.g. Fig. 2.10). In all other aspects, the early- versus late-successional PFTs were delineated the same way as EDor for CAX and TNF.

The third formula is a hydrodynamic pipe model that explicitly represents capacitance and hydraulic conductivity of the entire root to shoot path length to estimate change in leaf water potential (Ψ_l) over time (Jones, 1992; Williams *et al*., 1996). When applied to plants, a hydrodynamic pipe model relies on the fundamental assumption that water movement through xylem elements is controlled by pressure and gravitational potential differences, not solute potential differences, and thus can be represented by Darcy's law for water movement through a porous medium. In plants, however, a time lag (approximately 0.5 h for tropical trees) exists between the onset of transpiration and the basal flow of sap because water is initially drawn from storage in the stem (Meinzer *et al*., 2004). This hysteresis can be represented in the pipe model by including a stem capacitor (C_s), which becomes the governing equation in the form:

$$\frac{d\Psi_l}{dt} = \frac{g_x[\Psi_s - \Psi_l - \rho_{water} g h_t] - T_n}{C_s} \qquad \text{Eqn. 4}$$

where g_x represents xylem conductance (kg H_2O m^{-2} s^{-1} MPa). The physical effects of gravity on the transport of water is accounted for with $\rho_{water} g h_t$, which is water density (kg m^{-3}), acceleration of gravity (m s^{-2}) and tree height (m), respectively.

The variation in water-storage capacity of across tropical trees species is not well understood. Recent evidence suggests that wood density is a poor predictor of water storage since it is better explained by fiber cell-wall thickness than by total vessel lumen area (Poorter *et al*., 2010). However, one study found that stem diameter was a better predictor than species for stem water storage (Meinzer *et al*., 2004). Therefore, C_s (kg H_2O m^{-3}) is a function of stem volume (V_s, m^3):

$$C_s = \theta_{wood} V_s \qquad \text{Eqn. 5}$$

where θ_{wood} is a free parameter set equal across all PFTs and converts V_s to kg-H_2O m^{-3}.

Xylem vulnerability to cavitation is accounted for by using a Weibull function that reduces a tunable maximum xylem conductivity parameter ($K_{x,max}$, kg H_2O m^{-3} s^{-1} MPa^{-1}):

$$g_x = \frac{A_x K_{x,max}}{z} \exp\left[-\left(\frac{-\Psi_l}{c_1}\right)^{c_2}\right] \qquad \text{Eqn. 6a}$$

$$z = h_t h_p{}^{h_t} \qquad \text{Eqn. 6b}$$

The cross sectional active xylem area is given by A_x (m^2) and c_1 and c_2 are xylem vulnerability curve-fitting parameters. Xylem conductivity is divided by the path length, z (m), thus converting it to xylem conductance. The power function (Eqn. 6b) was incorporated into the path length to explore the effects of increased hydraulic resistance as trees grow taller (Ryan *et al*., 2006). The dimensionless parameter h_p was adjust between 1.00 (no additional effect beyond gravity) and 1.04 (increases the path length of the tallest trees by a factor of 4).

The new Ψ_l for the next timestep (t+1) is calculated by:

$$\Psi_l^{(t+1)} = \Psi_l^t + \Delta\Psi_l \qquad \text{Eqn. 7}$$

Although the mechanisms controlling stomatal closure are not completely understood and quite complex, there is a strong correlation between Ψ_l and stomatal conductance in tropical trees (Brodribb *et al*., 2003). Therefore, β becomes a Weibull function of Ψ_l in the EDhd formulation:

$$\beta = \left[-\left(\frac{-\Psi_l}{c_3}\right)^{c_4}\right]. \qquad \text{Eqn. 8}$$

where c_3 and c_4 are empirical curve fitting parameters that were tuned to set $\beta = 0.5$ when $\Psi_l = TLP$, the turgor loss point of the leaf (Brodribb *et al*., 2003).

One major advantage of EDhd is that Eqns 4 – 6 represent physiological mechanisms that control water movement through plants and their parameters can be derived directly from empirical measurements. Also, EDhd can be reasonably extrapolated to novel environments because the parameters remain within observed biological boundaries. For Eqn. 6, c_1 and c_2 were obtained from the PFT-dependent xylem vulnerability curves in Figure 3.4. For Eqn 8, the *TLPs* from Figure 3.1 were used to derived c_3 and c_4 for the drought-tolerant and intolerant PFTs. The photosynthetic parameterization for the late-successional type was the same as EDor and for the early-successional type was the same as the CAX early-successional for EDor. *SLA* was set to 21.66 and 15.06 $m^2\ kg^{-1}$-Cand ρ_{wood} was set to 0.60 and 0.85 g cm^{-3} for the early- and late-successional types, respectively. The remaining parameterization was unaltered from EDor.

The parameter values used in this analysis are given in Table 1. In EDor and EDsr, θ_s or Ψ_s is passed from the soil hydraulic module to the photosynthesis module where β is then calculated. In EDhd, Ψ_s is passed from the soil hydraulic module to the hydrodynamic module, which converts Ψ_s to Ψ_l, and then passes Ψ_l to the photosynthesis module where β is calculated (Fig. 4.3) (Xiangtao Xu and David Medvigy, personal communication). The hydrodynamic module was structured to interface with EDor in a manner that retains the original biophysical, ecological and demographic processes (Fig. 4.3) (Xiangtao Xu and David Medvigy, personal communication).

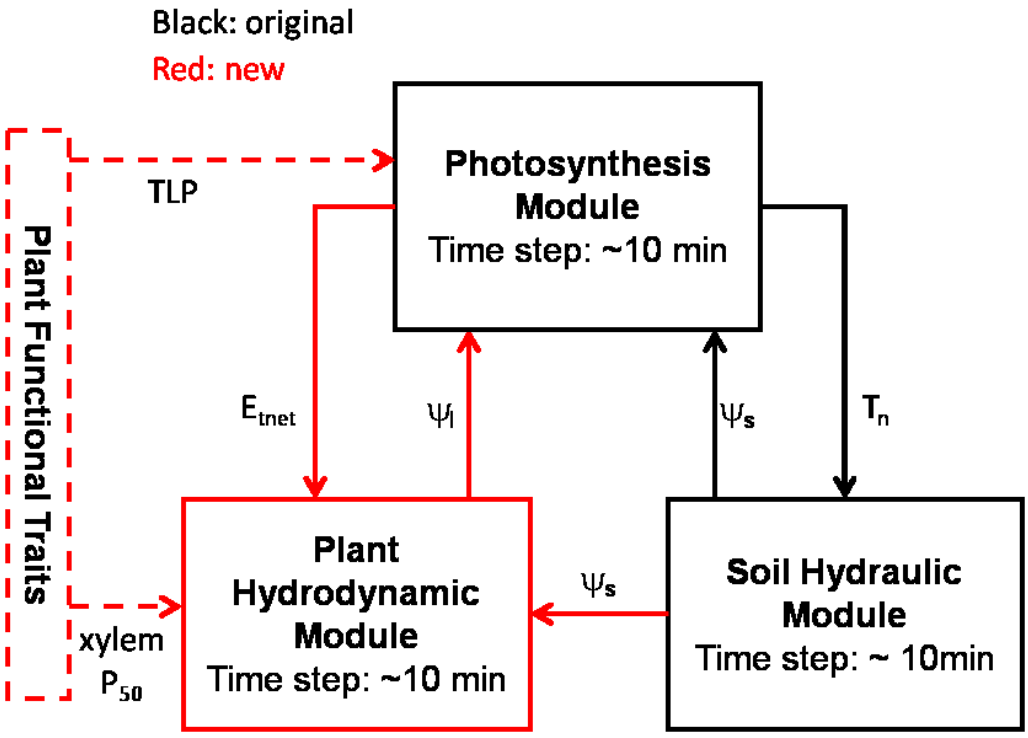

Figure 4.3. Schematic representing the modules from the original ED2 (black) and the new hydrodynamic module (red). Eqns. 4 – 7 are contained in the Plant Hydrodynamic Module. The β functions (Eqns. 2,3,8) are contain within the Photosynthesis Module. Xylem-P_{50} (Figure 3.4) is the plant functional trait used to parameterize Eqn. 6 and turgor loss point (*TLP*) is used to parameterize Eqn 8. Transpiration (T_n), leaf water potential (Ψ_l) and soil water potential (Ψ_s) are passed between modules to drive the hydraulic equations.

Methods

Study sites

Two throughfall exclusion experiments were established in the Caxiuanã (1.737ºS, 51.458ºW) and Tapajós National Forests (2.897ºS, 54.952ºW) Para, Brazil to assess whole ecosystem responses to soil moisture limitation. The two sites are separated by 400 km in the eastern Amazon rainforest. Mean annual precipitation at CAX is 2272 mm (Fisher *et al*., 2007) with a 7 month wet season (>100 mm mo^{-1}) from mid-December to mid-July (Rosolem *et al*., 2008). Mean annual precipitation at TNF is 2000 mm (Nepstad *et al*., 2002) with a 6 month wet season from mid-December to mid-June (Rosolem *et al*., 2008). Rainfall was normal at both sites except for the below average 2003 wet season at TNF (Rosolem *et al*., 2008). The soils at both sites are Oxisol, but the depth to the water table and the texture differs between them. Soils at CAX are comprised of 78% sand and 15% clay and a water table near 10 m during the wet season (Fisher *et al*., 2007). Soils at TNF are comprised of 38% sand and 68% clay and a water table >80 m (Nepstad *et al*., 2002). The aboveground biomass in 2000 for trees > 10 cm dbh at CAX was 20.4 kg C m^{-2} based on the average of 8 published allometric relationships (see Table 1 in da Costa *et al*., 2010). The aboveground biomass in 1999 for trees > 10 cm dbh at TNF was 15.0 kg C m^{-2} based on allometric equations from Chambers *et al*. (2001) (Nepstad *et al*., 2002).

A brief description of the experimental design is given below, but is described in greater detail elsewhere (Nepstad *et al*., 2002; Fisher *et al*., 2007). At each site, a 1-ha control plot and 1-ha treatment plot were established in floristically and structurally similar plots. A 1-m wide trench surrounding each plot separated the surface rooting

zones from the adjacent forests (Nepstad *et al*., 2002). In the treatment plot, a leaky septum was constructed of clear plastic panels 1-2 m above the forest floor and effectively intercepted 50% of total above-canopy precipitation (~60% of throughfall) from reaching the forest floor (Nepstad *et al*., 2002). A network of gutters and the surrounding trench transported the intercepted water off-site. The panels were overturned every 2-3 days to remove accumulated litter. The wooden frame supporting the panels and gutters was not constructed in the control plot due to the high cost and maintenance. The drought treatment at CAX was initiated in 2002 and in 2000 at TNF. At CAX, throughfall was excluded during the entire year, while at TNF throughfall was excluded only during the rainy season (January – June). The drought experiment ran from 2002 to 2008 in CAX and 2000 to 2004 in TNF.

The growth and survivorship of all trees >10cm dbh was recorded each year at both sites. Litterfall was collected using 0.5 m^2 mesh traps, 64 traps in each plot at TNF (Brando *et al*., 2008) and 25 at CAX (Metcalfe *et al*., 2010b). *NEP*, *GPP* and R_e were measured from a nearby eddy covariance tower at TNF (Hutyra *et al*., 2007). At CAX, R_l was estimated as the sum of light and dark respiration, where dark respiration was directly measured on leaves sampled from the canopy of each plot and light respiration was assumed to be 67% of dark respiration (Metcalfe et al. 2010b). R_w was estimated at CAX by multiplying a measured stem respiration rate of 0.6 μmol CO_2 m^{-2} stem-surface-area s^{-1} by the aboveground stem and branch surface area of the plot (Metcalfe *et al*., 2010b). Excised roots ≤5 mm diameter were collected from 0-30 cm depth soil cores to estimate R_r (Metcalfe *et al*., 2007), which is likely a conservative estimate because it does not include respiration from deep or larger roots.

Simulation protocol and meteorological drivers

All simulations followed the same initialization, spin-up, and drought simulation protocol described in detail in Appendix A. Briefly, site-level meteorological drivers were sequentially recycled over 500 years to spin-up, from a near-bare-ground initial condition, an equilibrium potential forest for present day atmospheric CO_2 concentrations (390 ppm). Three PFTs were prescribed for the spin-ups of EDor and EDsr following the parameterization described above; however, only two out of the three PFTs became established at each site (EDor description above). The PFT with higher ρ_{wood} was designated the late-successional type and the PFT with the lower ρ_{wood} was designated the early-successional type. The spin-ups for EDsr and EDhd used only the drought-tolerant early- and late-successional PFTs. After the EDsr and EDhd spin-ups completed, the two successional PFTs were divided equally into drought-tolerant and drought-intolerant PFTs, increasing the total PFTs to 4. The drought simulations were initialized from these spin-ups and run for seven years. The site years were selected to coincide with the actual TFE experiments (CAX: TFE 2002-2008 and TNF: 2000-2006).

The CAX meteorological drivers covered the entire seven year drought simulation (da Costa *et al*., 2010). The TNF meteorological drivers covered 2002 – 2004 (N. Restrepo-Coupe, unpublished data) and were recycled. Both sets of meteorological drivers were measured above the canopies from towers adjacent to the drought experiments. Consistent with the field experiment protocols, precipitation in the TNF simulations was reduced by 50% only during the wet season, while CAX precipitation was reduced by 50% all year. The other meteorological variables (e.g. humidity) were

not manipulated. The drought simulations are denoted throughout this paper as d50 and the control simulations are denoted as d0.

Soil textures were prescribed as reported for each site (see *Study sites*). Otherwise, the physical representation of the soil was standardized across both sites and all models in order to isolate the biological responses to drought under different soil types and meteorological conditions. The maximum soil depth was 8 m with sixteen layers of increasing thickness and free drainage as the lower boundary. Soil hydraulic parameters were derived following Clapp & Hornberger (1978) and Cosby *et al.* (1984). The hydraulic conductivity at field capacity, soil matrix potential at the wilting point, and the soil matrix potential at the air-dry point were defined as 0.1 mm d^{-1}, -1.5 MPa, -3.1 MPa, respectively (Clapp & Hornberger 1978). The maximum rooting depth was set to 5 m for the tallest (35 m) trees. A power function was used to describe the decline in root biomass through the soil profile.

A sensitivity analysis of EDhd was also performed to gain insight into underlying adaptations for drought tolerance. The stem capacitance parameter (θ_{wood}) was adjusted between 0.8 and 2.0. The height penalty parameter (h_p) was adjusted between 1.00 and 1.04. Maximum hydraulic conductivity ($K_{x,max}$) was adjusted between 1.8 and 2.7 for drought-intolerant and 1.5 and 2.5 for drought-tolerant PFTs. The drought phenology parameter (θ_{crit}, m^3 m^{-3}), which increases the soil moisture threshold triggering leaf drop, was adjusted from 0.0 (used for the main set of simulations) to 0.09. The adjustment of θ_{crit} to 0.09 was chosen for continuity with Chapter 2.

Results

Aboveground biomass

The overall ecosystem responses to the drought treatments predicted by the three water-stress formulas are summarized in Figure 4.4 for TNF and Figure 4.5 for CAX. EDor and EDsr marginally underpredict observed total aboveground biomass (*AGB*) (15.0 kg C m^{-2}) in the control plot at TNF (EDor: *AGB* = 10.4, EDsr *AGB* = 11.2 kg C m^{-2}) (Fig. 4.4a,b) and significantly underpredict (EDor: *AGB* = 12.5, EDsr *AGB* = 14.6 kg C m^{-2}) observed *AGB* (20.4 kg C m^{-2}) at CAX (Fig. 4.5 a,b). In contrast, EDhd predicts higher (18.9 kg C m^{-2}) than observed total AGB in the control plots of TNF (Fig. 4.4c), but is in agreement (21.7 kg C m^{-2}) with observed total AGB at CAX (Fig. 4.5c). Both EDor and EDhd capture almost exactly the timing and magnitude of the observed 22% reduction in total *AGB* after 5 years of drought treatment at TNF (Fig. 4.4a,c). In contrast, EDsr predicts a 50% smaller reduction in total *AGB* by the end of the drought treatment at TNF (Fig. 4.4e). All three models predict a <5% reduction in total *AGB* after 8 years in the drought treatment at CAX in comparison to the observed 21% reduction (Fig. 4.5d,e,f).

All three models predict differential drought responses by each PFT for *AGB* (Figs 4.4d,e,f, 4.5d,e,f). At both sites, EDor predicts the early-successional PFT to have a ~15% stronger response to the drought treatment compared to the late-successional PFT (Figs. 4.4d, 4.5d). This pattern is also predicted by EDsr and EDhd. However, the addition of the drought-tolerant and intolerant PFTs in both EDsr and EDhd resulted in both the early- and late-successional drought-intolerant PFTs accounting for most of the reduction in *AGB* in the TNF drought treatment (Figs. 4.4e,f), while at CAX the reduction in *AGB* is largely accounted for by only the early-successional drought-intolerant PFT

(Fig 4.5e,f). Also, EDhd predicts that the early-successional drought-intolerant PFT will be almost completely lost after the 4th year of drought at TNF (Fig. 4.4.f).

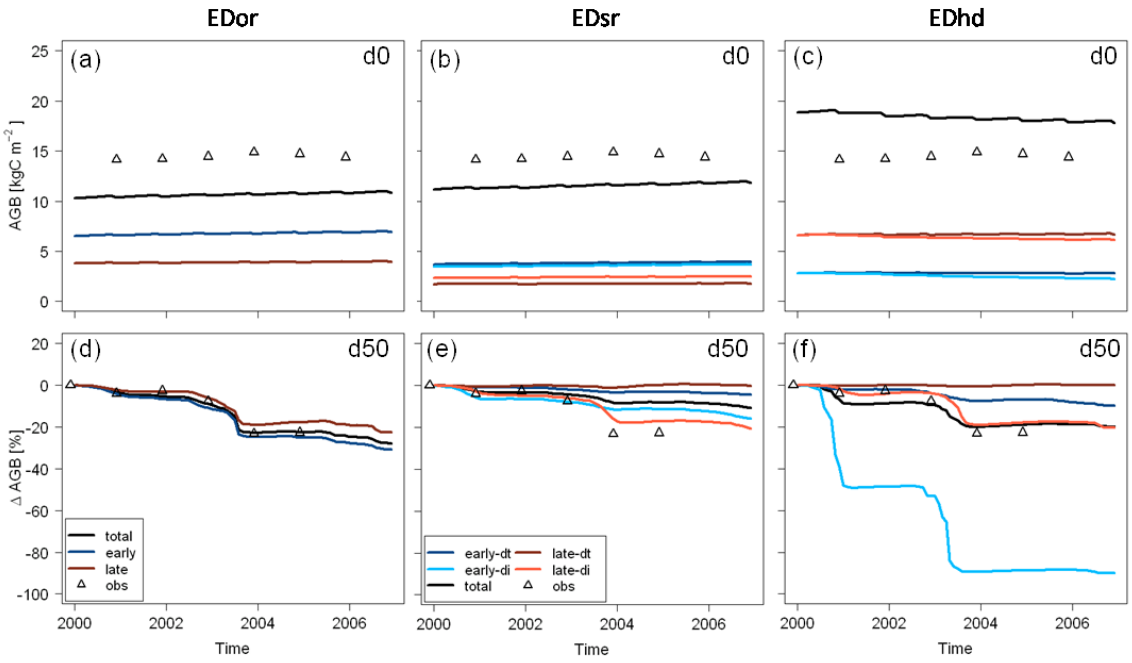

Figure 4.4. Seven year time series of aboveground biomass (*AGB*, kg C m^{-2}) predicted for the Tapajós National Forest using the original (EDor), single resistor (EDsr) and hydrodynamic (EDhd) water-stress formulations. Colored lines indicate early- (blue) and late- (red) successional plant functional types. Darker colors are drought-tolerant (dt), lighter colors are drought-intolerant (di), black is total *AGB*. Open symbols are published annual observations of *AGB* (Brando *et al.,* 2008). d0 and d50 are drought levels indicating a 0% and 50% reduction in precipitation. Panels a – c show the d0 control plot simulations. Panels d –f show the d50 treatment simulations and are presented as the percent the control plot *AGB* was changed (Δ) by the drought.

The reductions in *AGB* was subdivided into three diameter-at-breast-height (dbh) size classes—small (dbh: < 20 cm), medium (dbh: 20 – 40 cm), large (dbh: > 40 cm)—to evaluate if the models predict differential responses between the three size classes. EDor predicts the smallest size-class is the most vulnerable and the largest size class is the most resistant to the drought (Figs. 4.6a,d,g, 4.7a,d,g). Also, EDor predicts

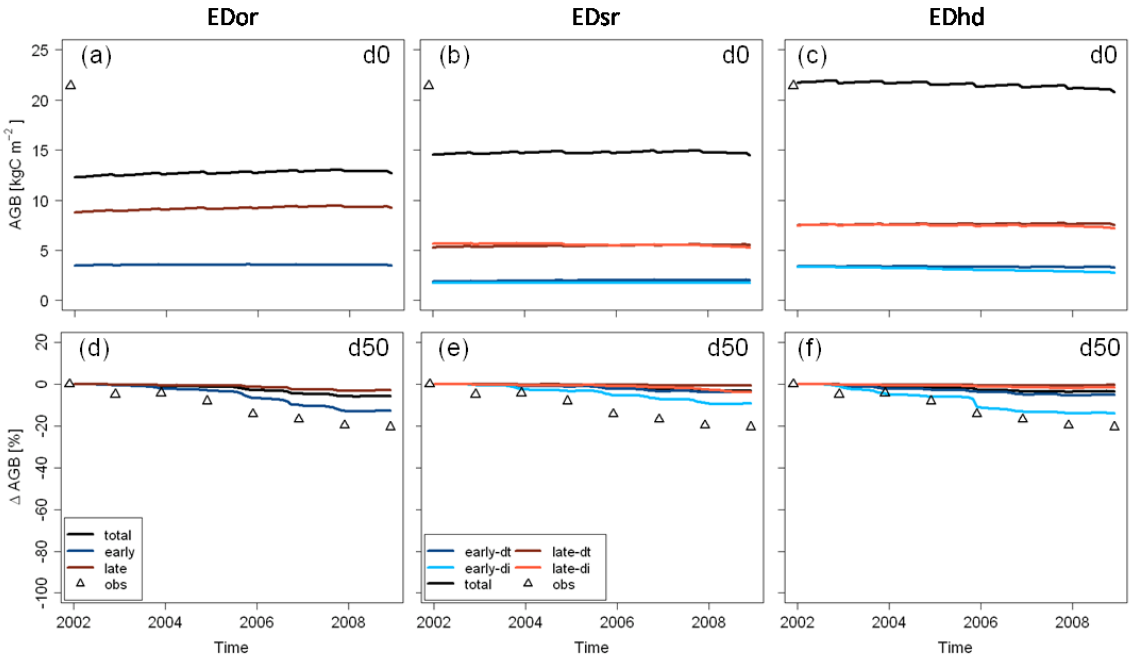

Figure 4.5. Seven year time series of aboveground biomass (*AGB*, kg C m^{-2}) predicted for the Caxiuanã National Forest using the original (EDor), single resistor (EDsr) and hydrodynamic (EDhd) water-stress formulations. Colored lines indicate early- (blue) and late- (red) successional plant functional types. Darker colors are drought-tolerant (dt), lighter colors are drought-intolerant (di), black is total *AGB*. Open symbols are published annual observations of *AGB* (da Costa *et al.,* 2010). d0 and d50 are drought levels indicating a 0% and 50% reduction in precipitation. Panels a – c show the d0 control plot simulations. Panels d –f show the d50 treatment simulations and are presented as the percent the control plot *AGB* was changed (Δ) by the drought.

the early-successional PFT is more vulnerable than the late-successional PFT in each size class (Figs. 4.6a,d,g, 4.7a,g), with one exception, the medium size class at CAX (Fig. 4.7d). The pattern is more variable for EDsr where the drought-tolerant PFTs in the smallest size class is generally the most vulnerable to the drought treatment (Figs. 4.6b, 4.7b). EDsr also predicts recovery by the end of the drought at TNF for the early-successional drought-intolerant PFT in the medium size class (Fig. 4.6e) and in the 4th and 5th years of the drought at CAX in the small size class (Fig. 4.7b). For TNF, EDhd contrasts with EDor where EDhd predicts the vulnerability to be even across size classes

for the late-successional drought-intolerant PFT and highest in the two larger size classes for the early-successional drought-intolerant PFT. For CAX, EDhd predicts the early-successional drought-intolerant PFT is equally vulnerable in all three size classes and the early-successional drought-tolerant PFT is vulnerable only in the medium size class while the other two PFTs are drought resistant in all three size classes (Fig. 4.7c,f,i). Also at both sites, the small and medium size classes of the early-successional drought-tolerant PFT has periods of recovery over the 8 year drought treatment (Figs. 4.6c,f, 4.7c,f).

EDor and EDsr underestimate control plot measurements of leaf area index (*LAI*) at TNF (EDor: *LAI* = 4.2, EDsr: *LAI* = 4.6, observation range: 5.2 – 6.9 m^2 m^{-2}) (Fig. 4.8a,b) but predict *LAI* similar in magnitude to measurements at CAX (EDor: *LAI* = 4.8, EDsr: *LAI* = 5.1 observation range: 4.2 – 5.8 m^2 m^{-2}) (Fig. 4.9a,b). In contrast, EDhd predictions of *LAI* are similar in magnitude to measurements at TNF (5.9 m^2 m^{-2}) (Fig. 4.8c), but overestimates measurements at CAX (6.3 m^2 m^{-2}) (Fig. 4.9c). None of the models capture the small seasonal dynamics in observed control plot *LAI* at TNF (Fig. 4.8 a,b,c). Under the drought treatment at TNF, both EDor and EDhd predict reductions in *LAI* that are similar in magnitude to the reductions observed by the end of the measurements in the 4^{th} year (~1.0 m^2 m^{-2}) (Fig. 4.8d,f). In comparison, EDsr predicts a much smaller reduction in *LAI* over the 4 year period (~0.5 m^2 m^{-2}) (Fig. 4.8e). The reductions in EDor *LAI* are accounted for by both PFTs, with the early-successional being slightly greater (Fig. 4.8d). The reductions in EDhd *LAI* are accounted for primarily by the early-successional drought-intolerant PFT, with the late-successional drought-intolerant PFT only beginning to show a significant response in the 4^{th} year (Fig. 4.8f). At CAX, all of the model formulations fail to capture the observed decline in *LAI* over

the 2 year measurement period (Fig. 4.9d,e,f). At both sites, the LAI patterns of each PFT mirror the *AGB* patterns over the entire 8 year simulation of the drought plots (data not shown).

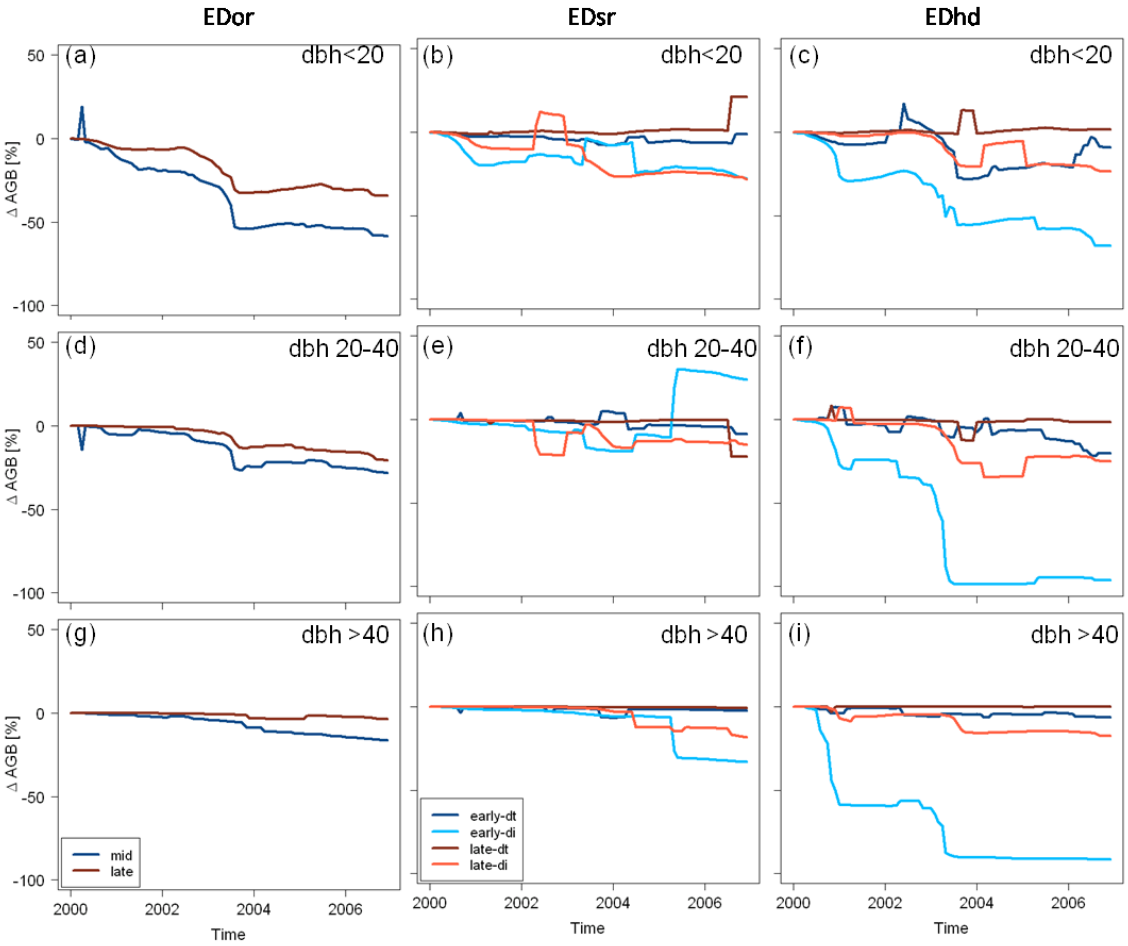

Figure 4.6. Seven year time series of the change (D) in aboveground biomass (AGB, kg C m^{-2}) predicted for the Tapajós National Forest for three size classes using the original (EDor), single resistor (EDsr) and hydrodynamic (EDhd) water-stress formulations. Panels a-c show trees of <20 cm diameter at breast height (dbh). Panels d-f show trees between 20-40 cm dbh. Panels g-i show trees >40cm dbh. Colored lines indicate early- (blue) and late- (red) successional plant functional types. Darker colors are drought-tolerant (dt), lighter colors are drought-intolerant (di). The Δ indicates the percent the control AGB was altered by the 50% drought treatment.

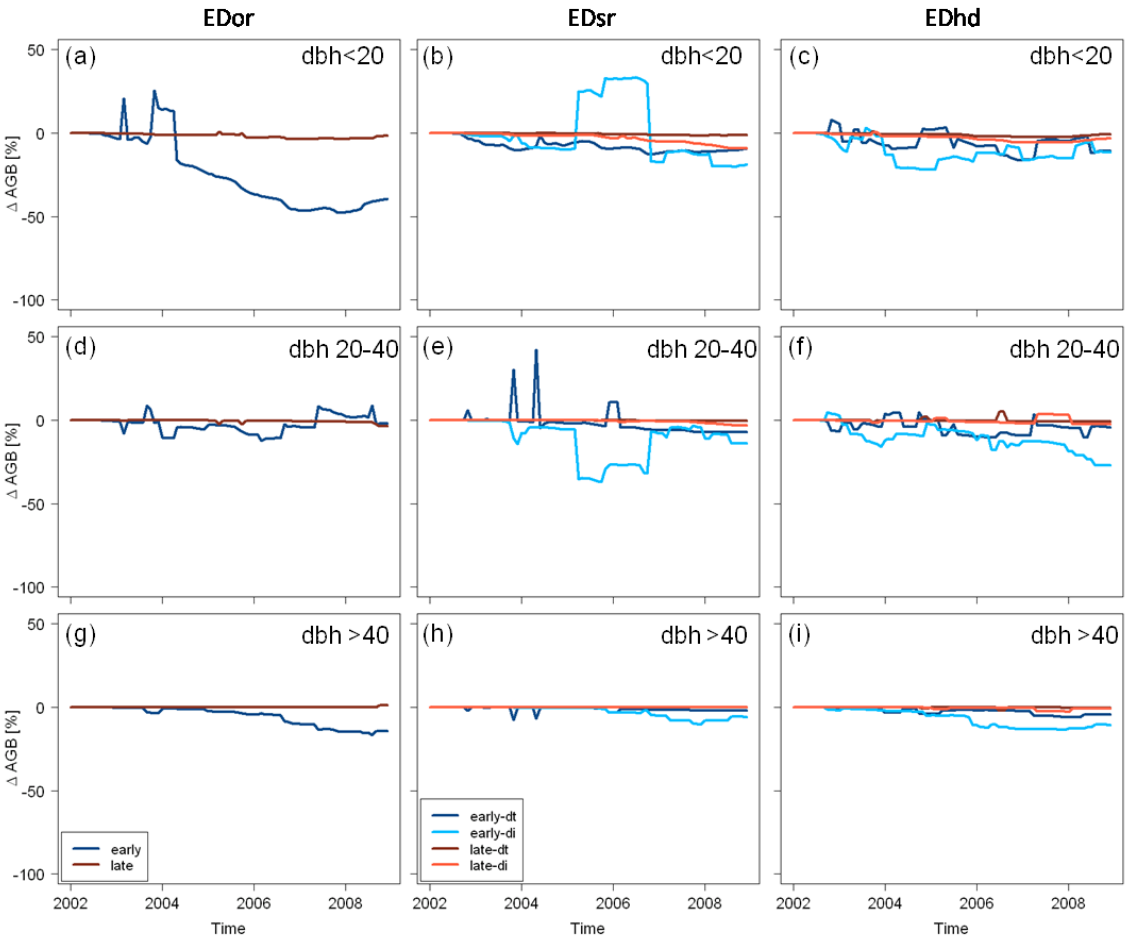

Figure 4.7. Seven year time series of the change (Δ) in aboveground biomass (*AGB*, kg C m^{-2}) predicted for the Caxiuanã National Forest for three size classes using the original (EDor), single resistor (EDsr) and hydrodynamic (EDhd) water-stress formulations. Panels a – c show trees of <20 cm diameter at breast height (dbh). Panels d – f show trees between 20 – 40 cm dbh. Panels g – i show trees >40cm dbh. Colored lines indicate early- (blue) and late- (red) successional plant functional types. Darker colors are drought-tolerant (dt), lighter colors are drought-intolerant (di). The Δ indicates the percent the control *AGB* was altered by the 50% drought treatment.

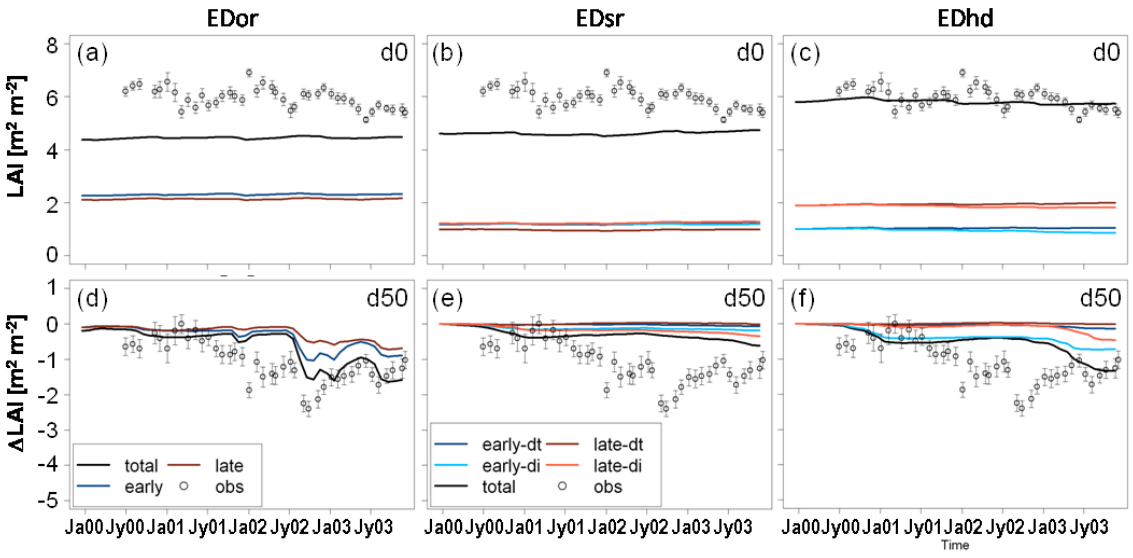

Figure 4.8. Three year time series of leaf area index (*LAI*, m^2 m^{-2}) predicted for the Tapajós National Forest using the original (EDor), single resistor (EDsr) and hydrodynamic (EDhd) water-stress formulations. Colored lines indicate early- (blue) and late- (red) successional plant functional types. Darker colors are drought-tolerant (dt), lighter colors are drought-intolerant (di), black is total *LAI*. Open symbols are published observations (Nepstad and Moutinho, 2008). d0 and d50 are drought levels indicating a 0% and 50% reduction in precipitation. Panels a – c show the d0 control plot simulations. Panels d –f show the d50 treatment simulations and are presented as the total amount the control plot *LAI* was changed (Δ) by the drought.

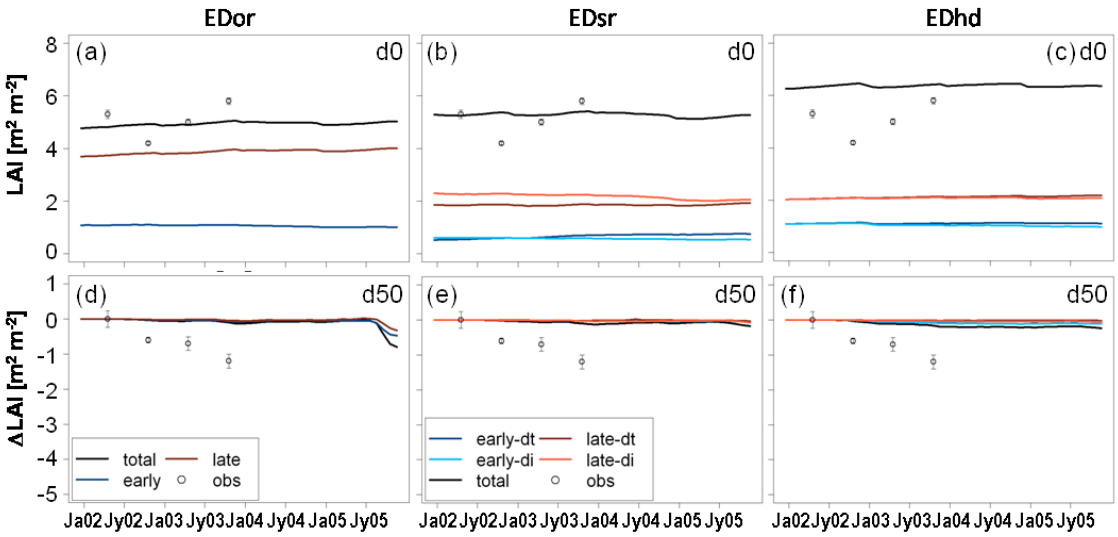

Figure 4.9. Three year time series of leaf area index (*LAI*, m^2 m^{-2}) predicted for the Caxiuanã National Forest using the original (EDor), single resistor (EDsr) and hydrodynamic (EDhd) water-stress formulations. Colored lines indicate early- (blue) and late- (red) successional plant functional types. Darker colors are drought-tolerant (dt), lighter colors are drought-intolerant (di), black is total *LAI*. Open symbols are published observations (Fisher *et al.,* 2007). d0 and d50 are drought levels indicating a 0% and 50% reduction in precipitation. Panels a – c show the d0 control plot simulations. Panels d –f show the d50 treatment simulations and are presented as the total amount the control plot *LAI* was changed (Δ) by the drought.

Carbon fluxes

The model predictions were compared to published observations of carbon fluxes measured at CAX and TNF. A detailed carbon budget was measured in the 4th year at CAX (Metcalfe *et al*., 2010b) and therefore, the 4th year is presented in this analysis for both sites as the evaluation of model predictions of photosynthesis and tissue scale respiration. Woody biomass production (NPP_w) and litter production were measured each year and are presented for the entire 8 year simulation. The purpose of this section is for model validation, and therefore, since the published observations are of the aggregate ecosystem, PFT specific fluxes are not reported for each model.

Table 4.2 List of observations and associated references.

Definition	Symbol	Units	Site and source
Aboveground biomass	*AGB*	kg C m^{-2}	CAX: da Costa *et al*., 2010 TNF: Brando *et al*., 2008
Gross primary production of carbon	*GPP*	kg C m^{-2} yr^{-1}	TNF: Hutyra *et al*., 2007
Leaf area index	*LAI*	m^2 m^{-2}	CAX: Fisher *et al*., 2007 TNF: Nepstad & Moutinho, 2008
Litter production		kg C m^{-2} yr^{-1}	TNF: Brando *et al*., 2008
Net ecosystem production of carbon	*NEP*	kg C m^{-2} yr^{-1}	TNF: Hutyra *et al*., 2007
Net primary production of carbon in wood	NPP_w	kg C m^{-2} yr^{-1}	CAX: da Costa *et al*., 2010 TNF: Brando *et al*., 2008
Autotrophic respiration	R_a	kg C m^{-2} yr^{-1}	CAX: Metcalfe *et al*., 2010b
Whole ecosystems respiration	R_e	kg C m^{-2} yr^{-1}	CAX: Metcalfe *et al*., 2010b TNF: Hutyra *et al*., 2007
Heterotrophic respiration	R_h	kg C m^{-2} yr^{-1}	CAX: Metcalfe *et al*., 2010b
Leaf respiration	R_l	kg C m^{-2} yr^{-1}	CAX: Metcalfe *et al*., 2010a,b
Root respiration	R_r	kg C m^{-2} yr^{-1}	CAX: Metcalfe *et al*., 2010b
Wood respiration	R_w	kg C m^{-2} yr^{-1}	CAX: Metcalfe *et al*., 2010b

EDor and EDsr predict net ecosystem production (NEP) of the control plots at both sites to be substantial carbon sinks (range: ~0.3 to 0.4 kg C m-2 yr-1) (Fig 4.10a,c). In contrast, EDhd predicts each site to be a small carbon source, which is in strong agreement with flux tower measurements of NEP at TNF(-0.09 ± 0.005 kg C m^{-2} yr^{-1}). (Note: error estimates are reported as ±95% CI). Under the drought treatment, EDsr

predicts both ecosystems to become even stronger carbon sinks in the fourth year, whereas both EDor and EDhd predict both sites as sources (Fig. 4.10e,g).

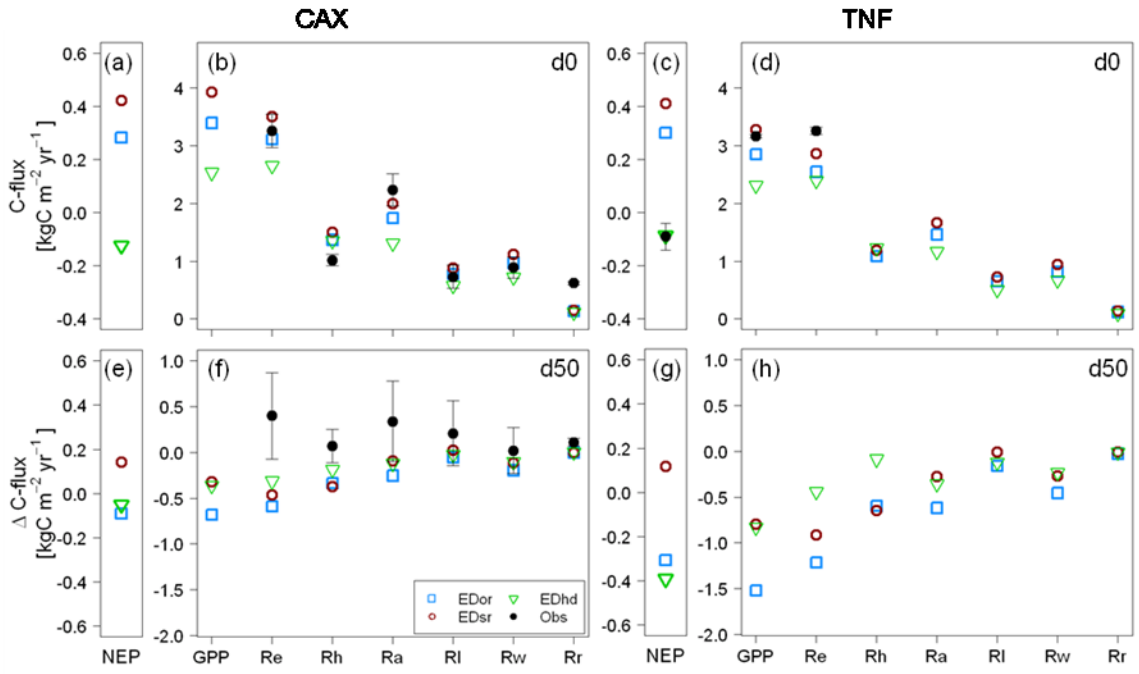

Figure 4.10. Net and component ecosystem carbon fluxes (kg C m^{-2} yr^{-1}) in the fourth year of the experiment for Caxiuanã (CAX, left side) and Tapajós (TNF, right side). Colored symbols indicate the original (EDor, blue), single resistor (EDsr, red) and hydrodynamic (EDhd, green) water-stress formulations. Black symbols are published observations (mean ± 95% CI; CAX: Metcalfe *et al*., 2010; TNF: Hutyra *et al*., 2007). Panels (a) to (d) show control plot (d0) carbon fluxes and panels (e) to (h) show drought treatment plot (d50) fluxes. The *D* indicates the total amount the control (d0) fluxes were altered by the 50% drought treatment. NEP: net ecosystem production, GPP: gross primary production, Re: ecosystem respiration, Rh: heterotrophic respiration, Ra: autotrophic respiration, Rl: leaf respiration: Rw: wood respiration, Rr: root respiration.

EDor and EDsr predictions of gross primary production (*GPP*) in the 4th year for the control plots are similar in magnitude at both sites and agree with flux tower estimates (3.17 ± 0.03 kg C m^{-2} yr^{-1}) at TNF (Fig. 4.10b,d). In comparison, *GPP* predictions by EDhd are approximately 1.0 kg C m^{-2} yr^{-1} lower than EDor at both sites and the measurements at TNF. All three models predict lower *GPP* under the drought

treatment at both sites, with EDor predicting a considerably greater reduction relative to EDsr and EDhd (Fig. 4.10f,h).

Respiration definitions are given in Table 4.2. All three models were within the range of observed ecosystem respiration (R_e) for the 4th year in the control plot at CAX (3.26 ± 0.29 kg C m^{-2} yr^{-1}) and were approximately 1.0 kg C m^{-2} yr^{-1} less than observations at TNF (3.26 ± 0.06 kg C m^{-2} yr^{-1}) (Fig. 4.10b,d). All three models are in agreement at both sites about the magnitude of heterotrophic respiration (R_h) in 4th year (TNF: ~1.2, CAX: ~1.5 kg C m^{-2} yr^{-1}), but are significantly higher than the control plot estimates at CAX (1.02 ± 0.10 kg C m^{-2} yr^{-1}) (Fig. 4.10b,d). EDor and EDsr predictions of autotrophic respiration (R_a) are similar in magnitude at both sites TNF: EDor = 1.5, EDsr = 1.7, CAX EDor = 1.7, EDsr = 2.0 kg C m^{-2} y^{-1}); however, only EDsr is within the CI of the 4th year control plot measurements at CAX (2.24 ± 0.28 kg C m^{-2} yr^{-1}). R_a for EDhd is comparatively lower at both sites (TNF: 1.2, CAX: 1.3 kg C m^{-2} yr^{-1}). Predictions of leaf (R_l) and wood (R_w) respiration in the 4th year at both sites is similar in magnitude across models (R_l = ~0.8, R_w = ~1.0 kg C m^{-2} yr^{-1}) and are within the ranges observed at CAX (R_l: 0.73 ± 0.20, R_w: 0.89 ± 0.18 kg C m^{-2} yr^{-1}) (Fig. 4.10b,d). All three models are in agreement at both sites but significantly underpredict the 4th year observations of root respiration (R_r) at CAX (0.62 0.03 kg C m^{-2} yr^{-1}) (Fig. 4.10b,d). Under the drought treatment, all models are in agreement about ecosystem and component respiration fluxes being suppressed in the 4th year at both sites(Fig. 4.10f,h), which is in contrast to the observed marginal increases in all of these fluxes at CAX. It should be noted however, that the drought predictions of R_l and R_w by all of the models are within the range of measurement error at CAX (Fig. 4.10f).

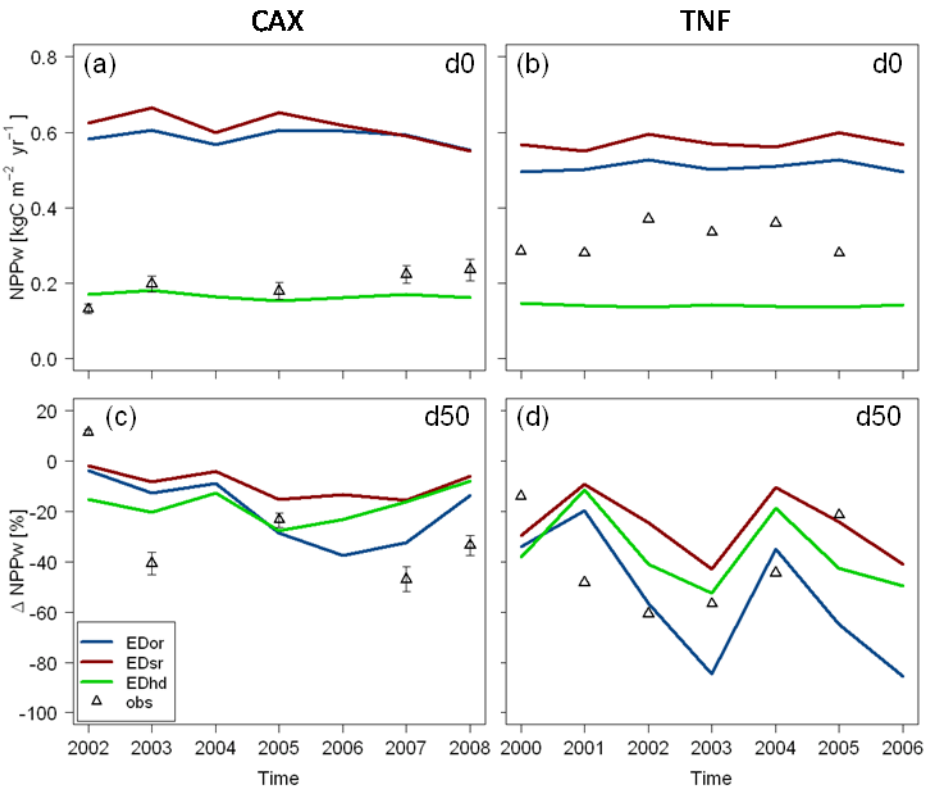

Figure 4.11. Seven year time series of annual NPP_w (kg C m^{-2} yr^{-1}) for (a, c) Caxiuanã (CAX) and (b, d) Tapajós (TNF). Colored lines indicate the original (EDor, blue), single resistor (EDsr, red) and hydrodynamic (EDhd, green) water-stress formulations. Open symbols are published observations (mean ± 95% CI (when reported), TNF: Brando *et al.,* 2008, CAX: da Costa *et al.,* 2010). d0 and d50 are drought levels indicating a 0% and 50% reduction in precipitation. The Δ plots (c, d) show the percent the control (a, b) NPP_w was altered by the 50% drought treatment.

EDor and EDsr systematically over predict the observed NPP_w for the control plots of both sites (TNF: EDor = ~0.50, EDsr =~0.59 observations = ~0.31, CAX: EDor = ~0.59, EDsr =~0.61, observations = ~0.20 kg C m^{-2} yr^{-1}) (Fig. 4.11a,b). In contrast, predictions of NPP_w by EDhd is similar in magnitude to observed NPP_w in the control plot of CAX (~0.2 kg C m^{-2} yr^{-1}), but lower than observations in the control plot of TNF (~0.18 kg C m^{-2} yr^{-1}) (Fig. 4.11a,b). Lower NPP_w predicted by EDhd relative to EDor and EDsr reflects lower available carbon for assimilation resulting from lower *GPP* (Fig.

4.10b,d). Under the drought treatment, the observed interannual variability is weakly captured by all three models at TNF and not capture at CAX (Fig. 4.11c,d). However, the magnitude of the reduction in *NPPw* under the drought treatment is realistically captured by EDor at TNF, but in all other cases the predicted reduction is too small (Fig. 4.11c,d). Furthermore, the patterns of the drought response of NPP_w is similar between the models at both sites, but varies in magnitude with EDor having the strongest, while EDsr having the weakest response (Fig. 4.11c,d).

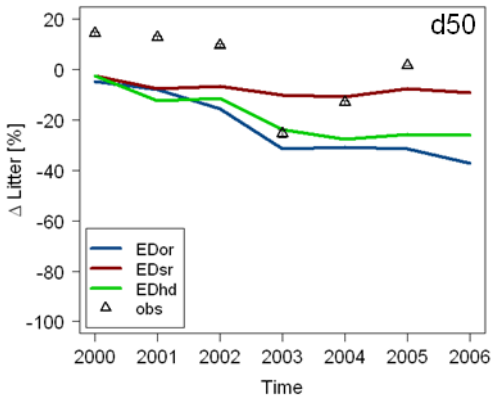

Figure 4.12. Seven year time series of the change in annual litterfall (kg C m^{-2} yr^{-1}) for the Tapajós drought experiment. Colored lines indicate the original (EDor, blue), single resistor (EDsr, red) and hydrodynamic (EDhd, green) water-stress formulations. Open symbols are published observations (mean ± 95% CI, TNF: Brando *et al.,* 2008). The Δ indicates the percent the control litterfall was altered by the drought treatment.

Litter production in the control plot is similar between all three models at both sites (TNF; ~0.18, CAX: ~0.20 kg C m^{-2} yr^{-1}), thus indicating that the water stress-formulations and alternative PFTs do not produce systematic differences in leaf shedding under normal precipitation. The drought response of litter production predicted by each model reflects its total AGB response, where EDsr has a weak response at both sites and

EDor and EDhd have ~10% and ~25% decline in litter production at CAX and TNF, respectively. All three models predict a sustained reduction in litter production from the beginning, which is in contrast to the observed increase in litter production in the first three years of the TNF drought experiment (Fig 4.12).

Plant hydrodynamics

Diurnal patterns of GPP_{leaf} (expressed per unit leaf area), β, and leaf temperature (T_{leaf}) were evaluated for EDhd and then GPP_{leaf} and β were compared to predictions by EDor. October 10, 2003 is used for illustrative purposes, since it was in the dry season and was preceded by several rain-free days. Both β and T_{leaf} can affect the magnitude of GPP_{leaf}, the former through a down-regulation of stomatal conductance and the latter through temperature dependent maintenance respiration. Since β and T_{leaf} are dependent on canopy position, all three variables were separated into small (dbh: <20 cm), medium (dbh: 20 – 40 cm) and large (dbh: >40 cm) size classes. GPP_{leaf} for all PFTs in both plots follows a typical diurnal pattern with the highest rates occurring in the morning followed by a midday suppression (Fig. 4.13). The midday suppression is particularly steep for the early-successional PFTs, but a late afternoon recovery is also predicted in the drought plots (Fig 4.13a,c,e). The magnitude of GPP_{leaf} is dependent on both PFT and size. In terms of PFT, in the control plot GPP_{leaf} of the early-successional PFT is typically more than double (range: 3.5 – 6.0 μmol CO_2 m^{-2} s^{-1}) that of the late-successional PFTs (range: 1.8 – 2.8 μmol CO_2 m^{-2} s^{-1}) (Fig. 4.13). In the drought plots, GPP_{leaf} of the early-successional drought-tolerant PFT is still double that of the late-successional drought-

tolerant PFT. But, GPP_{leaf} of both the early- and late-successional drought-intolerant PFTs are approximately the same after 11:00. In terms of size effects, predictions of

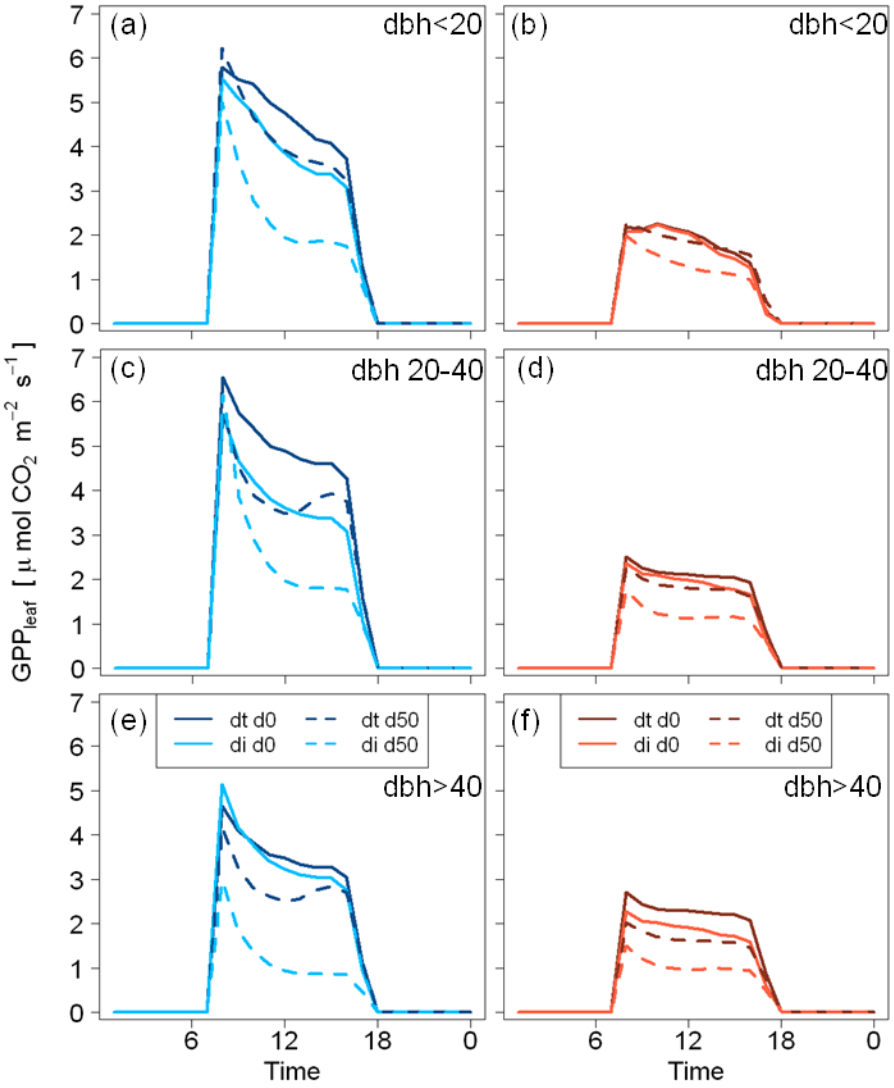

Figure 4.13. Diurnal pattern of leaf-level gross primary productivity (GPP_{leaf}, µmol CO_2 m^{-2}leaf s^{-1}) for trees of different size classes and plant functional types simulated for the Tapajós for October 2, 2003 using the hydrodynamic (EDhd) formulation. GPP_{leaf} is divided between size classes: (a,b) trees <20 cm diameter at breast height (dbh), (c,d) trees between 20-40 cm dbh, (e,f) trees >40cm dbh. Colored lines indicate early- (blue, left) and late- (red, right) successional plant functional types. Darker colors are drought-tolerant (dt), lighter colors are drought-intolerant (di). d0 and d50 indicate drought levels of 0% and 50% reductions in precipitation.

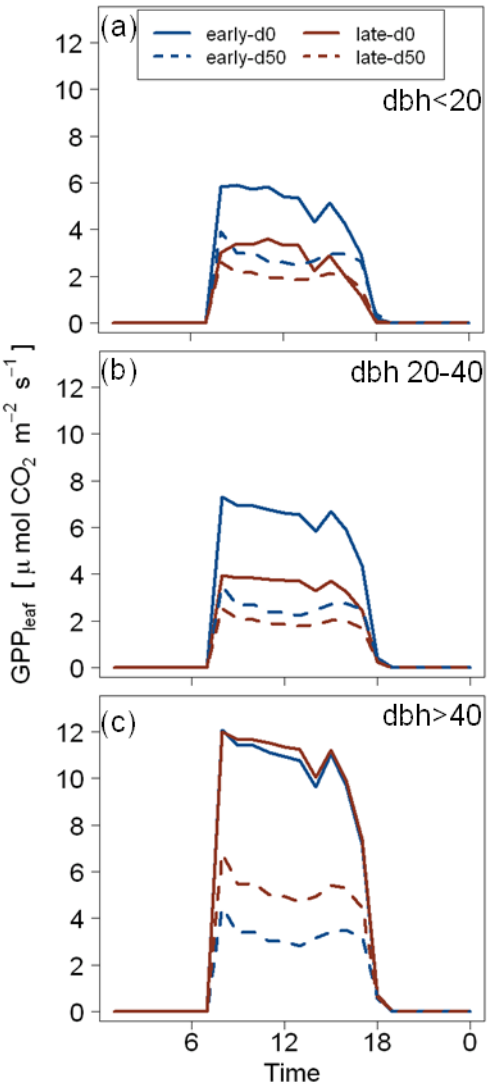

Figure 4.14. Diurnal pattern of leaf-level gross primary productivity (GPP_{leaf}, μmol CO_2 m^{-2}leaf s^{-1}) for trees of different size classes and plant functional types simulated for the Tapajós for October 2, 2003 using the original (EDor) formulation. GPP_{leaf} is divided between size classes: (a) trees <20 cm diameter at breast height (dbh), (b) trees between 20-40 cm dbh, (c) trees >40cm dbh. Colored lines indicate early- (blue, left) and late- (red, right) successional plant functional types. d0 and d50 (dashed lines) indicate drought levels of 0% and 50% reductions in precipitation. Note the difference in scale on the y-axis compared to Figure 4.13.

GPP_{leaf} of the early-successional PFTs in the largest size class of the control plot (Fig. 4.13e) is generally 1.0 μmol CO_2 m^{-2} s^{-1} lower throughout the day compared to the medium and small size classes (Fig. 4.13a,c). In contrast, *GPP_{leaf}* of the late-successional

PFTs is similar in magnitude across all size classes (Fig. 4.13b,d,f). The drought-tolerant PFTs also has higher GPP_{leaf} than the drought-intolerant PFTs (Fig. 4.13), particularly in the early-successional PFTs (Fig. 4.13a,c,e). In comparison, in the control plot EDor also predicts the early-successional PFT to have higher GPP_{leaf} than the late-successional PFT in the small and medium size classes (Fig. 4.14a,b); but in contrast, the rates are the same in the largest size class (Fig. 4.14c). Also in contrast to EDhd, GPP_{leaf} increases in magnitude with size and it does not have the same midday suppression pattern. Finally, the overall magnitude of GPP_{leaf} predicted by EDhd (Fig 4.13) is lower than predictions by EDor (Fig. 4.14) for the two larger size classes, but the same for the smallest size class. This difference is caused by the diurnal differences in β described below.

The overall diurnal pattern of β in the EDhd simulations is U-shaped with a broad minimum occurring during the midday (Fig. 4.15). The PFT and size class pattern of β is similar to that of GPP, where the larger sized trees compared smaller trees, the early-successional PFTs compared to late-successional, and drought-intolerant PFTs compared to drought-tolerant, all experience greater relative reductions over the course of the day (Fig. 4.15). β down regulates the stomata most strongly for the drought-intolerant early-successional PFTs. For example in the control plot, the midday values of β for the medium and large size classes drops below 0.7 and 0.6, respectively, and in the drought plots it drops below 0.4 for both (Fig. 4.15c,e). The stomata began the day partially closed ($\beta < 1.0$) for both drought-intolerant PFTs in the largest size class of the control plot (Fig. 4.15e,f) and for all PFTs of all size classes in the drought plot (Fig. 4.15a-f). In comparison, midday values of β in the EDor simulations are considerably higher and never drop below 0.9 for all size classes (Fig. 4.16). In the drought plot, EDor β for both

PFTs in all size classes begin the day near 1.0 (Fig. 4.16), but each drop to a similar value as its EDhd drought-intolerant counterpart (Fig. 4.15).

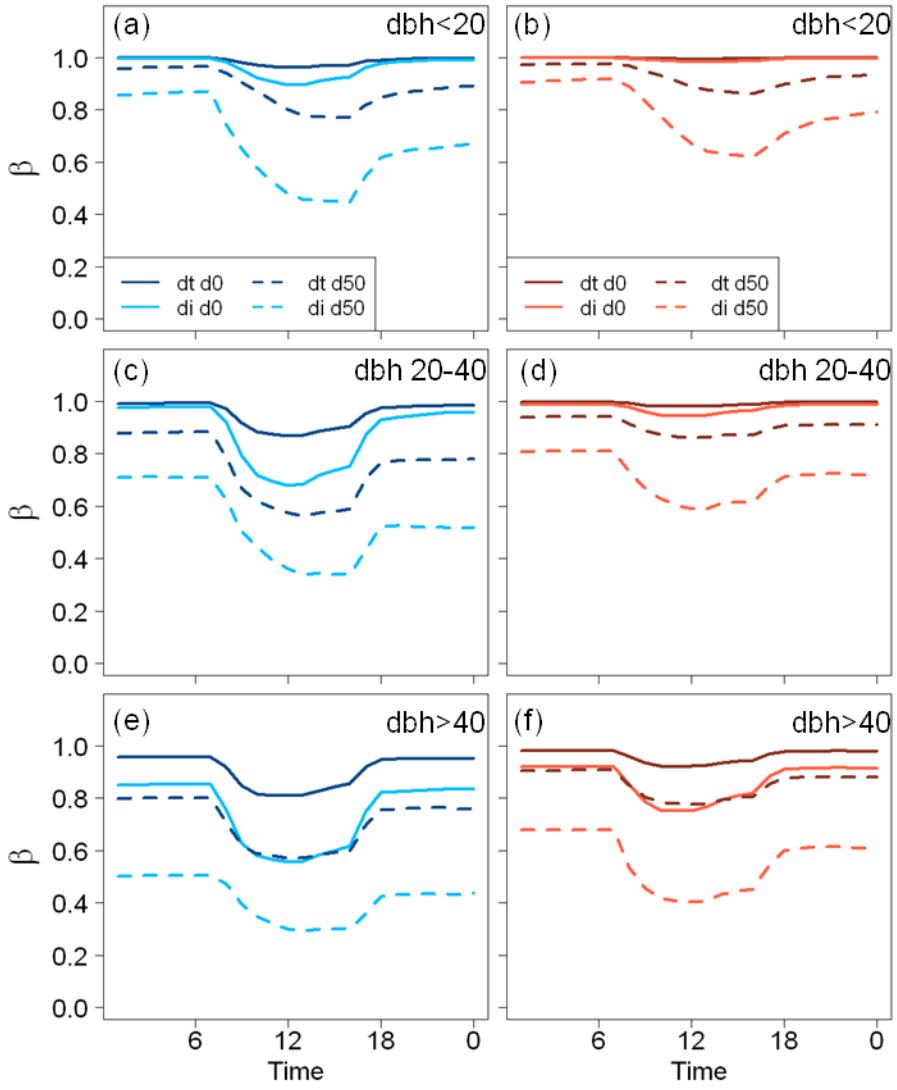

Figure 4.15. Diurnal pattern of the soil water-stress scaling factor, β (dimensionless), for trees of different size classes and plant functional types simulated for the Tapajós for October 2, 2003 using the hydrodynamic (EDhd) formulation. β is divided between size classes: (a,b) trees <20 cm diameter at breast height (dbh), (c,d) trees between 20-40 cm dbh, (e,f) trees >40cm dbh. Colored lines indicate early- (blue, left) and late- (red, right) successional plant functional types. Darker colors are drought-tolerant (dt), lighter colors are drought-intolerant (di). d0 and d50 indicate drought levels of 0% and 50% reductions in precipitation.

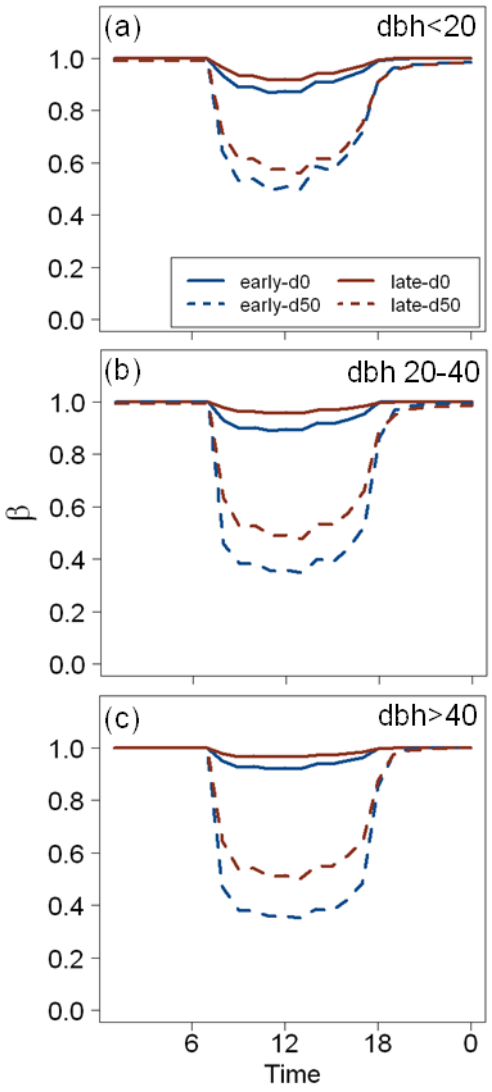

Figure 4.16. Diurnal pattern of the soil water-stress scaling factor, β (dimensionless), for trees of different size classes and plant functional types simulated for the Tapajós for October 2, 2003 using the original (EDor) formulation. β is divided between size classes: (a) trees <20 cm diameter at breast height (dbh), (b) trees between 20-40 cm dbh, (c) trees >40cm dbh. Colored lines indicate early- (blue, left) and late- (red, right) successional plant functional types. d0 and d50 (dashed lines) indicate drought levels of 0% and 50% reductions in precipitation.

The diurnal pattern of T_{leaf} in the EDhd simulations is hump-shaped with a peak occurring between 11:00 and 12:00 (Fig. 4.17). Leaf temperatures are about 1 – 2 ^{o}C higher for the drought-intolerant PFTs compared to the drought-tolerant PFTs in the

smallest size class (Fig. 4.17a,b). In the two larger size classes, differences between the PFTs are marginal (Fig. 4.17c-f), with the exception of the early-successional drought-intolerant PFT (Fig. 4.17c,e). Finally, the large late-successional PFTs have leaf temperatures approximately 2.5 ^{o}C greater than the two smaller size classes (Fig. 4.17f).

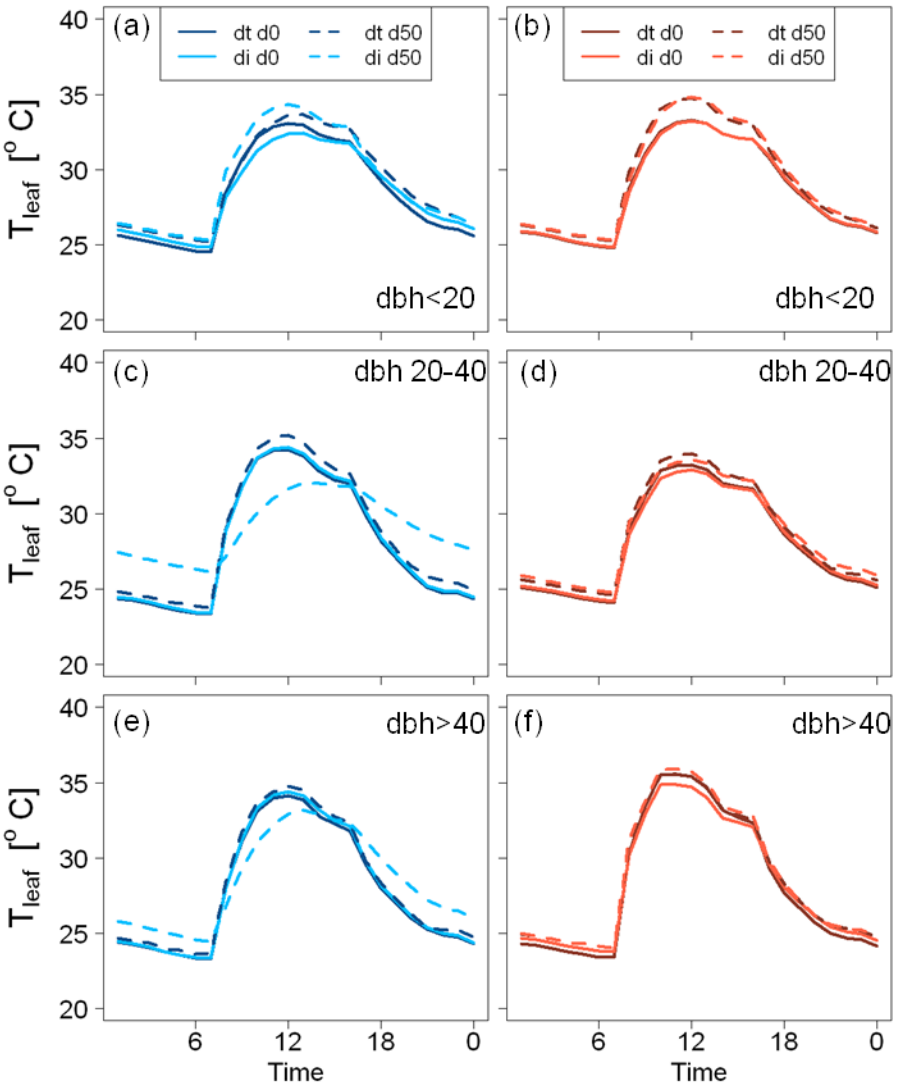

Figure 4.17. Diurnal pattern of leaf temperatures (T_{leaf}, ^{o}C) for trees of different size classes and plant functional types simulated for the Tapajós for October 2, 2003. Panels a-b show trees of <20 cm diameter at breast height (dbh). Panels c-d show trees between 20-40 cm dbh. Panels e-f show trees >40cm dbh. Colored lines indicate early- (blue, left) and late- (red, right) successional plant functional types. Darker colors are drought-tolerant (dt), lighter colors are drought-intolerant (di). d0 and d50 indicate drought levels of 0% and 50% reductions in precipitation.

The sensitivity analysis revealed that individually adjusting $K_{w,max}$, θ_{wood}, and h_p only modified the *AGB* drought responses shown in Figure 4.4f by <5% for the drought-intolerant PFTs and <2% for the drought-tolerant PFTs. In contrast, raising the soil moisture threshold, θ_{xcrit}, to 0.09 m^3 m^{-3} produced a large drought response across all models (Fig. 4.18). However, the largest reductions in *AGB* incorrectly occurred with the late-successional PFTs instead of the drought-intolerant PFTs, most notably with EDor and EDhd (Fig. 4.18a,c).

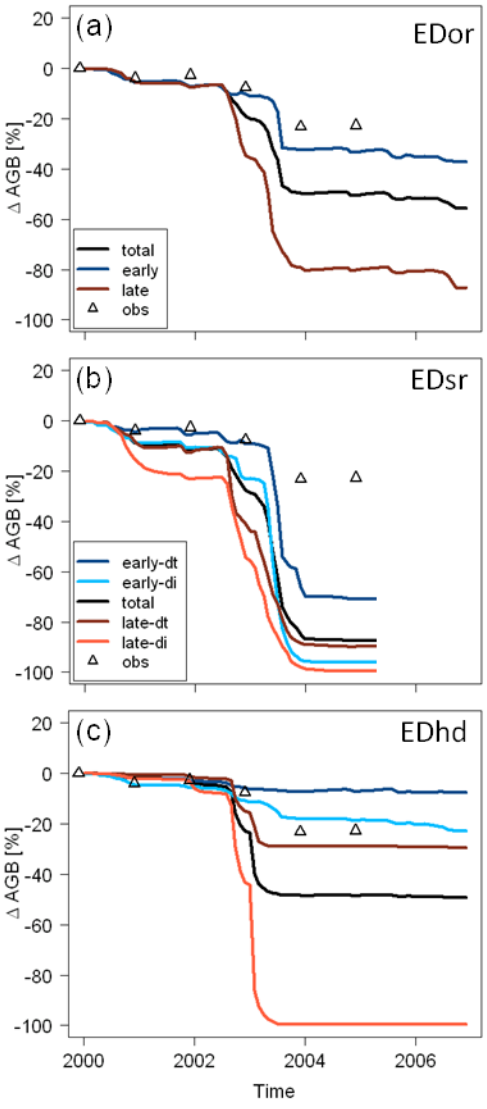

Figure 4.18. Seven year time series of the change (*D*) in aboveground biomass (*AGB*, kg C m^{-2}) predicted for drought plots of the Tapajós National Forest using the (a) original (EDor), (b) single resistor (EDsr) and (c) hydrodynamic (EDhd) water-stress formulations. This differs from Fig 4.4d,e,f in that the drought phenology parameter (θ_{crit}) is set to 0.09. Colored lines indicate early (blue) and late (red) successional plant functional types. Darker colors are drought-tolerant (dt), lighter colors are drought-intolerant (di), black is total *AGB*. Open symbols are published annual observations of *AGB* (Brando *et al.,* 2008).

Discussion

Climate models project many regions of the Amazon basin will experience more extreme precipitation patterns or general drying by the end of this century (Joetzjer *et al*., 2013). Higher tree mortality rates are likely to be a significant consequence of these changes (Phillips *et al*., 2010). However, DVMs are poorly formulated to capture losses in live biomass during extreme drought events (McDowell *et al*., 2013; Powell *et al*., 2013), which arises from our still nascent understanding of the complex mechanisms underlying drought induced mortality (McDowell *et al*., 2008). In this study, two potentially important mechanisms were evaluated for the first time within the framework of a DVM: (1) hydrodynamic water-transport from the root to the leaf and (2) competition arising from diversity in plant hydraulic strategies.

To evaluate the role of plant hydrodynamics, three water-stress formulations were tested in the Ecosystem Demography model (Fig. 4.2): (1) a single-resistor formulation as a function of soil moisture (Eqn. 2a) (EDsr), (2) a supply and demand formulation as a function of soil moisture (Eqn. 3) (EDor), and (3) a supply and demand formulation as a function of leaf water potential (Eqn. 4) (EDhd). The later requires a hydrodynamic formulation to transfer the soil water potential to the leaf. Many DVMs (e.g. CLM3.5, IBIS and JULES, shown in Powell *et al*., 2013) use a variant of the single-resistor water-stress formulation as a function of soil moisture. However, using a DVM with such a formulation to evaluate ecosystem drought responses has been the subject of considerable scientific scrutiny (e.g. McDowell *et al*., 2013; Sperry and Love, 2015). Stomata respond to the leaf water balance, which is simultaneously modulated by the supply of water from the soil and the demand from the atmosphere. Therefore, a DVM with a more

mechanistic soil water-stress formulation that includes both supply of and demand for water in the leaf (Sperry and Love, 2015) should theoretically be more successful at capturing drought responses.

Currently available DVMs use a single water-stress parameterization (Powell *et al*., 2013) to represent the range of hydraulic trait diversity found in the tropical biome (e.g. Figs. 3.1, 3.2, 3.4; see also Baltzer *et al*., 2008; Anderegg, 2014). Species compositional shifts may be a consequence of extreme droughts in the tropics (da Costa *et al*., 2010), which underscores the imperative to develop DVMs with hydraulically diverse PFTs. EDsr was parameterized to represent multiple PFTs that spanned a range of hydraulic and successional diversity (Fig. 4.2a) to determine if the single-resistor formulation alone could be remedied with only greater diversity. Similarly, EDhd was also parameterized to represent both hydraulic and successional diversity (Fig. 4.2b), to evaluate if both diversity and hydrodynamics must be included in order to capture observed ecosystem responses to drought.

EDsr was able to capture the correct PFT dependent reductions in *AGB* at TNF, however, it was unable to replicate the magnitude of the observed reduction in total *AGB* (Figs. 4.4b,e, 4.5b,e) or the size-dependent reductions in *AGB* (Figs. 4.6b,e,h, 4.7b,e,h). Therefore, one key result from this analysis is that increasing functional diversity in the water-stress formula alone is not sufficient enough for improving the ability of DVMs to make reliable drought response predictions for tropical forests.

Although none of the models correctly captured the magnitude and timing of the drought response of *AGB* or NPP_w at both sites (Figs, 4.4, 4.5, 4.11), predictions by EDhd possess characteristics that suggest its formula should be preferentially selected that of

EDor and EDsr when evaluating the fate of Amazon rainforests in a drier climate. For example, unlike EDor, EDhd includes greater biodiversity with four PFTs that operate along both successional and drought axes of competition. While the exact fraction of drought-tolerant and drought-intolerant species has not been reported for either CAX or TNF, EDhd (and EDsr) captured the resistance of the drought-tolerant PFTs to biomass loss (Figs. 4.4e,f, 4.5e,f) that was reported by da Costa *et al*. (2010). Secondly, most of the biomass loss predicted by EDor is from the smallest size class (Figs. 4.6a and 4.7a). In contrast, predictions by EDhd more closely resemble the observations (CAX: da Costa *et al*., 2010, TNF: Nepstad *et al*. 2007), where the early-successional drought-intolerant PFT in the two larger size classes is the most vulnerable to drought (Figs. 4.6c,f,i, 4.7c,f,i). These size dependent differences between EDor and EDhd are explained by the size dependent differences in β (Figs. 4.15, 4.16), which in turn controls the size dependent differences in GPP_{leaf} (Figs. 4.13, 4.14). Also, EDhd predicts that T_{leaf} does not play a role in the size dependent drought responses of GPP_{leaf} and by extension AGB (Fig. 4.17).

EDhd predicts a relatively strong midday suppression in GPP_{leaf} for both early-successional PFTs across all size classes (Fig4.13a,c,d) compared to the EDor predictions (Fig. 4.14). This prediction by EDhd is consistent with empirical evidence that suggests canopy trees at CAX use an isohydric strategy by closing their stomata during the day to conserve water (Fisher *et al*., 2006). Moreover, Edhd predicts that the isohydric strategy becomes very influential during severe droughts. Caution should be taken with the early morning prediction of β by EDhd for the largest trees and trees growing in the drought plot (Fig. 4.15). For those trees, EDhd predicts β to begin the day suppressed, being as

low as 0.5 for the early-successional drought-intolerant PFT. Yet, Ψ_l measurements for the four PFTs measured in the drought plot at CAX revealed that only trees from the early-successional drought-tolerant PFT begin the day under water-stress (Table 3.1). The other three PFTs start the day with Ψ_l near 0.0 MPa.

In each model formulation, each PFT was given an equivalent parameterization for CAX and TNF. The only two differences between the simulations for the two sites were edaphic and meteorological. EDhd and EDor predict that the plants should respond differently to these two physical differences (Figs. 4.4d,f vs 4.5d,f and Figs. 4.8d,f vs 4.9 d,f). Yet despite these differences, the observations showed similar reductions in *AGB* and *LAI* (Brando *et al*., 2008; da Costa *et al*., 2010). Spatial variation in hydraulic traits may account for the disagreement between the observed drought responses and model predictions. However, none of the parameterizations from the sensitivity analysis reproduced the observed reductions in *AGB* at CAX. Plus, empirical evidence suggests that the two measured hydraulic traits used to parameterize EDhd (*TLP* and xylem-P_{50}) are spatially conserved for the *terra firma* forests of the eastern Brazilian Amazon (Figs. 3.1, 3.4). Nevertheless, it is possible that either spatial variation in other plant traits exists and must be represented, or additional ecological or physiological processes need to be included. A few possible explanations are elucidated below.

Under current climate conditions, EDhd correctly predicts that *NEP* at TNF is a small C source in the fourth year (Fig. 4.10c). However, Edhd under predicts *GPP* and R_e, the two components of NEP, relative to both the observations and the other two models (Fig 4.10d). Also under current climate, all three formulations correctly captured the pattern of the component respiratory fluxes observed in the fourth year at CAX (Fig.

4.10b). Under the drought conditions, all three models failed to capture the increase in R_a, R_l, and R_w at CAX (Fig. 4.10f). This result is consistent with the diagnosis of Powell *et al*. (2013), which includes multiple DVMs, suggesting that we need a more complete understanding of the respiratory costs associated with different drought survival strategies.

The drought phenology scheme used in all formulations causes a fraction of the leaves to drop once soil moisture falls below a critical threshold. The magnitude of leaf-shedding is dependent on the severity and duration of the soil moisture deficit, both of which can be modulated by θ_{crit}. The permanent wilting point of the soil (-1.5 MPa) was used as the leaf shedding threshold (Clapp & Hornberger 1978). For the main set of simulation, θ_{crit} was set to 0.0—meaning that the leaf shedding threshold was unaltered. Under normal precipitation, the drought phenology scheme fails to capture the seasonal dynamics in *LAI* (Fig. 4.8a,b,c, see also Fig. 2.6a,b for EDor when $\theta_{crit} = 0.09$). Yet, EDor and EDhd, but not EDsr, captured the magnitude of the reduction in LAI by the 3rd year in the TNF drought plots (Fig. 4.8).

Leaf-shedding has been suggested as a preemptive adaptation to avoid drought (Pineda-García *et al*., 2013). The models failed to capture the increase in litter production in the initial years for the TNF drought plot (Fig. 4.12). Therefore, the soil moisture threshold causing leaves to shed was tested by increasing $\theta_{crit,}$ to 0.09. Across all models, increasing θ_{crit} caused significant reductions in *AGB* in the drought plots of TNF (Fig. 4.17). However, the reductions were most extensive in the late-successional PFTs, not the drought-intolerant PFTs. This result suggests that drought phenology is an important adaptive ecological process, but it requires better understanding and

representation in DVMs. For example, leaves of deciduous species in tropical dry forests have higher *TLPs* relative to the coexisting evergreen species (Sobrado, 1986), which suggests an important link between plant hydraulics and phenology. Indeed, linking drought phenology to plant hydraulics in EDhd has shown promise for capturing seasonal dynamics, but it is still untested under severe droughts (Xiangtao Xu, personal communication).

Xylem recovery may also explain the observed similarity in the drought responses between the two sites. However, the ability of air-filled xylem to refill while functional vessels are under tension is a topic of considerable debate. One side asserts that a plausible mechanism has yet to be presented; one which can overcome the physical constraints imposed by the instantaneous expansion of gas as water that is pumped into air-filled vessels comes in contact with water under negative pressure (Wheeler *et al*., 2013; Cochard and Delzon, 2013). The other side claims that while they indeed do lack a formal mechanism, empirical evidence clearly demonstrates its existence (Nardini *et al*., 2008; Brodersen and McElrone, 2013; Ogasa *et al*., 2013). The EDhd formula presented here has the potential to provide valuable insight about the ecological importance and evolutionary stability of xylem recovery when the vessels are under tension, and thus might help to resolve this debate. The EDhd formulation tested in this analysis has xylem recovery tightly coupled to recovery of soil moisture. Therefore, the formulation would need to include a new PFT with a time dimension for xylem recovery that is decoupled from the recovery of soil moisture. Furthermore, because xylem recovery was coupled to soil moisture in this analysis, this may explain why CAX, the site with higher annual precipitation, continued to have a muted drought response and both sites were relatively

insensitive to parameter tuning. Decoupling xylem recovery from soil moisture should be tested in future analyses.

Vessel tapering (West *et al*., 1999, Petit *et al*., 2008) and stem water storage (Pineda-García *et al*., 2013) have been invoked as adaptations that buffer trees against water-stress. An increase in vessel diameter from the apex to the base allows for more efficient flow at the base while reducing cavitation risk in the branches where xylem tension is greatest. The sensitivity test on the effects of height indicates that the EDhd formulation is congruent with this hypothesis because increasing h_p produced minimal reductions in *AGB* in the drought plot. On the other hand, stem water-storage provides a local reservoir of water, which allows for narrower, yet less conductive, vessels on the outer branches. The sensitivity test on θ_{wood} did not support this hypothesis, where increasing capacitance did not provide any additional buffer against biomass loss in the drought plots.

Conclusions

The results of this study support the hypothesis that functional diversity related to differences in plant hydrodynamics is an important ecosystem property because compositional shifts in tropical forest tree species that arise from differences in plant hydrodynamics is predicted to be a consequence of changes in precipitation patterns. Also, plant hydrodynamics capture size-dependent physiological processes, which in turn enable DVMs to more correctly capture structural shifts associated with size-dependent mortality caused by droughts. Therefore, representing drought-tolerance functional

diversity and plant hydrodynamics is essential in DVMs that are used to predict the fate of tropical ecosystems exposed to more frequent and extreme droughts.

Acknowledgments

This research was graciously supported by a grant from the Andes-Amazon Initiative of The Gordon and Betty Moore Foundation and by the National Science Foundation Partnership for International Research and Education in Amazon Climate Interactions grant (NSF award #OISE-0730305), and graduate research funding provided by the Department of Organismic and Evolutionary Biology, Harvard University. I acknowledge the LBA-DMIP project (NASA award #NNX09AL52G) for providing the TNF meteorological data. I am also deeply indebted to Marcos Longo, Naomi Levine, Ke Zhang, and Xiangtao Xu for all the instruction they provided me about working with ED.

References

Anderegg WRL (2014) Spatial and temporal variation in plant hydraulic traits and their relevance for climate change impacts on vegetation. *New Phytologist*, 205, 1008-1014. doi: 10.1111/nph.12907.

Baker IT, Prihodko L, Denning AS, Goulden M, Miller S, da Rocha HR (2008) Seasonal drought stress in the Amazon: Reconciling models and observations. *Journal of Geophysical Research* 113, G00B01. doi: 10.1029/2007JG000644

Baldocchi, D. D. (1997). "Measuring and modeling carbon dioxide and water vapor exchange over a temperate broad-leaved forest during the 1995 summer drought." Plant, Cell and Environment. 20, 1108-1122.

Ball JT, Woodrow IE, Berry JA (1986) A model predicting stomatal conductance and its contribution to the control of photosynthesis under different environmental conditions. In: *Progress in Photosynthesis Research* (ed. Biggins I), pp. 221-224. Martinus Nijhoff, Netherlands.

Baltzer JL, Davies SJ, Bunyavejchewin S, Noor NSM (2008) The role of desiccation tolerance in determining tree species distributions along the Malay–Thai Peninsula *Functional Ecology*, 22, 221–231 doi: 10.1111/j.1365-2435.2007.01374.x

Boisier JP, Ciais P, Ducharne A, Guimberteau M (2015) Projected strengthening of Amazonian dry season by constrained climate model simulations. *Nature Climate Change*, 5, 656-660. doi: 10.1038/nclimate2658.

Bonan GB (2008) Forests and climate change: Forcings, feedbacks, and the climate benefits of forests. *Science*, 320, 1444. doi: 10.1126/science.1155121.

Brando PM, Nepstad DC, Davidson EA, Trumbore SE, Ray D, Camargo P (2008) Drought effects on litterfall, wood production and belowground carbon cycling in an Amazon forest: results of a throughfall reduction experiment. *Philosophical Transactions of the Royal Society B*. 363, 1839–1848. doi:10.1098/rstb.2007.0031

Brodersen CR, McElrone AJ (2013) Maintenance of xylem network transport capacity: a review of embolism repair in vascular plants. *Frontiers in Plant Science*, 4. doi: 10.3389/fpls.2013.00108

Brodribb TJ, Holbrook NM, Edwards EJ, Gutiérrez MV (2003) Relations between stomatal closure, leaf tugor and xylem vulnerability in eight tropical dry forest trees. *Plant, Cell and Environment,* 26, 433-450.

Chambers JQ, dos Santos J, Ribeiro RJ, Higuchi N (2001) Tree damage, allometric relationships, and above-ground net primary production in central Amazon forest. *Forest Ecology and Management,* 152, 73-84.

Clapp RB, Hornberger GM (1978) Empirical equation for some soil hydraulic properties. *Water Resources Research*, 14, 601-604.

Clark DB, Mercado LM, Sitch S, *et al.* (2011) The Joint UK Land Environment Simulator (JULES), model description—Part 2: carbon fluxes and vegetation dynamics. *Geoscientific Model Development* 4, 701-722. doi:10.5194/gmd-4-701-2011

Cochard H, Delzon S (2013) Hydraulic failure and repair are not routine in trees. *Annals if Forest Science*, 70, 659-661. doi: 10.1007/s13595-013-0317-5.

Cosby BJ, Hornberger GM, Clapp RB, Ginn TR (1984) A statistical exploration of the relationships of soil moisture characteristics to the physical properties of soils. *Water Resources Research*, 20, 682-690.

Costa MH, Pires GF (2010) Effects of Amazon and Central Brazil deforestation scenarios on the duration of the dry season in the arc of deforestation. *International Journal of Climatology*, 30, 1970-1979.

Cox PM (2001) Description of the TRIFFID Dynamic Global Vegetation Model. Hadley Centre Technical Note 24, Hadley Centre, Met Office, Bracknell, UK.

Cox PM, Betts RA, Collins M, Harris PP, Huntingford C, Jones CD (2004) Amazonian forest dieback under climate-driven cycle projections for the 21st century. *Theoretical and Applied Climatology*, 78, 137-156. doi: 10.1007/s00704-004-0049-4.

da Costa ACL, Galbraith D, Almeida S, *et al.* (2010) Effect of 7 yr of experimental drought on vegetation dynamics and biomass storage of an eastern Amazonian rainforest. *New Phytologist* 187: 579–591. doi: 10.1111/j.1469-8137.2010.03309.x

Farquhar GD, von Caemmerer S, Berry JA (1980) A biochemical model of photosynthetic CO_2 assimilation in leaves of C_3 species. *Planta*, 149, 78-90.

Fisher RA, Williams M, do Vale RL, da Costa AL, Meir P (2006) Evidence from Amazonian forests is consistent with isohydric control of leaf water potential. *Plant, Cell and Environment*, 29, 151-165.

Fisher RA, Williams M, da Costa AL, Malhi Y, da Costa RF, Almeida S, Meir P (2007) The response of an Eastern Amazonian rain forest to drought stress: results and modelling analyses from a throughfall exclusion experiment. *Global Change Biology*, 13, 2361-2378.

Foley JA, Prentice IC, Ramankutty N, Levis S, Pollard D, Sitch S, Haxeltine A (1996) An integrated biosphere model of land surface processes, terrestrial carbon balance, and vegetation dynamics. *Global Biogeochemical Cycles*, 10, 603–628.

Harper AB, Denning AS, Baker IT, Branson MD, Prihodko L, Randal DA (2010) Role of deep soil moisture in modulating climate in the Amazon rainforest. *Geophysical Research Letters*, 37, L05802. doi:10.1029/2009GL042302.

Huntingford C, Zelazowski P, Galbraith D, et al. (2013) Simulated resilience of tropical rainforests to CO_2-induced climate change. *Nature Geoscience*, 6, 268-273. doi: 10.1038/ngeo1741.

Hutyra LR, Munger W, Saleska SR, Gottlieb E, *et al*. (2007) Seasonal controls on the exchange of carbon and water in an Amazonian rain forest . *Journal of Geophysical Research*, 112, G03008. doi:10.1029/2006JG000365.

Joetzjer E, Douville H, Delire C, Ciais P (2013) Present-day and future Amazonian precipitation in global climate models: CMIP5 versus CMIP3. *Climate Dynamics*, 41, 2921-2936. doi: 10.1007/s00382-012-1644-1

Jones H (1992) Plants and microclimate. pp. 88-102. Cambridge University Press, Cambridge.

Leuning R (1995) A critical appraisal of a combined stomatal-photosynthesis model for C_3 Plants. *Plant Cell and Environment*, 18, 339-355.

Lintner B, Biasutti M, Diffenbaugh NS, Lee J-E, Niznik MJ, Findell KL (2012) Amplification of wet and dry month occurrence over tropical land regions in response to global warming, *Journal of Geophysical Research,* 117, D11106, doi:10.1029/2012JD017499.

Malhi Y, Roberts JT, Betts RA, Killeen TJ, Li W, Nobre CA (2008) Climate change, deforestation, and the fate of the Amazon. *Science* 319: 169. doi: 10.1126/science.1146961

Malhi Y, Aragão, Galbraith D, *et al*. (2009) Exploring the likelihood and mechanism of a climate-change-induced dieback of the Amazon rainforest. *Proceedings of the National Academy of Sciences*, 106, 20610–20615. doi: 10.1073/pnas.0804619106.

McDowell N, Pockman WT, Allen CD, *et al*. (2008) Mechansims of plant survival and mortality during drought: why do some plants survive while other succumb to drought? *New Phytologist*, 178, 719-739. doi: 10.1111/j.1469-8137.2008.02436.x.

McDowell NG, Fisher RA, Xu C, et al., (2013) Evaluating theories of drought-induced vegetation mortality using multimodel-experiment framework. *New Phytologist*, 200, 304-321. doi: 10.1111/nph.12465.

Medvigy D, Wofsy SC, Munger JW, Hollinger DY, Moorcroft PR (2009) Mechanistic scaling of ecosystem function and dynamics in space and time: Ecosystem Demography model version 2. *Journal of Geophysical Research*, 114, G01002, doi:10.1029/2008JG000812.

Meinzer FC, James SA, Goldstein G (2004) Dynamics of transpiration, sap flow and use of stored water in tropical forest canopy trees. *Tree Physiology*, 24, 901-909.

Metcalfe DB, Meir P, Aragão LEOC, *et al*. (2007) Factors controlling spatio-temporal variation in carbon dioxide efflux from surface litter, roots, and soil organic matter at four rain forest sites in the eastern Amazon. *Journal of Geophysical Research – Biogeosciences*, 112, G04001. doi: 10.1029/2007JG000443.

Metcalfe DB, Lobo-do-Vale R, Chaves MM, *et al.* (2010a). Impacts of experimentally imposed drought on leaf respiration and morphology in an Amazon rainforest. *Functional Ecology*, 24, 524-533. doi: 10.1111/j.1365-2435.2009.01683.x

Metcalfe DB, Meir P, Aragão LEOC, *et al* .(2010b) Shifts in plant respiration and carbon use efficiency at a large-scale drought experiment in the eastern Amazon. *New Phytologist*, 187, 608–621. doi: 10.1111/j.1469-8137.2010.03319.x

Moorcroft PR, Hurtt GC, Pacala SW (2001) A method for scaling vegetation dynamics: The Ecosystem Demography model (ED). *Ecological Monographs*, 71, 557-587.

Nardini A, Ramani M, Gortan E, Salleo S (2008). Vein recoveryfrom embolism occurs under negative pressure in leaves of sunflower (*Helianthus annuus*). *Physiologia Plantarum*, 133, 755–764. doi: 10.1111/j.1399-3054.2008.01087.x

Nemani R, Keeling C, Hashimoto H *et al*. (2003) Climate-driven increases in global terrestrial net primary production from 1982 to 1999. *Science* 300, 1560-1563.

Nepstad DC, Moutinho PR (2008) LBA-ECO LC-14 Rainfall Exclusion Experiment, LAI, Gap Fraction, TNF, Brazil: 2000-05. Data set. Available on-line [http://lba.cptec.inpe.br/] from LBA Data and Information System, National Institute for Space Research (INPE/CPTEC), Cachoeira Paulista, Sao Paulo, Brazil [accessed 17 November 2012].

Nepstad DC, Moutinho P, Dias-Filho MB, *et al.* (2002) The effects of partial throughfall exclusion on canopy processes, aboveground production, and biogeochemistry of an Amazon forest. *Journal of Geophysical Research*, 107(D20), 8085. doi:10.1029/2001JD000360.

Nepstad DC, Tohver IM, Ray D, Moutinho P, Cardinot G. 2007. Mortality of large trees and lianas following experimental drought in an Amazon forest. *Ecology*, 88, 2259-2269.

Ogasa M, Miki NH, Murakami Y, Yoshikawa K (2013) Recovery performance in xylem hydraulic conductivity is correlated with cavitation resistance for temperate deciduous tree species. *Tree Physiology*, 33, 335-344. doi:10.1093/treephys/tpt010.

Oleson KW, Niu G-Y, Yang Z-L, *et al*. (2008) Improvements to the Community Land Model and their impact on the hydrological cycle. *Journal of Geophysical Research*, 113, G01021. doi:10.1029/2007JG000563.

Petit G, Anfodillo T, Mencuccini M (2008) Tapering of xylem conduits and hydraulic limitations in sycamore (*Acer pseudoplantanus*) trees. *New Phytologist*, 177, 653-664. doi: 10.1111/j.1469-8137.2007.02291.x

Pineda-García F, Paz H, Meinzer FC (2013) Drought resistance in early and late secondary successional species from a tropical dry forest: the interplay between xylem resistance to embolism, sapwood water storage and leaf shedding. *Plant Cell and Environment*, 36, 405-418. doi: 10.1111/j.1365-3040.2012.02582.x

Phillips OL, van der Heijden G, Lewis S, *et al*. (2010) Drought-mortality relationships for tropical forests. *New Phytologist*, 187, 631-646. doi: 10.1111/j.1469-8137.2010.03359.x

Poorter L, McDonald I, Alarcon A, *et al*. (2010) The importance of wood traits and hydraulic conductance for the performance and life history strategies of 42 rainforest tree species. *New Phytologist*, 185, 81-492. doi: 10.1111/j.1469-8137.2009.03092.x.

Powell TL, Galbraith DR, Christoffersen BO, *et al*. (2013) Confronting model predictions of carbon fluxes with measurements of Amazon forests subjected to experimental drought. *New Phytologist*, 200, 350-364. doi: 10.1111/nph.12390

Rosolem R, Shuttleworth WJ, Gonçalves LGG (2008) Is the data collection period of the Large-Scale Biosphere-Atmosphere Experiment in Amazonia representative of long-term climatology? *Journal of Geophysical Research*, 113, G00B09, doi:10.1029/2007JG000628.

Ryan MG, Phillips N, Bond BJ (2006) The hydraulic limitation hypothesis revisited. *Plant, Cell and Environment*, 29, 367-381. doi: 10.1111/j.1365-3040.2005.01478.x.

Sakaguchi K, Zeng X, Christoffersen BJ, Restrepo-Coupe N, Saleska SR, Brando PM (2011) Natural and drought scenarios in an east central Amazon forest: Fidelity of the Community Land Model 3.5 with three biogeochemical models. *Journal of Geophysical Research*, 116, G01029. doi:10.1029/2010JG001477.

Sellers PJ, Randall DA, Collatz GJ, Berry JA, Field CB, Dazlich DA, Zhang C, Collelo GD, Bounoua L (1996) A revised land surface parameterization (SiB2) for atmospheric GCMs. Part I: Model formulation. *Journal of Climate*, 9, 676-705.

Sobrado MA, (1986) Aspects of tissue water relations and seasonal changes of leaf water potential components of evergreen and deciduous species coexisting in tropical dry forests. *Oecologia*,68, 413-416.

Sperry JS, Love DM (2015) What plant hydraulics can tell us about responses to climate-change droughts. *New Phytologist*, 207, 14-27. doi: 10.1111/nph.13354

von Caemmerer S, Farquhar GD (1981) Some relationships between the biochemistry of photosynthesis and the gas exchange of leaves. *Planta*, 153, 376-387.

West GB, Brown JH, Enquist BJ (1999) A general model for the structure and allometry of plant vascular systems. *Nature*, 400, 664-667.

Wheeler JK, Huggett BA, Tofte AN, Rockwell FE, Holbrook NM (2013) Cutting xylem under tension or supersaturated with gas can generate PLC and the appearance of rapid recovery from embolism. *Plant Cell Environment*, 36, 1938-1949. doi:10.1111/pce.12139

Williams M, Rastetter EB, Fernandes DN, *et al*. (1996) Modelling the soil-plant-atmosphere continuum in a *Quercus-Acer* stand at Harvard Forest: the regulation of stomatal conductance by light, nitrogen and soil/plant hydraulic properties. *Plant, Cell and Environment*, 19, 911–927.

Zhang K, Castanho ADDA, Galbraith DR, *et al*. (2015) The fate of the Amazonian ecosystems over the coming century arising from changes in climate, atmospheric CO2, and land use. *Global Change Biology*, 21, 2569–2587. doi: 10.1111/gcb.12903.

Chapter 5

Conclusions

This dissertation explores the ecological implications of the projected reductions in precipitation across the Amazon basin. Climate models are converging on either more extreme wet and dry seasons, a lengthening of the dry season length, or general drying in different regions across the basin (Malhi *et al*. 2008, Lintner *et al*., 2012, Joetzjer *et al*., 2013, Boisier *et al*., 2015). It is of considerable ecological interest to understand how these changes in precipitation may affect ecosystem services and where to target conservation efforts. While incredibly informative about fundamental mechanisms, manipulations on individuals and whole ecosystems are limited by issues associated with spatial and temporal scaling because of the difficulty in capturing emergent properties that arise in higher scales of organization. Therefore, state of the art terrestrial biosphere models, which dynamically track vegetation responses to physical forcings and scales to the landscape, are theoretically among our best tools, if not the only tool, for making this assessment.

The current formulations in terrestrial biosphere models are, however, untested against a robust set of benchmarks for tropical forest responses to drought. Therefore, the Chapter 2 of this dissertation explores whether or not a collection of terrestrial biosphere and ecosystem models that have been used to assess Amazon drought responses (e.g. Cox *et al*., 2004, Baker *et al.,* 2008) are properly formulated in the first place. This model intercomparison standardized for the first time, the physical environment across all models so that the range of formulations representing the biological processes, such as photosynthesis, respiration, carbon allocation and storage, and competition could be evaluated. This study demonstrates that terrestrial biosphere models can reliably predict plant and ecosystem carbon fluxes under the present climate, but still require substantial

development for predicting the consequences of severe drought. Model development should be focused on testing hypotheses associated with enhanced autotrophic respiration under severe water-stress, controls over leaf phenology, stomatal responses to soil water-stress, and drought induced mortality.

An important finding of Powell *et al*. (2013) and others (e.g. Sakaguchi et al. 2011, Anderegg, 2014) calls into question how soil water-stress and water-transport are represented in terrestrial biosphere models. One concern is the lack of functional diversity in the soil water-stress parameterization, which precludes explicit competition between species with alternative growth versus xylem-safety strategies. Previous research has shown considerable diversity in plant hydraulic traits among tropical forest tree species (e.g. Baltzer *et al*., 2008; Bartlett *et al*., 2012), but very few have linked this physiological diversity to functional diversity at the ecosystem scale. Chapter 3 of this dissertation explores how plant hydraulic traits vary between species identified as early successional versus late successional and between species identified as drought tolerant versus drought intolerant. Chapter 3 also explores how plant hydraulic traits vary temporally and spatially for each of the four plant functional types. The evidence from this study suggests that traits associated with drought tolerance are orthogonal to wood density, which is an important life history trait associated with succession. The evidence also suggests that hydraulic traits of *terra firma* trees are largely conserved spatially and temporally. However, lack of plasticity in hydraulic traits indicates that mature trees belonging to the drought intolerant functional type are vulnerable to reductions in precipitation because of their limited ability to adjust. Finally, insights from this study

provide valuable information about plant hydraulic traits needed to parameterize more realistic water-stress functions in terrestrial biosphere models.

To date, formulations for representing soil water-stress and water transport are fairly simplistic relative to the detailed level of understanding we have about these processes (Sperry and Love, 2015). Chapter 4 of this dissertation explores the level of sophistication required in the soil water-stress and water transport formulations in order for terrestrial biosphere models to make robust predictions about tropical forest drought responses. Three different water-stress and water transport formulations, ranging in degrees of complexity, were evaluated using the Ecosystem Demography model (ED): (1) a single-resistor formulation as a function of soil moisture (EDsr), (2) a supply and demand formulation as a function of soil moisture (EDor), and (3) a hydrodynamic supply and demand formulation as a function of leaf water potential (EDhd). The hydrodynamic formulation transfers the soil water potential to the leaf. The results of this study support the hypothesis that functional diversity related to differences in plant hydrodynamics is an important ecosystem property because compositional shifts in tropical forest tree species that arise from differences in plant hydrodynamics is predicted by this analysis to be a consequence of changes in precipitation patterns. Also, plant hydrodynamics capture size-dependent physiological processes, which in turn enable terrestrial biosphere models to more correctly capture structural shifts associated with the observed size-dependent mortality that occurs during severe droughts (da Costa *et al*., 2010). Therefore, including functional diversity along a drought-tolerance gradient and plant hydrodynamics are essential when terrestrial biosphere models are used to predict the fate of tropical ecosystems subjected to severe droughts.

References

Baker IT, Prihodko L, Denning AS, Goulden M, Miller S, da Rocha HR (2008) Seasonal drought stress in the Amazon: Reconciling models and observations. *Journal of Geophysical Research* 113, G00B01. doi: 10.1029/2007JG000644

Baltzer JL, Davies SJ, Bunyavejchewin S, Noor NSM (2008) The role of desiccation tolerance in determining tree species distributions along the Malay–Thai Peninsula *Functional Ecology*, 22, 221–231 doi: 10.1111/j.1365-2435.2007.01374.x

Bartlett MK, Scoffoni C, Sack L (2012) The determinants of leaf tugor loss point and prediction of drought tolerance of species and biomes: a global meta-analysis. *Ecology Letters*: 15, 393-405. dio: 10:1111/j.1461-0248.2012.01751.x.

Boisier JP, Ciais P, Ducharne A, Guimberteau M (2015) Projected strengthening of Amazonian dry season by constrained climate model simulations. *Nature Climate Change*, 5, 656-660. doi: 10.1038/nclimate2658.

Cox PM, Betts RA, Collins M, Harris PP, Huntingford C, Jones CD (2004) Amazonian forest dieback under climate-driven cycle projections for the 21st century. *Theoretical and Applied Climatology*, 78, 137-156. doi: 10.1007/s00704-004-0049-4.

da Costa ACL, Galbraith D, Almeida S, *et al.* (2010) Effect of 7 yr of experimental drought on vegetation dynamics and biomass storage of an eastern Amazonian rainforest. *New Phytologist* 187: 579–591. doi: 10.1111/j.1469-8137.2010.03309.x

Joetzjer E, Douville H, Delire C, Ciais P (2013) Present-day and future Amazonian precipitation in global climate models: CMIP5 versus CMIP3. *Climate Dynamics*, 41, 2921-2936. doi: 10.1007/s00382-012-1644-1

Lintner B, Biasutti M, Diffenbaugh NS, Lee J-E, Niznik MJ, Findell KL (2012) Amplification of wet and dry month occurrence over tropical land regions in response to global warming, *Journal of Geophysical Research,* 117, D11106, doi:10.1029/2012JD017499.

Malhi Y, Roberts JT, Betts RA, Killeen TJ, Li W, Nobre CA (2008) Climate change, deforestation, and the fate of the Amazon. *Science* 319: 169. doi: 10.1126/science.1146961

Powell TL, Galbraith DR, Christoffersen BO, *et al*. (2013) Confronting model predictions of carbon fluxes with measurements of Amazon forests subjected to experimental drought. *New Phytologist*, 200, 350-364. doi: 10.1111/nph.12390

Sperry JS, Love DM (2015) What plant hydraulics can tell us about responses to climate-change droughts. *New Phytologist*, 207, 14-27. doi: 10.1111/nph.13354

Appendix A

Protocol for drought manipulations

See the Table 1 below for a summary and check-list of the required simulations.

GENERAL NOTE:

The simulations for both sites should begin with one baseline year using normal precipitation (i.e. do not impose a drought) and then the drought manipulation with be imposed for the following seven years. The baseline year for TNF is 1999 and the manipulations years are 2000-2006. The baseline year for CAX is 2001 and the manipulations years are 2002-2008.

SITE SPECIFIC INFORMATION:

Tapajos National Forest (TNF)

Experiment information (Nepstad et al. 2002):

1 ha treatment plot, 1 ha control plot. Rainfall input was reduced by 50%. Throughfall was reduced by 60%. Stem flow was not excluded. Throughfall exclusion occurred only during wet season (approx. Jan – Jun). Treatment period was Jan 2000 – Dec 2004

Simulation information:

1. General information:
    a. Coordinates: Use S83 lat: -3.02, lon:-54.97
    b. Soil depth: 8 meters.

c. Soil type: 60%clay, 38% sand (Nepstad et al., 2002)

d. Use free drainage.

e. Meteorological drivers: SOImet is from the km67 tower and covers 2002-2004 (supplied by Natalia). SHF met covers 1970 to 2008

2. Understanding the interaction between local and regional met driver, and the impacts of drought on an equilibrium forest:

   a. *Summary*: We will do two sets of simulations; both initialized with bare-ground spin ups. The first set will use the Sheffield met drivers (SHF), the second set will use SOImet drivers (SOImet). Both sets will cover drought levels ranging from 0% - 90% reduction in above canopy precipitation.

   b. *Spin up initialization*: Do one bare ground spin up using the SHF met drivers and do one bare ground spin up using the SOImet drivers. Follow the same bare-ground spin up protocol described in the SiteLevelSimulations document. Therefore, spin up to equilibrium (approximately 500yrs)with pre-industrial CO_2(280 ppm) level . Then, perform a transient simulation from 1720 to 2000 with increasing atmospheric CO_2 to present day levels. (Tip: Run this just like the S67 site level spin ups, except change the soils and coordinates.)

      For each set of simulations, use the same met drivers throughout the spin up and manipulation period. (If you use the SHF met drivers for the spin up, then use the SHF met drivers for the manipulation period. And, if you use the SOImet drivers for the spin up then use the SOImet drivers for

the manipulation period.) The meteorological forcing data should cycle sequentially throughout the spin up and manipulations periods.

c. *Manipulations*: Generate hourly and monthly output following the Moore Simulations Output document. See Table 1 for summary of all simulations.

   i. Run a one year baseline period for 1999. NOTE: For the SOImet drivers, DO NOT USE 2002 for the baseline year. Use 2004 to create the baseline year (See Table 2). We need to use 2004, because 2002 is a dry year and we do not want to start the drought manipulation with the ecosystem already water-stressed by a natural drought. And, 1999 in the SHF met drivers is not a dry year, so this will remove an artefact when we compare the two.

   ii. MONTHLY OUTPUT: Run all monthly simulations for a total of 8 years (1999-2006) using both meteorological drivers. The first year (1999) is a baseline year where no drought is imposed. Impose the treatment in the second year for the remaining 7 years of the simulation (2000-2006). For the treatment, reduce above canopy precipitation by 0% (control) and in 10% increments from 10% to 90% (drought treatments) between January and June. Use unadjusted precipitation for the months of July to December (similar to the actual TFE experiment).

   iii. HOURLY OUTPUT: Run all hourly simulations for three years. Run 0% drought for the baseline year (1999). Then, impose all treatment levels (d00 to d90) in the second and third years of the

simulation. Use unadjusted precipitation from July to December each year.

Validation biomass information:

Raw data: Document LBA-ECO LC-14. Published results: Nepstad et al., (2007), Brando et al., (2008). *Biomass citation*: Nepstad, D.C. and P.R. Moutinho. 2008. **LBA-ECO LC-14** Rainfall Exclusion Experiment, LAI, Gap Fraction, TNF, Brazil: 2000-05. Data set. Available on-line [http://lba.cptec.inpe.br/] from LBA Data and Information System, National Institute for Space Research (INPE/CPTEC), Cachoeira Paulista, Sao Paulo, Brazil. (Note: the data are easier to locate through the link on the Moore website.)

Caxiuana (CAX)

Experiment information:

Measurements were taken in a pre-treament year (2001) to establish a baseline for both the control and throughfall exclusion plots. The treatment period was Jan 2002 – present. Rainfall input was reduced by 50% throughout the whole year (i.e., panels were not removed during the dry season as in Tapajós). Two exceptions to this were: a) a 2-week period in November 2002 when the panels were completely removed and b) all of 2004, where panel damage reduced the amount of excluded rainfall to approximately 30 % (Antonio Carlos Lola da Costa, pers. comm.).

Simulation information:

1. General information:
    a. Coordinates: (Fisher et al. 2007) lat:-1.72, lon:-51.46.
    b. Soil depth: 8 meters.
    c. Soil type: 78% sand, 15% clay, 7% silt (following mid-values of Fisher et al. 2007).
    d. Use free drainage.
    e. Meteorological drivers: SOImet is from the CAX06 tower and covers 2001-2008 (supplied by D. Galbraith). SHEF met covers 1970 to 2008
2. Understanding the interaction between local and regional met driver, and the impacts of drought on an equilibrium forest:
    a. *Summary*: Similar to TNF, do two sets of simulations; both initialized with bare-ground spin ups. The first set will use the Sheffield met drivers (SHF), the second set will use Site Level met drivers (SOImet). Both sets will cover drought levels ranging from 0% - 90% reduction in above canopy precipitation.
    b. *Spin up initialization*: Do one bare ground spin up using the SHF met drivers and do one bare ground spin up using the SOImet drivers. Follow the same bare-ground spin up protocol described in the SiteLevelSimulations document. Therefore, spin up to equilibrium (approximately 500yrs)with pre-industrial CO_2(280 ppm) level . Then, perform a transient simulation from 1720 to 2000 with increasing

atmospheric CO_2 to present day levels. (Tip: Run theses just like the CAX06 spin ups, except change the soils and coordinates.)

For each set of simulations, use the same met drivers throughout the spin up and manipulation period. The meteorological forcing data should cycle sequentially throughout the spin up and manipulations periods.

c. *Control and drought simulations*: Generate hourly and monthly output following the Moore Simulations Output document. See Table 1 for summary of all simulations.

   i. Run a one year baseline period for 2001 using the met year of 2001 for both the SHF and SOImet drivers.

   ii. MONTHLY OUTPUT: Run these simulations for a total of 8 years (2001-2008) using both meteorological drivers. The first year (2001) is a baseline year where no drought is imposed. Impose the treatment in the second year for the remaining 7 years of the simulation (2002-2008). Reduce above canopy precipitation by 0% (control) and in 10% increments from 10% to 90% for the <u>whole year during the drought period (2002-2008)</u>.

   iii. HOURLY OUTPUT: Run all hourly simulations for three years. Run 0% drought for the baseline year (2001). Then, in the second and third years of the simulation impose all treatment levels (d00 to d90) for the entire year.

Validation biomass and summary of measurements:

Ecosystem carbon stocks, wood production and tree mortality: da Costa *et al*., (2010).

Photosynthetic parameters Vcmax, Jmax: Fisher *et al*., (2007).

Leaf area index: Fisher *et al*., (2007).

Litterfall and coarse woody debris: Metcalfe *et al*., (2010).

Stomatal conductance, sap flow, leaf water potential, xylem water potential: Fisher *et al*., (2006)

Soil respiration: Sotta *et al*., (2007).

Net primary production of leaves, roots, wood: Metcalfe *et al*., (2010).

Leaf, stem, root respiration: Metcalfe et al., (2010).

Soil moisture: Fisher et al. (2007), da Costa *et al*., (2010).

Table A1. Required drought simulations:

Simulation	base-line yr[1]	Manipulation drought levels									
		0%	10%	20%	30%	40%	50%	60%	70%	80%	90%
Monthly Output											
CAX_TFE manipulation years											
CAX_TFE BGspin SHEFmet											
CAX_TFE BGspin SOImet											
TNF_TFE manipulation years											
TNF_TFE BGspin SHEFmet											
TNF_TFE BGspin SOImet											
Hourly Output											
CAX_TFE											
CAX_TFE BGspin SHEFmet											
CAX_TFE BGspin SOImet											
TNF_TFE											
TNF_TFE BGspin SHEFmet											
TNF_TFE BGspin SOImet											

Table 1 Notes:

1. In all of the simulations (d00 to d90), include the baseline year with drought level set to 0. Baseline years: CAX: 2001, TNF: 1999.
2. Manipulations years: CAX: 2002 to 2008, TNF 2000 to 2006.
3. Output Years: CAX(hourly): 2001 to 2003), CAX(monthly): 2001 to 2008); TNF(hourly): 1999 to 2001, TNF(monthly): 1999 to 2006.
4. BGspin: drought simulations initialized from a bare ground spin up.
5. SHEFmet: Sheffield meteorological driver.
6. SOImet: Site of interest meteorological driver.

Table A2. Match-up between the met driver year and the year of the simulation.

Simulation year	Meteorological driver year			
	TNF		CAX	
	SHEFmet BGspin	SOImet BGspin	SHEFmet BGspin	SOImet BGspin
1999	1999*	2004*	--	--
2000	2000	2003	--	--
2001	2001	2004	2001*	2001*
2002	2002	2002	2002	2002
2003	2003	2003	2003	2003
2004	2004	2004	2004	2004
2005	2005	2002	2005	2005
2006	2006	2003	2006	2006
2007	--	--	2007	2007
2008	--	--	2008	2008

Notes: * denotes the baseline year (do not impose a drought).

References:

Meteorological forcing data:

Sheffield J, Goteti G, Wood EF (2006) Development of a 50-year high-resolution global dataset of meteorological forcings for land surface modeling. *Journal of Climate*, 19, 3088-3111.

Tapajos National Forest

Brando PM, et al. (2008) Drought effects on litterfall, wood production and belowground carbon cycling in an Amazon forest: results of a throughfall reduction experiment. *Philosophical Transactions of the Royal Society B,* 363, 1839-1848. doi: 10.1098/rstb.2007.0031.

Nepstad DC, et al. (2002) The effects of partial throughfall exclusion on canopy processes, aboveground production, and biogeochemistry of an Amazon forest. *Journal of Geophysical Research* 107(D20), 8085. doi:10.1029/2001JD000360.

Nepstad DC, et al. (2007) Mortality of large trees and lianas following experimental drought in an Amazon forest. *Ecology*, 88, 2259-2269.

Caxiuana

da Costa A.C.L., et al. (2010) Effect of seven years of experimental drought on the aboveground biomass storage of an eastern Amazonian rainforest. *New Phytologist*, 187, 579-591. doi: 10.1111/j.1469-8137.2010.03309.x

Fisher R M, et al. (2006) Evidence from Amazonian forests is consistent with isohydric control of leaf water potential, *Plant, Cell and Enironment.*, *29*, 151-165.

Fisher RA, et al. (2007) The response of an Eastern Amazonian rain forest to drought stress: results and modelling analyses from a throughfall exclusion experiment. *Global Change Biology, 13*, 2361-2378.

Metcalfe DB, *et al.* (2007) Factors controlling spatio-temporal variation in carbon dioxide efflux from surface litter, roots, and soil organic matter at four rain forest sites in the eastern Amazon. *Journal of Geophysical Research*, *112*, G04001, doi:10.1029/2007JG000443.

Metcalfe DB, et al. (2010) Shifts in plant respiration and carbon use efficiency at a large-scale drought experiment in the eastern Amazon. *New Phytologist,* 187, 608-621. doi: 10.1111/j.1469-8137.2010.03319.x

Metcalfe DB, et al. (2008) The effects of water availability on root growth and morphology in an Amazon rainforest. *Plant and Soil*, *311*, 189-199.

Sotta ED, et al. (2007), Effects of an induced drought on soil CO2 efflux and soil CO2 production in an Eastern Amazonian rainforest, Brazil, *Global Change Biology,* 13, 2218-2229. doi: 10.1111/j.1365-2486.2007.01416.x.

Appendix B

(as published in New Phytologist)

Chapter 2 Supporting Information: Notes S1–S5, Tables S2.1–S2.4 and Figures S2.1-S2.7.

Table S2.1 Net and component ecosystem carbon fluxes (kg C m^{-2} yr^{-1}) in the fourth[1] year of the experiment for TNF and CAX. Carbon flux definitions and observation sources are given in Table 2.2. d0 and d50 are drought levels indicating a 0% and 50% reduction in precipitation. The Δ indicates the amount the control (d0) fluxes were altered by the 50% drought treatment. Observations are the mean ± 95% CI (when reported) of samples collected within each 1 ha plot.

Flux	TNF							CAX						
	CLM3.5	ED2	IBIS	JULES	SIB3	SPA	Obs	CLM3.5	ED2	IBIS	JULES	SIB3	SPA	Obs
AGB d0[1]	16.6	10.6	9.0	12.4		30.8	14.4	17.0	12.3	9.4	14.0		20.8	21.4 ± 1.4
Δ*AGB* d50[1]	-0.2	-5.4	-0.2	-0.6		-0.3	-3.2	-0.3	-1.4	-0.1	-0.2		-0.3	-3.8 ± 0.2
NEP d0	0.16	0.30	0.13	-0.07	-0.16	0.17	-0.09 ± 0.05	-0.06	0.26	0.29	0.10	0.18	0.09	
Δ*NEP* d50	-0.49	-0.31	-0.64	-0.31	-0.45	-0.24		-0.09	-0.03	0.01	-0.41	-0.22	-0.12	
GPP d0	3.63	2.87	3.09	2.95	3.36	3.05	3.17 ± 0.03	3.82	3.37	3.52	3.53	3.94	3.23	
Δ*GPP* d50	-0.98	-1.86	-0.75	-1.15	-1.15	-0.55		-0.39	-0.71	-0.05	-1.33	-0.51	-0.42	
R_e d0	3.47	2.57	2.96	3.02	3.52	2.88	3.26 ± 0.06	3.88	3.11	3.23	3.43	3.76	3.14	3.26 ± 0.09
ΔR_e d50	-0.50	-1.54	-0.11	-0.83	-0.70	-0.31		-0.30	-0.68	-0.06	-0.93	-0.28	-0.30	0.40 ± 0.47
R_h d0	1.00	1.08	0.91	0.93	1.79	1.33		1.16	1.35	1.03	1.15	1.84	0.94	1.02 ± 0.10
ΔR_h d50	-0.2	-0.61	0.12	-0.34	-0.30	-0.03		-0.12	-0.34	-0.05	-0.39	-0.11	-0.01	0.07 ± 0.18

Table S2.1 continued.

Flux	TNF							CAX						
	CLM3.5	ED2	IBIS	JULES	SIB3	SPA	Obs	CLM3.5	ED2	IBIS	JULES	SIB3	SPA	Obs
R_a d0	2.48	1.49	2.05	2.08	1.74	1.56		2.72	1.75	2.20	2.28	1.92	2.20	2.24 ± 0.28
ΔR_a d50	-0.29	-0.93	-0.22	-0.49	-0.40	-0.28		-0.18	-0.34	-0.01	-0.54	-0.17	-0.29	0.34 ± 0.44
R_{lf} d0	0.70	0.67	0.72	0.73	0.61	0.32		0.81	0.79	0.77	0.83	0.76	0.43	0.73 ± 0.20
ΔR_{lf} d50	-0.45	-0.40	0.01	-0.32	-0.25	-0.08		-0.06	-0.15	0.00	-0.34	-0.12	-0.08	0.21 ± 0.35
R_w d0	0.85	0.82	0.01	0.54		0.83		0.81	0.96	0.01	0.61		0.85	0.89 ± 0.18
ΔR_w d50	0.79	-0.53	0.00	-0.09		-0.11		-0.15	-0.19	0.00	-0.11		-0.08	0.02 ± 0.25
R_r d0	0.92	0.13	0.46	0.81	1.13	0.41		1.10	0.15	0.47	0.83	1.16	0.91	0.62 ± 0.03
ΔR_r d50	-0.63	-0.07	-0.02	-0.08	-0.15	-0.09		0.03	-0.01	-0.01	-0.09	-0.06	-0.13	0.11 ± 0.04
R_s d0	1.58	1.21	1.37	1.86	2.92	1.73	1.28 ± 0.01	1.85	1.5	1.49	2.11	2.99	1.85	1.63
ΔR_s d50	-0.75	-0.68	0.10	-0.44	-0.45	-0.12	0.0 ± 0.16	-0.02	-0.35	-0.06	-0.5	-0.17	-0.14	-0.42
NPP_w d0	0.48	0.47	0.52	0.32		0.45	0.34	0.26	0.56	067	0.49		0.31	0.18 ± 0.02

Table S2.1 continued.

Flux	TNF							CAX						
	CLM3.5	ED2	IBIS	JULES	SIB3	SPA	Obs	CLM3.5	ED2	IBIS	JULES	SIB3	SPA	Obs
ΔNPP_w d50	-0.48	-0.36	-0.26	-0.25		-0.08	-0.19	-0.13	-0.18	-0.02	-0.31		-0.04	-0.04 ± 0.02
Litter d0	0.23	0.18	0.31	0.06		0.67	0.34 ± 0.01	0.25	0.20	0.36	0.07		0.46	
ΔLitter d50	-0.02	-0.11	0.00	0.00		-0.10	-0.09 ± 0.01	-0.02	-0.03	0.00	0.00		-0.05	

1. TNF AGB estimates are for 2005. CAX AGB estimates are for 2001 at the d0 level and 2008 at the d50 level, which are the reported years of observations.

Notes S1 Explanation of symbols

Table S2.2 Explanation of symbols

Symbol	Definition	Value	Units
This paper:			
d0	No drought		
d30	30% reduction in precipitation		
d50	50% reduction in precipitation		
d80	80% reduction in precipitation		
Δ	Difference between drought and reference (e.g. d50-d0)		
model variables:			
A_g	Leaf-level gross C assimilation		μmol CO_2 m^{-2} s^{-1}
A_n	Leaf-level net C assimilation		μmol CO_2 m^{-2} s^{-1}
A_p	Leaf-level potential C assimilation (JULES)		μmol CO_2 m^{-2} s^{-1}
AGB	Aboveground biomass		kg C m^{-2}
B_j	Biomass in tissue *j*		g C m^{-2}
B_{fri}	Fraction of root biomass a soil layer *i*	0-1	unitless
$B_{fri,ap}$	Apparent fraction of root biomass a soil layer *i*	0-1	unitless
D	Total canopy demand for soil water (ED2)		kg H_20 m^{-2} s^{-1}
ET_{max}	Maximum evapotranspiration (ED2)		kg H_20 m^{-2} s^{-1}
GPP	Gross primary production of carbon		kg C m^{-2} yr^{-1}
g_s	Stomatal conductance of CO_2		mmol CO_2 m^{-2} leaf s^{-1}
i	Index of vertical layer		
j	Index of leaf, wood and fine root components		
LAI	Leaf area index		m^2 m^{-2}
f(N)	Nitrogen limitation function		
NEP	Net ecosystem production of carbon		kg C m^{-2} yr^{-1}

Table S2.2 continued.

Symbol	Definition	Value	Units
NPP_w	Net primary production of carbon in wood		kg C m^{-2} yr^{-1}
R_a	Autotrophic respiration		kg C m^{-2} yr^{-1}
R_e	Whole ecosystems respiration		kg C m^{-2} yr^{-1}
R_g	Growth respiration		kg C m^{-2} yr^{-1}
R_h	Heterotrophic respiration		kg C m^{-2} yr^{-1}
R_{lf}	Leaf respiration		kg C m^{-2} yr^{-1}
R_m	Maintenance respiration		kg C m^{-2} yr^{-1}
R_r	Root respiration		kg C m^{-2} yr^{-1}
R_s	Soil respiration		kg C m^{-2} yr^{-1}
R_w	Wood respiration		kg C m^{-2} yr^{-1}
S_i	Supply of available water in layer i (ED2)		kg H_20 m^{-2} s^{-1}
T_{lf}	Leaf temperature		CLM3.5: °K ED2: °C
V_{cmax}	Maximum carboxylation capacity of Rubisco		μmol CO_2 m^{-2} s^{-1}
VPD	Vapor pressure deficit		kPa
θ_i	Volumetric soil water content in soil layer i		m^3 m^{-3}
ψ_i	Soil water matric potential in soil layer i		m
model parameters:			
a_{vmax}	Q10 for V_{c25}	CLM: 2.4	
cn_j	Carbon to nitrogen ratio in tissue j (leaf, wood, fine roots)	CLM3.5: 29, 330, 29 SPA: 23, 97, 23	gC gN^{-1}
K_w	Soil-plant conductivity parameter	ED: 1.4260×10^{-5}	m^2 s^{-1} (kg C root)$^{-1}$

Table S2.2 continued.

Symbol	Definition	Value	Units
V_{c25}	Value of V_{cmax} at 25 ℃	CLM: 76.1 SiB: 100	μmol CO_2 m^{-2} s^{-1}
α	Factor that determines strength of β	IBIS: -5.0 SiB3: 0.2	unitless
β_i	Soil water-stress factor a for soil layer *i*	0-1	unitless
β_t	Total soil water-stress factor integrated over the soil column	0-1	unitless
θ_f	Volumetric soil water content at field capacity	CAX: 0.193 TNF: 0.327	m^3 m^{-3}
θ_w	Volumetric soil water content at the wilting point	CAX: 0.089 TNF: 0.246	m^3 m^{-3}
ψ_{so}	Soil matrix potential when stomata are fully open	CLM: -66	m
ψ_w	Soil matrix potential at wilting point	-153	m
$_{CLM}$	Respiration coefficient, rate g C converted g N (see note 1)	CLM: 3.17×10^{-7}	gC gN^{-1} s^{-1}
γ_{lf}	Proportionality constant to convert V_{cmax} to R_{lf} (see note 1)	0.015	unitless
γ_r	Root respiration coefficient	ED: 0.528 IBIS: 4.76×10^{-10}	s^{-1} s^{-1}

Note: 1. Parameter is PFT dependent; value given is for broadleaf tropical trees.

Notes S2 Model specific soil water-stress functions (β)

The model specific β functions used to down-regulate *GPP* as soils dry are given in Table S3. Two unique features of the β function in CLM3.5 were that it scaled the leaf-level calculation of the maximum carboxylation capacity of Rubisco (V_{cmax}) and it was parameterized for soil matrix potential (ψ). The β calculation of ED2 differed from the other models by including leaf-water demand. Consequently for ED2, β had a hyperbolic functional form with respect to water-stress (i.e. β vs D/S). By contrast, β in the other models followed a sigmoidal shape as water-stress increased (i.e. β vs ψ or θ); however, its sensitivity to available soil moisture differed across models (Fig. 2.9). CLM, IBIS and JULES coupled the amount of soil water drawn from each layer (i) to the root biomass fraction contained in that layer (B_{ri}). By contrast, SiB3 and ED2 did not impose a cap on the amount of water drawn from a single soil layer when $\theta_i > \theta_w$. Both models prioritized water uptake across the different soil layers according to the amount of root biomass in each layer. However, when the supply of water was insufficient in any given soil layer, both models allowed water uptake to be passed onto different soil layers by adjusting the actual fraction of root biomass in each soil layer to an apparent root fraction ($B_{ri,apparent}$) that reflected the available soil moisture in that layer. In this manner, the relative contribution of water from each soil layer to transpiration was dynamic, thereby representing hydraulic redistribution.

Reference

Cox PM. 2001. *Description of the TRIFFID Dynamic Global Vegetation Model. Hadley Centre Technical Note 24.* Bracknell, UK: Hadley Centre, Met Office.

Table S2.3 Formulations for the soil water-stress functions for CLM3.5, ED2, IBIS, JULES and SiB3. Explanations of symbols are given in Table S2.2.

Model	Soil water-stress functions (β)	References
CLM3.5	$V_{cmax} = V_{c25}(a_{vmax})^{\frac{T_{lf}-25}{10}} f(T_{lf})\beta_t f(N)$ $\beta_t = \sum_i \beta_i B_{ri}$ $\beta_i = \left(\frac{\psi_i - \psi_w}{\psi_{so} - \psi_w}\right)$ $total\ i = 12$	Oleson *et al.,* 2008
ED2	$A_n = A_g \beta_t - (1 - \beta_t) R_{lf}$ $\beta_t = \sum_i \frac{1}{1+\frac{D}{S_i}}$ $D = ET_{max}\ LAI$ $S_i = K_w\ \theta_i\ B_{ri}$ $total\ i = 16$	Medvigy *et al.,* 2009
IBIS	$A_n = A_g \beta_t - R_{lf}$ $\beta_t = \sum_i \beta_i B_{ri}$ $\beta_i = \frac{1-\exp\left(\alpha\frac{\theta_i - \theta_w}{\theta_f - \theta_w}\right)}{1-\exp(\alpha)}$ $total\ i = 6$	Foley et al. 1996

Table S2.3 continued.

Model	Soil water-stress functions (β)	References
JULES	$A_n = \beta_t A_p$ $A_p = A_g - R_{lf}$ $\beta_t = \sum_i \beta_i B_{ri}$ $\beta_i = \frac{\theta_i - \theta_w}{\theta_f - \theta_w}$ $total\ i = 4$	Cox 2001, Clark et al. 2011
SiB3	$V_{cmax} = V_{cmax,0} f(T_{lf}) \beta_t$ $\beta_t = \sum_i \beta_i B_{ri,apparent}$ $B_{ri,apparent} = \left(\frac{1-\frac{\theta_w}{\theta_i}}{1-\frac{\theta_w}{\theta_f}}\right) B_{ri}$ $\beta_i = \frac{(1+\alpha)\left(\frac{\theta_i - \theta_w}{\theta_f - \theta_w}\right)}{\alpha + \left(\frac{\theta_i - \theta_w}{\theta_f - \theta_w}\right)}$ $total\ i = 10$	Sellers *et al.,* 1996, Baker *et al.,* 2008

Notes S3 Model specific autotrophic respiration formulations

Model specific formulations for calculating R_a are given in Table S2.4. Note that the respiration terms in Table S2.4 are calculated at the tissue level and therefore, are in units of μmol CO_2 m^{-2} tissue s^{-1}; while the respiration terms in the main text have been scaled up to the ecosystem and are in the units given in Table S2.2. The description of the

respiration terms given in Table S2.2 applies to both the main text and the Equations in Table S2.4.

Table S2.4 Autotrophic respiration (R_a) formulations for CLM3.5, ED2, IBIS, JULES, SiB3 and SPA. Explanations of symbols are given in Table S2.2 but see note above about the units.

Model	Respiration functions	References
CLM3.5	$R_a = R_g + \sum_j R_{mj}$ $R_{mj} = \gamma_{CLM} \frac{B_j}{cn_j} f(T_j)$ $R_g = 0.25(GPP - \sum_j R_{mj})$	Levis *et al.,* 2004
ED2	$R_a = R_g + R_m$ $R_m = R_{lf} + R_r$ $R_{lf} = \gamma_{lf} V_{cmax} f(T_{lf})$ $R_r = \gamma_r B_r f(T_s)$ $R_g = \max[0, 0.333(GPP - R_m)]$	Medvigy *et al.,* 2009
IBIS	$R_a = R_g + R_m$ $R_m = R_{lf} + R_r$ $R_{lf} = \gamma_{lf} V_{cmax} f(T_{lf})$ $R_r = \gamma_r B_r f(T_s)$ $R_g = 0.30(GPP - R_m)$	Foley *et al.,* 1996

Table S2.4 continued.

Model	Respiration functions	References
JULES	$R_a = R_g + R_m$ $R_{mj} = \gamma_{lf} V_{cmax} (\beta_t + f(N))$ $R_g = 0.25(GPP - R_m)$ β_t = 1 for wood and roots	Cox 2001; Clark *et al.,* 2011
SiB3	$R_m = R_{lf} + R_r$ $R_{lf} = \gamma_{lf} V_{cmax} f(T_{lf}) \beta_t$ $R_r = 0.5GPP - R_{lf}$	Sellers *et al.,* 1996
SPA	$R_a = 0.68GPP$ $R_{aj} = R_a \left[\frac{\frac{B_j}{cn_j}}{\sum_j \frac{B_j}{cn_j}} \right]$	Williams *et al.,* 1996, Williams *et al.,* 2005

Notes S4 TFE site description and C-flux methods

The TFE experiments were comprised of two one-hectare plots, one as a control and one as a treatment. The control and treatment plots were selected to be structurally and floristically similar. The throughfall exclusion system followed the same design for both sites (Nepstad *et al*., 2002; Fisher *et al*., 2007). Transparent plastic panels (~0.5 m × 3 m) were installed throughout the treatment plot 1–2 m above the forest floor to channel

the intercepted throughfall off site. In total, ~75% of the forest floor was covered by the panels with the remainder being openings around the stems. Stemflow (assumed to be ~1–2% of total rainfall) was allowed to reach the forest floor. The panels caused the forest floor temperature to increase by < 0.3^{o}C. The panels were overturned every 2–3 d to transfer litterfall to the forest floor. One by one meter drainage ditches were installed along the boundary of both plots to duplicate root damage. A deuterium tracer analysis demonstrated that a the drainage ditches were effective in preventing trees within the exclusion plot from accessing soil water outside the plot boundary (Nepstad *et al.,* 2002). The panels and gutter system was effective in removing *c*. 50% of total rainfall measured across a range of storm intensities (quantified at TNF (Nepstad *et al.,* 2002) and assumed to be similar at CAX). The wooden structure supporting the panels was not installed in the control plots. One difference in experimental design between the two sites was that throughfall was only excluded during the wet season (January–June) at TNF, while it was excluded during the entire year at CAX. The TFE experiment ran from 2000 to 2004 in TNF and from 2002 to 2008 in CAX.

For the TNF TFE site, aboveground NPP_w was estimated using a singular diameter based allometric relationship (Chambers *et al.,* 2001) applied to the annual census of trees in each plot (Brando *et al.,* 2008). Litterfall was collected using 64 0.5 m^2 mesh traps situated on the forest floor in the control plot and above the panels in the treatment plot. R_s was measured periodically using a dynamic chamber placed on each of 18 pvc soil collars within each plot (Davidson *et al.,* 2008). *NEP*, *GPP*, and R_e were measured from a nearby eddy covariance tower in a floristically and structurally similar stand (Hutyra *et al.,* 2007).

For the CAX TFE site, aboveground NPP_w was estimated using an average of 8 diameter based allometric relationships (see Table 1 in da Costa *et al.,* 2010) applied to the annual census of trees in each plot (da Costa *et al*., 2010). Fine litterfall (Metcalfe *et al.,* 2010b) and R_s (Sotta *et al.,* 2007) were collected/measured similar to TNF TFE site with sample sizes of 25 and 16, respectively, within each plot. Canopy leaf biomass was estimated by multiplying *LAI* by specific leaf area sampled in 2004 and 2007. R_{lf} was estimated for 2005 as the sum of dark and light respiration per unit leaf area scaled up to the canopy by *LAI* (Metcalfe *et al.,* 2010a, Metcalfe *et al.,* 2010b). The dark respiration component was directly measured from leaves sampled through the canopy in both plots. The light respiration component was estimated as 67% of dark respiration. Stem respiration was estimated in both plots by multiplying a respiration rate of 0.6 μmol CO_2 m^{-2} stem surface area s^{-1} by the total estimated stem surface area within the plot (Metcalfe *et al.,* 2010b). R_r was estimated in 2005 from measurements of excised roots ≤ 5 mm diameter collected from 0-30 cm soil cores (Metcalfe *et al*., 2007). These estimates of R_r are likely to be conservative because they do not include deep roots, mycorrhizae and microbial contributions.

References

Clapp RB, Hornberger GM. 1978. Empirical equation for some soil hydraulic properties. *Water Resources Research* **14**: 601–604.

Cosby BJ, Hornberger GM, Clapp RB, Ginn TR. 1984. A statistical exploration of the relationships of soil moisture characteristics to the physical properties of soils. *Water Resources Research* **20**: 682–690.

Notes S5 Soil standardization protocol

Soil hydraulic parameters, soil matrix potential at saturation (Ψ_s, MPa), hydraulic conductivity at saturation (K_s, m s^{-1}), and soil water content at saturation (θ_s, m^3 m^{-3}) were derived following Cosby *et al.* (1984). Volumetric soil water content (m^3 m^{-3}) at field capacity (θ_{fc}), wilting point (θ_{wp}), and air-dry point (θ_{ad}) were derived following Clapp & Hornberger (1978). The hydraulic conductivity at field capacity (K_{fc}) was defined as 0.1 mm d^{-1}; the soil matrix potential at the wilting point was defined as -1.5 MPa; and, the soil matrix potential at the air-dry point was defined as -3.1 MPa (Clapp & Hornberger 1978). Soil textures used for the simulations were prescribed as reported for each site: TNF had 60% clay and 38% sand (Nepstad *et al*., 2002) and CAX was 15% clay and 78% sand (Fisher *et al*., 2007). All models used 8 m depth and free drainage as the lower boundary condition. This physical standardization successfully yielded a similar soil physical environment across all of the models (B.O. Christoffersen, unpublished). The depth and distribution of roots, a biological property, was, however, model dependent.

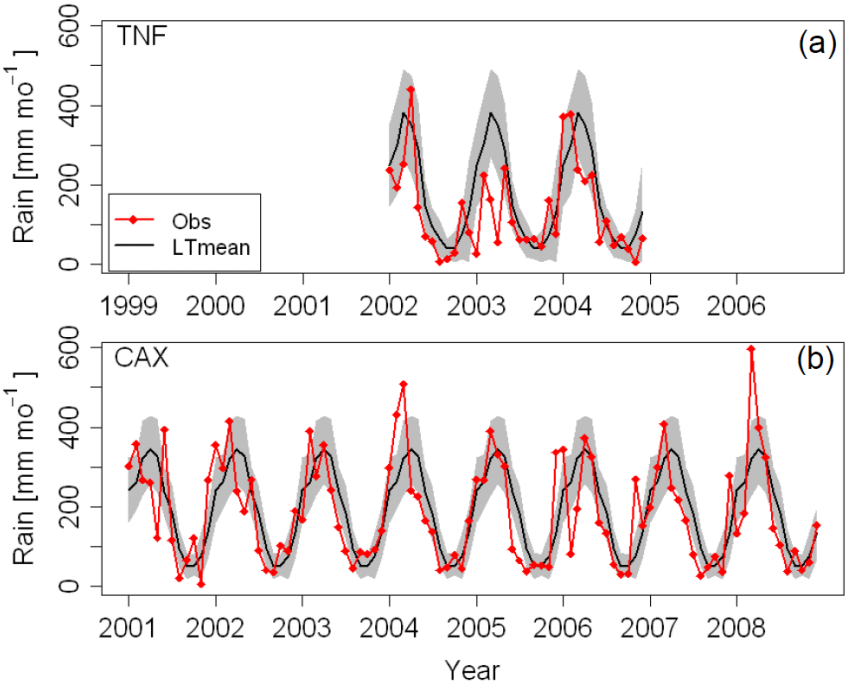

Figure S2.1. Monthly rainfall (mm mo^{-1}) measured at (a) TNF from 2002 to 2004 and (b) CAX from 2001 to 2008 (red line and symbols). The black line and shaded area shows long-term (>30 years) precipitation patterns (mean±stdev.) for each site reported by Rosolem *et al.,* (2008).

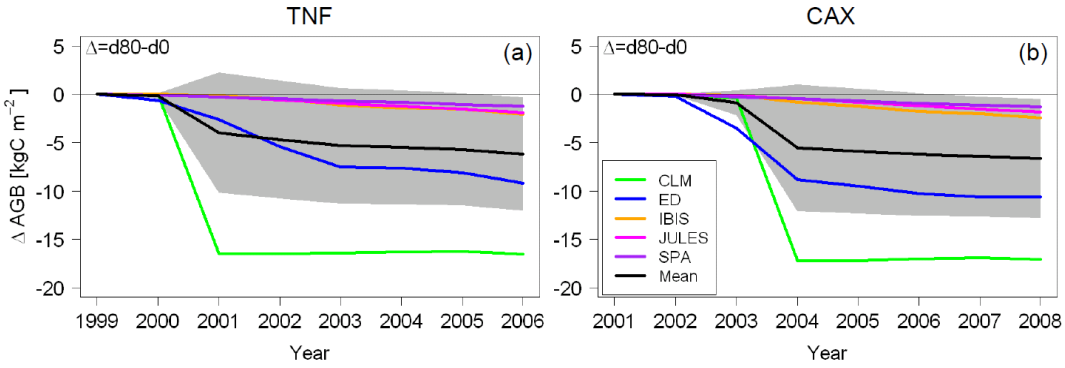

Figure S2.2. Change in aboveground biomass (*AGB*, kg C m^{-2}) with an 80% reduction (d80) in precipitation relative to the control (d0) simulations shown in Figure 1. Colored lines are individual model predictions and black line is the 5 model ensemble mean. Shaded area is the 95% CI of the models. (a) Tapajós National Forest. (b) Caxiuanã National Forest.

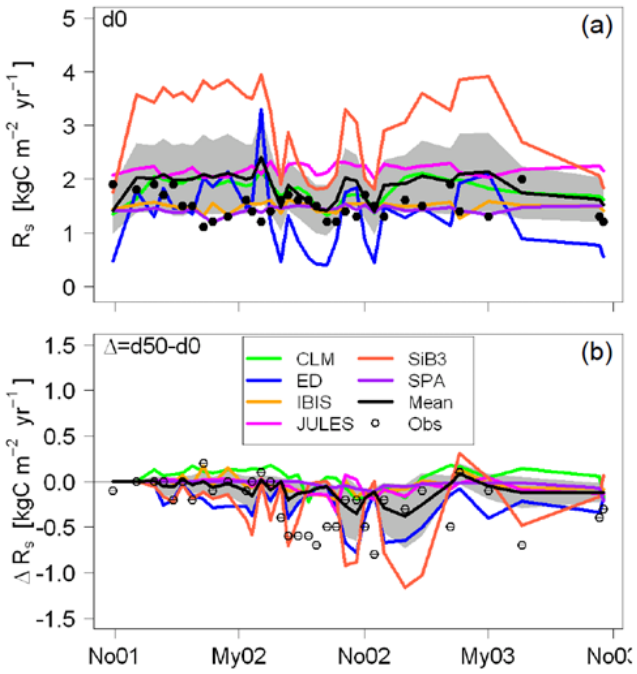

Figure S2.3. Time series of published periodic measurements of soil respiration (R_s) for CAX (Sotta *et al.,* 2007) and concurrent individual model estimates for the (a) control (d0) and (b) treatment (d50) plots of CAX. Color lines are individual model predictions and the black line is the 6 model ensemble mean. Shaded area is the 95% CI of the models. d0 and d50 are drought levels indicating a 0% and 50% reduction in precipitation. The Δ plot (b) shows the amount the control (a) R_s was altered by the 50% drought treatment.

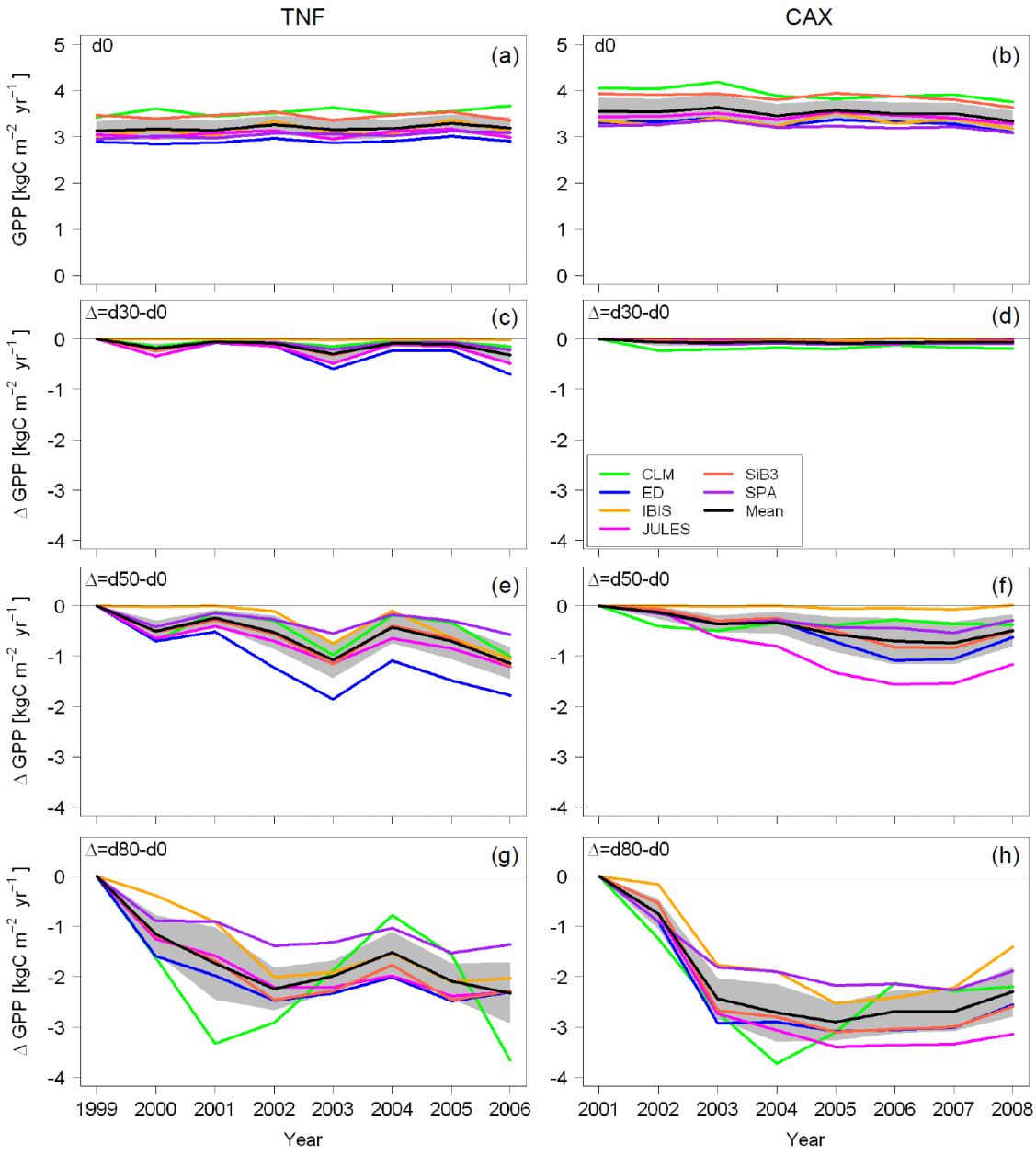

Figure S2.4. Annual gross primary production (*GPP*, kg C m^{-2} yr^{-1}) for TNF (left side) and CAX (right side). Colored lines are individual model predictions and the black line is the 6 model ensemble mean. Shaded area is the 95% CI of the models. Drought levels are indicated by d30, d50 and d80, which are respectively 30%, 50% and 80% reductions in precipitation. The Δ indicates the amount the d0 carbon fluxes were altered by the indicated drought level.

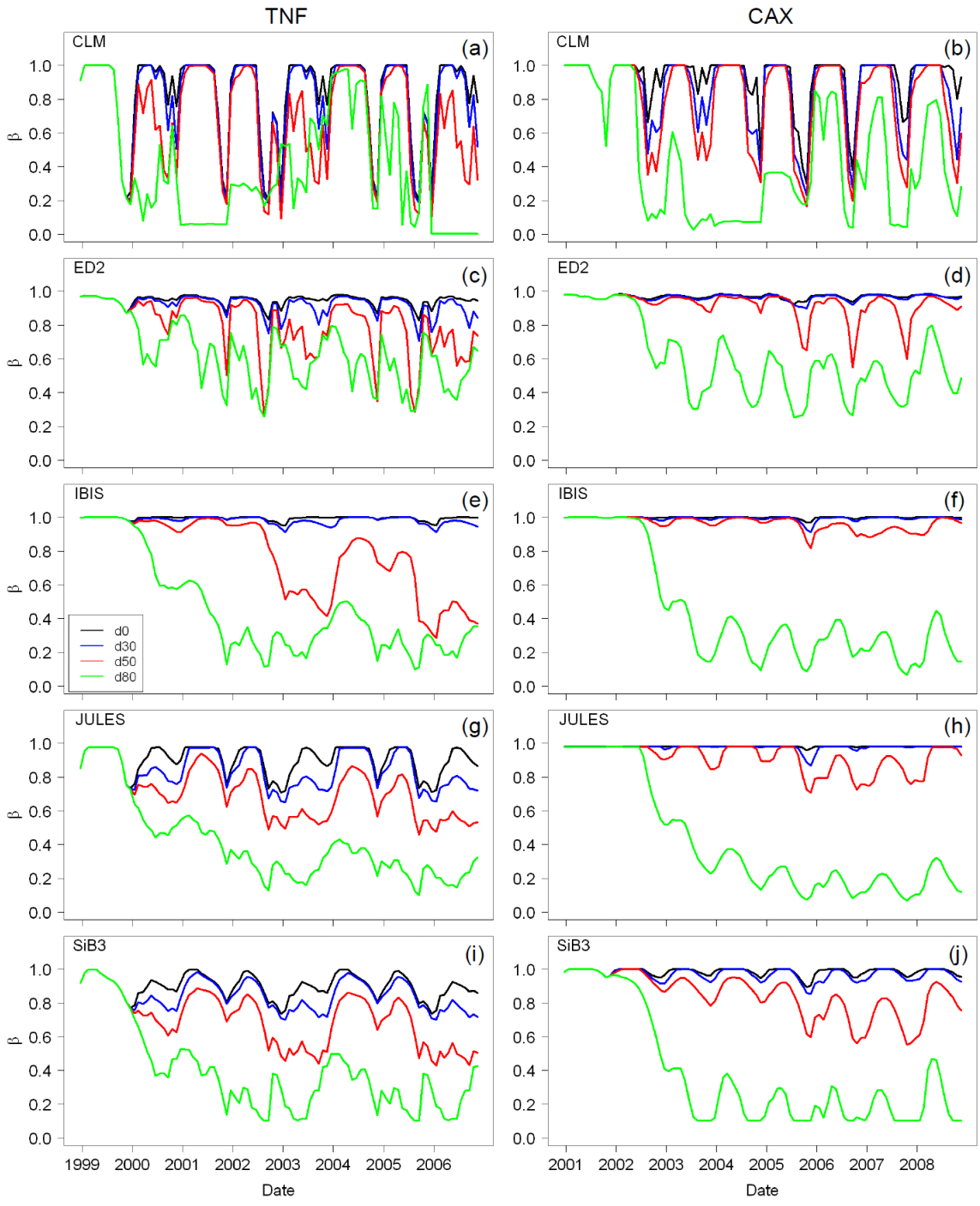

Figure S2.5. Full 7 year time series of the monthly mean water-stress factor (β) for (a, b) CLM3.5, (c, d) ED2, (e, f) IBIS, (g, h) JULES, (i, j) SiB3 at each treatment level (colored lines) for TNF (left side) and CAX (right side).

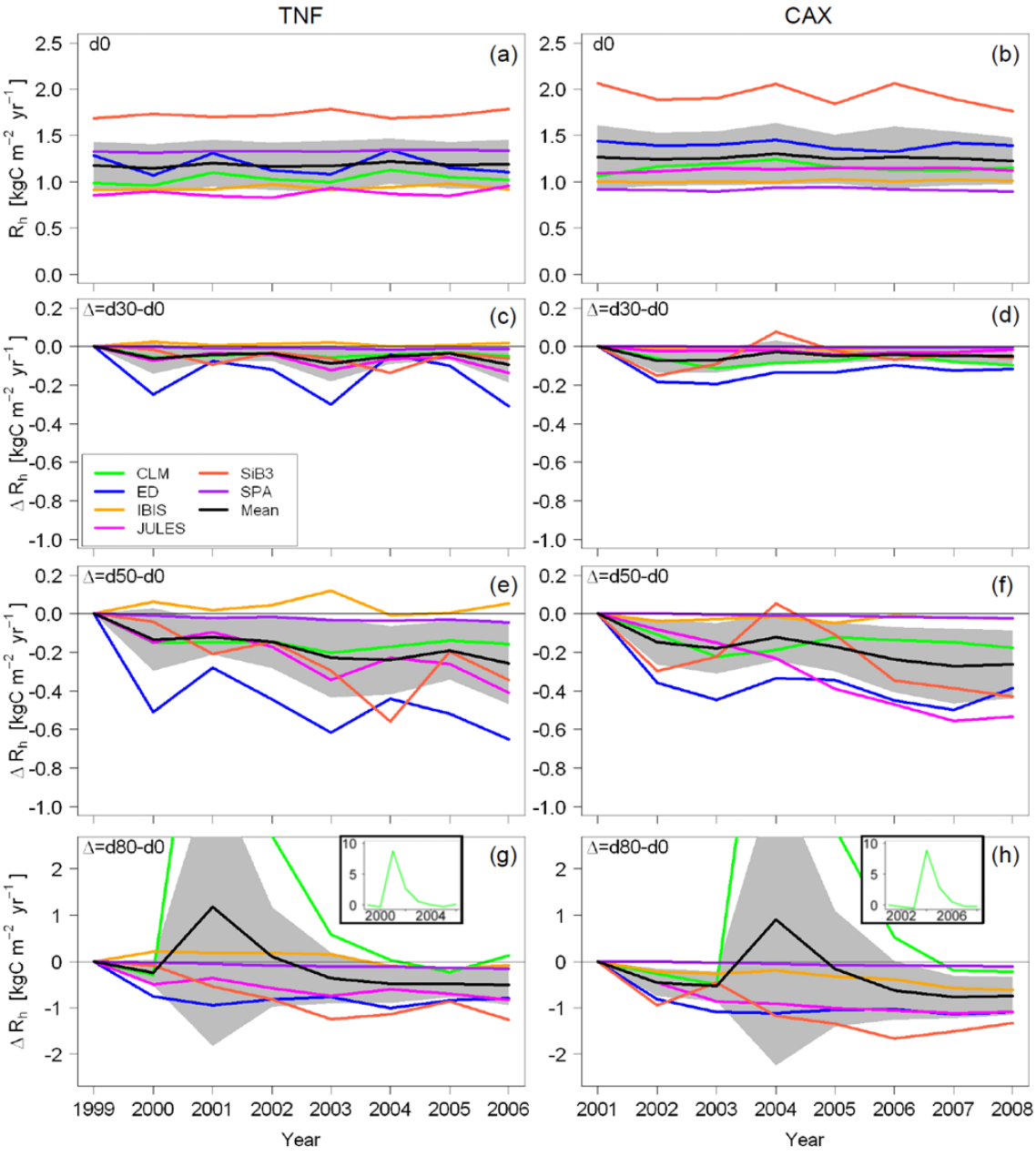

Figure S2.6. Annual heterotrophic respiration (R_h, kg C m^{-2} yr^{-1}) for TNF (left side) and CAX (right side). Colored lines are individual model predictions and the black line is the 6 model ensemble mean. Shaded area is the 95% CI of the models. Drought levels are indicated by d30, d50 and d80, which are respectively 30%, 50% and 80% reductions in precipitation. The Δ indicates the amount the d0 carbon fluxes were altered by the indicated drought level. Insets in (g) and (h) show full range for CLM3.5.

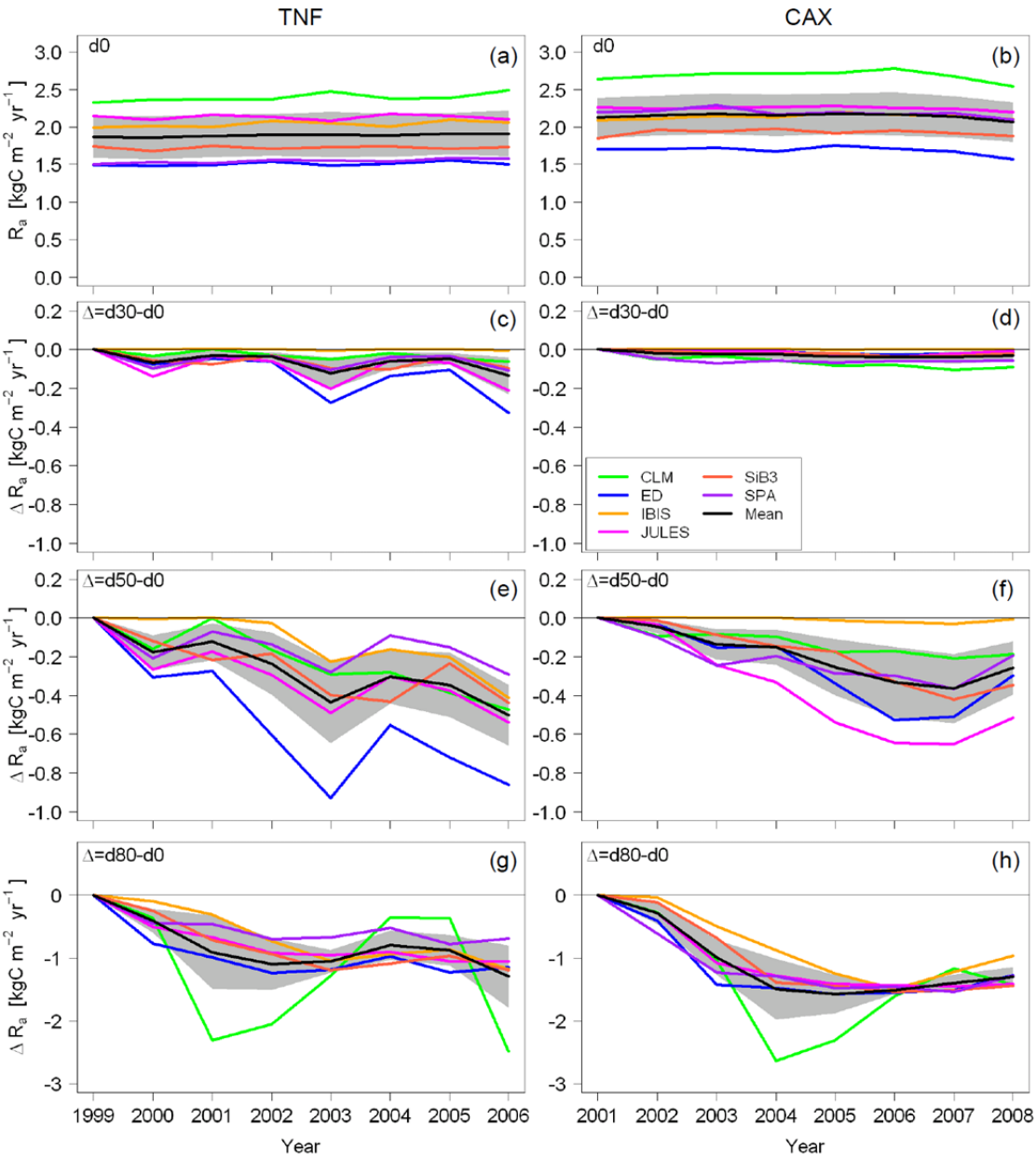

Figure S2.7. Annual autotrophic respiration (R_a, kg C m^{-2} yr^{-1}) for TNF (left side) and CAX (right side). Colored lines are individual model predictions and the black line is the 6 model ensemble mean. Shaded area is the 95% CI of the models. Drought levels are indicated by d30, d50 and d80, which are respectively 30%, 50% and 80% reductions in precipitation. The Δ indicates the amount the d0 carbon fluxes were altered by the indicated drought level.

Appendix C

Chapter 3 Supporting Information: Table S3.1 and Figures S3.1-S3.4.

Table S3.1. Leaf and branch sample sizes for each species at each site. Leaves were used to construct the pressure-volume curves shown in Figure 3.1 and branches were used to construct the xylem vulnerability curves shown in Figure 3.4. Sites are indicated by CAX for Caxiuanã and TNF for Tapajós National Forests.

	Pressure volume curves				Xylem vulnerability curves			
Site:	CAX*		TNF		CAX*		TNF	
Species	trees	leaves	trees	leaves	trees	branches	trees	branches
Inga species	4(2)	15(7)	4	12	6(4)	10(6)	6	7
Eschweilera coriacea	4(2)	19(10)	4	14	9(5)	11(5)	7	10
Protium species	4(2)	18(8)	4	10	10(6)	10(6)	8	9
Licania species	5(2)	23(10)	3	12	9(5)	13(6)	6	7

* Total sample size of control plus treatment plots. Parentheses indicate sample size from control plots only.

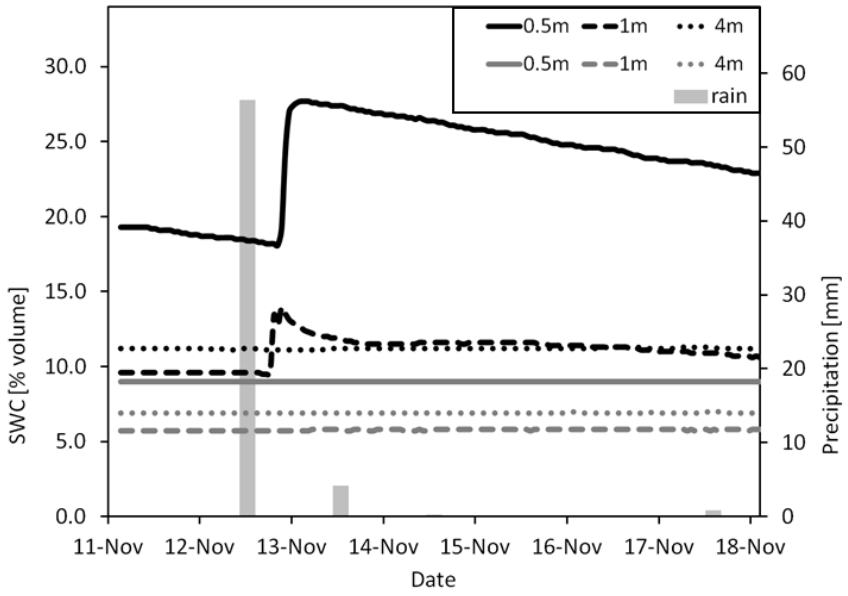

Figure S3.1. Soil water content (SWC, % volume, left axis) at three depths in the rooting zone, 0.5 m (solid), 1.0 m (dash) and 4.0 m (dot), of the control (black) and drought treatment (grey) plots at Caxiuana. Soils were 78% sand. Soil moisture was measured continuously over the 8 year study and the differences between plots remained consistent (Fisher *et al*., 2007). Measurement shown here are from the 7 days immediately preceding the leaf water potential measurements on 18 November 2011. Precipitation (mm, bar) is shown on the right axis.

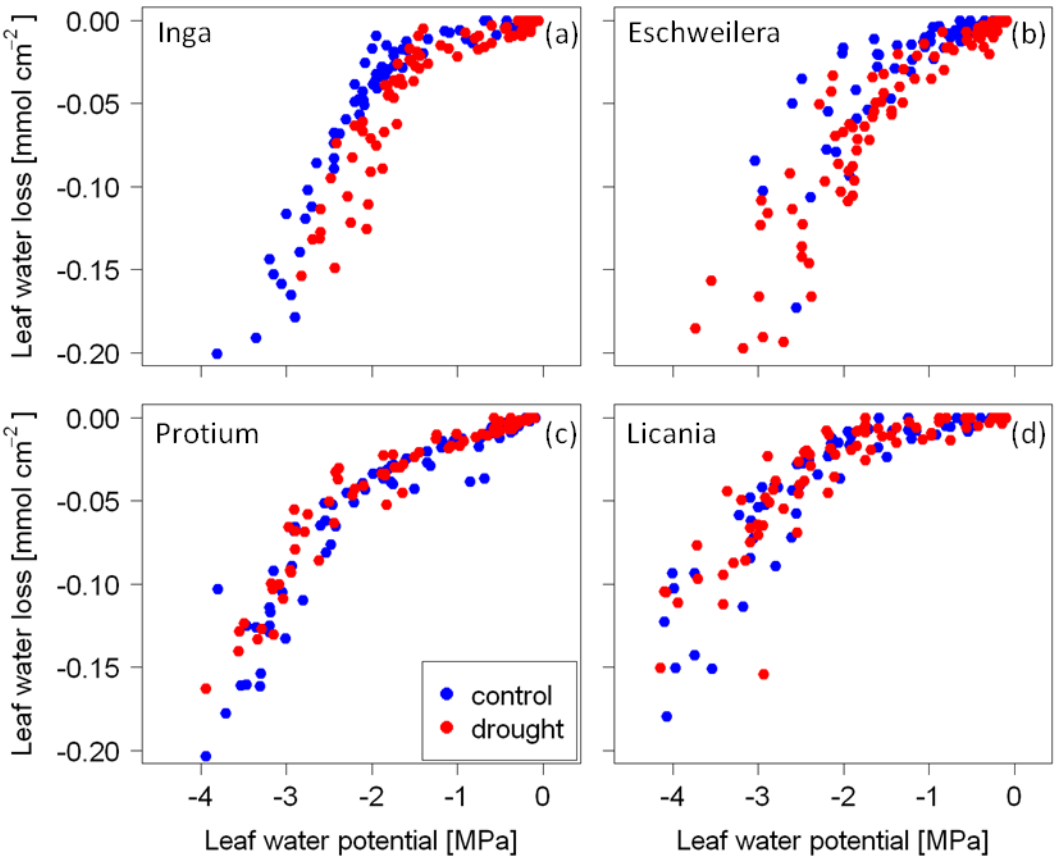

Figure S3.2. Pressure-volume curves showing the relationship between leaf water potential (MPa) and leaf water loss (mmol H_2O cm^{-2}) for each plant functional type measured in the control and drought plots at Caxiuanã. (a) *Inga* genus represents early-successional drought-intolerant. (b) *Eschweilera* genus represents late-successional drought-intolerant. (c) *Protium* genus represents early-successional drought-tolerant. (d) *Licania* genus represents late-successional drought-tolerant .

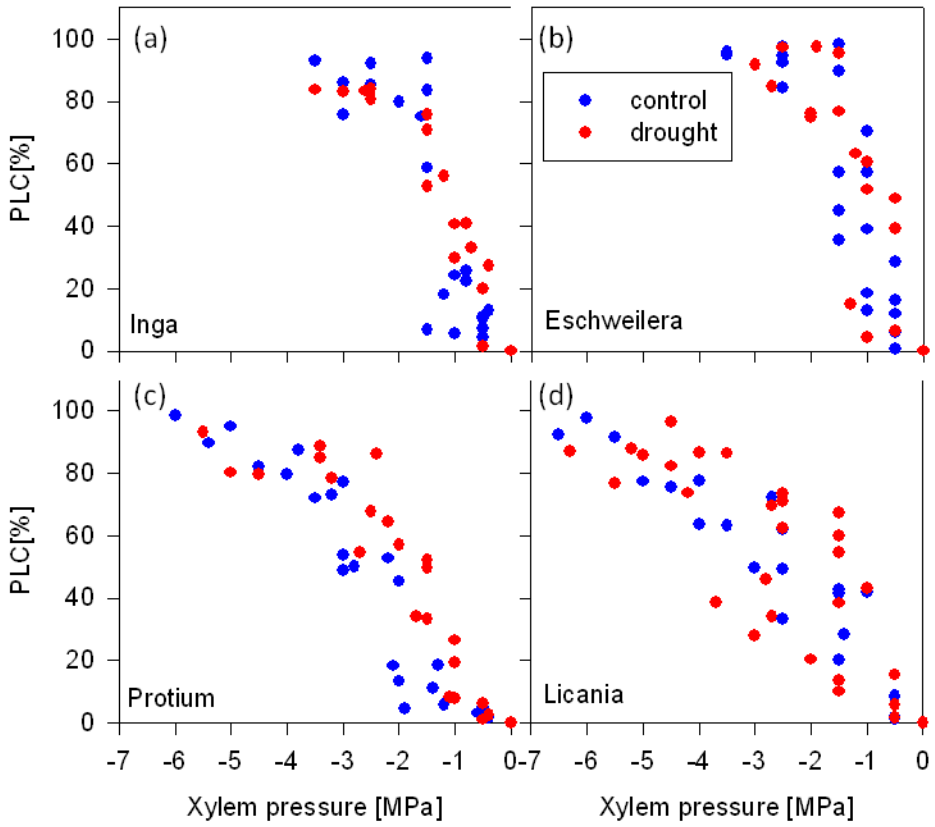

Figure S3.3. Xylem vulnerablity curves showing the percent loss in conductance (PLC, %) with decreasing xylem pressure (MPa) for species measured at Caxiuana. The P_{50} values indicate the xylem pressure when 50% of the conductance is lost. (a) *Inga* genus represents early-successional drought-intolerant. (b) *Eschweilera* genus represents late-successional drought-intolerant. (c) *Protium* genus represents early-successional drought-tolerant. (d) *Licania* genus represents late-successional drought-tolerant.

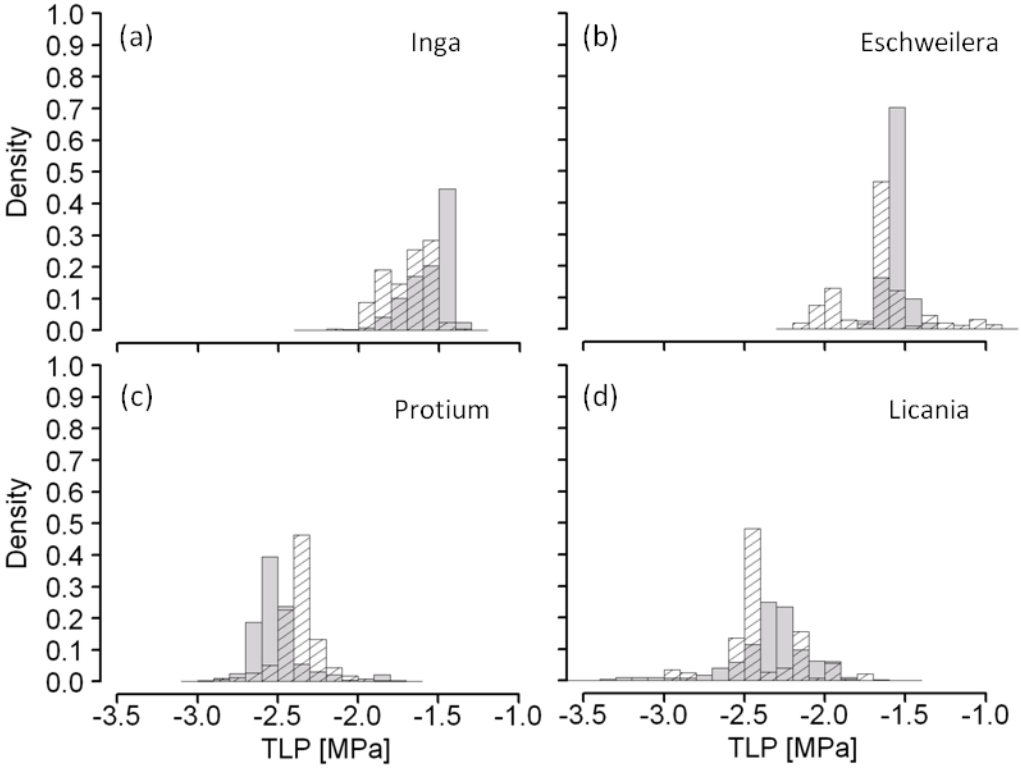

Figure S3.4. Frequency distribution of turgor loss point (TLP) estimates from a 10000 iteration bootstrap of the change point detection routine. Tapajós: grey bars. Caxiuanã: textured bars. (a) *Inga* represents early-successional drought-intolerant. (b) *Eschweilera* represents late-successional drought-intolerant. (c) *Protium* represents early-successional drought-tolerant. (d) *Licania* represents late-successional drought-tolerant.